POLITECNICO DI MILANO

Department of Civil and Environmental engineering

Master of Science – Civil engineering for risk mitigation

Landslide susceptibility assessment. A case study in central Norway

Advisor: **Prof: Laura Longoni**
Co-advisor: **Prof: Ivan Depina**

Loza Ayehutsega Awgechew

Student ID: 966527

Academic year: 2022-23

Acknowledgment

Table of Contents

List of Figures

List of Tables

ABSTRACT

Rainfall-induced Landslide susceptibility assessment using a detailed investigation of environmental factors, geotechnical parameters, hydrological parameters, and topography condition is important. A physical base model can be used to investigate the impact in the study area and investigate the elements at risk.

This research attempts to quantify landslide susceptibility assessment in a case study in Norway using a physical base model assessment. The study area is located in Trøndelag county, central Norway in the east of Trondheim. The selected area is 250 km^2 in size. This thesis project was done with the partner university NTNU (Norwegian university of since and technology), Norway in the department of civil and environmental engineering.

Firstly, the objective of the study, research question, and delimitation of the project studied. The main objective of the project is to perform a rainfall-induced landslide susceptibility assessment on a case study in central Norway with a physical-based landslide model. Accordingly, landslide analysis using inventory data and triggering factors was adopted. The geotechnical, geological, and hydrological data and topographic maps were collected and studied for the detailed assessment of landslide susceptibility in the case study. A physical-based landslide model, LISEM used for slope stability assessment and runout model. From the assessment result, it was possible to investigate the parameters controlling the stability of the slope in the case study area and the triggering parameters. The model was calibrated using the landslide inventory from the recent rainfall-triggered landslide event. Rainfall data analysis was applied in the case study and the runout model was investigated using the observed precipitation. This model was chosen because of its applicability for the multi-process of simulating slope stability, sensitivity analysis, and runout model. The calibration is based on slope stability assessment. The parameters that change the factor of safety and failure depth result selected for calibration are, (cohesion, internal friction angle (IFA), and soil depth). Further, a detailed investigation of this parameter using sensitivity analysis is presented in this research. Result from slope stability assessment used for the runout model and elements at risk in the study area observed. The result from the model well predicted the landslide in the study area. The calibration showed that slope failure results and inventory map were almost consistent in most of the area. However, some areas were also not predicted well by the model according to the inventory data. Therefore, a detailed conclusion regarding the model result and calibration are discussed in this research project. In addition, limitations and recommendations are also drawn for future studies.

Keywords: (slope stability, physical-based landslide model, calibration, sensitivity analysis, geotechnical and hydrological parameters)

1. INTRODUCTION

1.1.   Statement of the problem

Landslides are hazardous phenomena that have a tremendous negative impact on people's lives, on the environment, and infrastructures. Landslide susceptibility assessment can be difficult and time-consuming particularly when detailed hazard inventory maps and data for risk assessment are not available or properly recorded. The major cause of landslide mass movement is the exceedance of shear stress on the slope material over the material shear strength. As its well-known landslides occur worldwide, however, certain regions are particularly susceptible due to environmental factors, soil material conditions, and topography conditions. According to recent studies, landslides cause thousands of fatalities and injuries, and significant economic damage annually (Mikoš & Sassa, 2015).

Landslide damage covers many aspects, including direct and indirect damage. Direct damage can be physical damage that occurs due to direct contact with the hazard. Examples of this include death or serious injuries to people, environmental damage, damage to the building, damage to infrastructures (e.g., roads, railways, electricity, utility pipelines), and damage to agriculture (farmland). The indirect damage can be defined as those resulting from the event but not from direct contact with the impacts. Some examples are economic loss, social (political) disruption, loss of industrial production, emergency cost, traffic disruptions, and trauma/ stress to people. More than 2000 deaths due to snow avalanches and landslides are recorded in Norway over the past 150 years (Nadim, 2016). The frequency of water-triggered landslides today in Norway is steadily increasing, both due to huge amounts of snowmelt and rainfall events. The climate research report in Norway (NVE., 2022) predicted an intense increase in precipitation.

One of the major problems in landslide assessment and hazard mapping is the limited availability of data on various parameters controlling the stability of slopes assessing the likelihood of landslide occurrence, detecting areas susceptible to land sliding, detailing topography, and conducting geomorphology study of the area, acquiring knowledge about the major cause of historic landslide and the consequences of damage, and quantitative and qualitative studies of hazard, exposure and vulnerability are critical information tools for the hazard assessment.

.

1.2. Research objective

1.2.1. General objective

➢ To perform rainfall-induced landslide susceptibility assessment on a case study in central Norway with a physical-based landslide model.

1.2.2. Specific Objectives

➢ Analyse landslide inventory and examine landslide triggering parameters in the case study area.
➢ Collect and analyse geotechnical, geological, and hydrological data, topographic maps, meteorological records, and other parameters controlling the stability of slope in the case study area.
➢ Implement a physics-based landslide model, LISEM, in the case study area.
➢ Perform sensitivity and calibration analyses of the LISEM model.
➢ Perform landslide susceptibility assessment by conducting slope stability and runout analyses with LISEM.

1.3. Research question

➢ What are the parameters controlling the stability of slopes in the case study area?
➢ What are the typical triggering parameters for water-induced landslides in the case study area?
➢ Which method of assessment is applicable for mapping and modelling water-induced landslide hazards in the case study area?
➢ What are the most important parameters in the slope stability model?
➢ Can the implemented landslide model reasonably assess landslide susceptibility in the case study area?
➢ Which are the elements/properties exposed to landslide in the case study area?

1.4. Significance of the project

It is important to assess the conditions that trigger landslides and the parameters controlling the stability of slopes in a given area for the prediction of landslide occurrence and its propagation. Therefore, the assessment of probable conditions and parameters that caused the slope to become unstable and the investigation of triggering factors are significant to reduce the damage to exposed elements.

This project will examine the most probable condition for the occurrence of landslides in the specified area based on the available landslide inventory. This assessment will help to mitigate the landslide occurrence due to the triggering factor in unstable slope from the back analysis of rainfall-triggered landslide event. Even though it is not possible to stop the occurrence of natural hazards, proper hazard mitigation and risk assessment have a positive outcome to reduce the damage cost to the people and the property.

Rainfall-induced landslide hazard assessment is done based on a historical event recorded by NVE. Norwegian Water Resources and Energy Directorate (NVE, 1921) classifies landslides in Norway based on the different materials involved: bedrock, loose material, and snow. In Norway water is always contributing factor to the occurrence of a landslide which is mostly caused by heavy rainfall with a combination of the high ground water table (Trøan, 2017).

Climate change will increase the risk of landslides. Yearly precipitation is expected to increase by 20% with significant seasonal variation (Hisdal et al, 2017). Consequently, the vulnerability will increase in the study areas. This project studies the potential slope failure of the study area by considering the appropriate initial hydrological conditions (infiltration, initial soil saturation, wetting front height, and groundwater height,) and different slope stability parameters particularly (soil cohesion, soil depth, and internal friction angle (IFA)) for the physically based modelling of failure. The climate conditions and rainfall data of the study area are assessed for different return periods. The observed precipitation data was applied for slope stability assessment and the runout model. The result is used for susceptibility assessment in the given area. The approach to landslide susceptibility and hazard mapping can be categorized into different methodologies. According to (Bobrowsky, 2009), the methodologies can be categorized into (qualitative, heuristic approaches, quantitative analysis of landslide inventories, statistical approaches, and physically based models). Each methodology is described in the literature review section.

Firstly, the study area and its geological and hydrological properties are described with the aid of aerial photography and /or satellite image analysis using a Geographic Information System (GIS) environment in chapter 2. Then, historical landslide case studies were assessed in chapter 3. Landslide hazard

assessment research has predominantly focused on on-site investigations (Kirschbaum & Hong, 2006). Landslide inventories and rainfall information are used to provide an estimate of static landslide hazard susceptibility. The landslide inventory database was used from (NVE, 1921) datasets recorded from 2005. In addition, information was collected from journal articles, government, and media reports. It's worthless to state the methodology of the assessment without a brief description of the literature review that has been done to select the appropriate approaches. For this project several literature reviews are presented for the point of interest then the methodology for hazard assessment is selected in chapter 4 based on the available data, environment condition, research objective, and computational cost. Chapter 5 briefly discusses the slope stability assessment, calibration (validation of the result), and sensitivity analysis of selected parameters. Conclusion and discussion of the result drawn in chapter 6.

1.5.   Delimitation of the project

1. For this project, a single landslide assessment approach is chosen based on the availability of data. The approaches are selected mainly based on the objective of the project and the availability of input data. Two or more evaluation approaches and a comparison of the result could give a better susceptibility assessment. However, this project only considers a single approach due to the limitation of input data.

2. Input data availability and accuracy.

Data used for this project can be categorized into three: - (landslide inventory data, triggering factor/ rainfall data, soil property data, and element at-risk data). Among all these landslide inventory data is the most important one as it should give insight into the location of the unstable area, failure mechanism, and frequency of occurrence. Landslide inventory data used for this project is the data recorded after 2005. Field information data are not enough to use in the selected physical base model, for example, a soil depth map modelled using an empirical formula extracted from the available DEM map. The model may not precisely and accurately predict the actual soil depth in all over the area.

3. Rainfall data is considered for the triggering effect of landslides. Snowmelt data are not considered for this project. The back analysis of landslide events in the study area considers a single landslide event due to the heavy rainfall. However, the snowmelt data during this event were not the major triggering factor. Therefore, for this project, it was decided to focus only on the rainfall trigger landslide susceptibility assessment.

2. STUDY AREA

2.1. Study area description

The study area is located in Trøndelag county, central Norway in the east of Trondheim, and is 250 km^2 in size. The area is located between the municipality of Stjørdal and the municipality of Meråker (Depina & Oguz, KlimaDigital Case Study, 2021). The Meråker railway line and the European E14 highway route are the main transportation line in the area and follow the river through the length of the valley. Along Stjørdalselva river the slope angle is greater than 30 degrees. The study area is very susceptible to landslides (NVE, Norwegian Water Resources and Energy Directorate, 1921). The DEM of the study area was obtained from "hoydedata.no" with a resolution of 10 m. slope angle, drainage direction, and channels of the flow are derived from the DEM data.
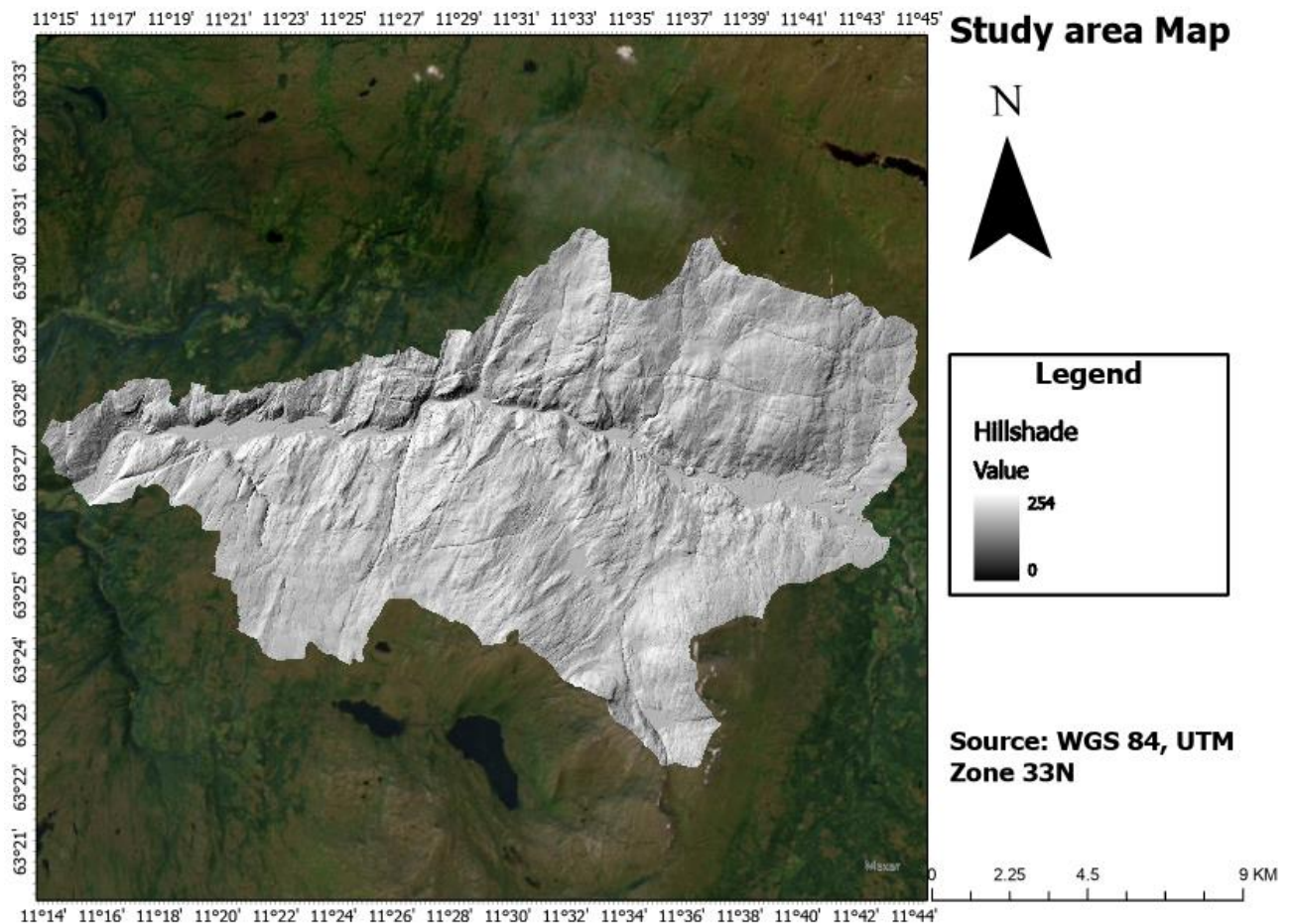
Figure 1. Study area DTM

2.2. Geology

The study area bedrock is a composition of Proterozoic and Cambrian metamorphic rock deformed during Caledonian orogenesis (Depina & Oguz, 2021). In the eastern sector rock groups are categorized as dark gray, black phyllites, calcium-rich gray, metasandstone, and greenstone. To the west, the rocks vary from greenstone with local conglomerate, gray to green phyllites, and dark gray to black phyllites. The bedrock is covered by a thin cover of quaternary deposits of different origins, the thick cover is above the bedrock that is at the bottom of the valley. On the west side, there is a shallow cover that is formed by the chemical and physical decomposition of altered material abounds on the top of the bedrock. Organic soil and peat cover formed from dead plant remains with a thickness greater than 0.5 m were observed. In the central or eastern part of the section, the bedrock is covered by till or moraine deposits with a thickness of less than 0.5 m. This material is composed of hard-packed and well-sorted material which contains silt-to-stone fractions (Depina & Oguz, 2021) . In addition, humus cover/pit cover can also be observed over the bedrock. The bottom of the valley is filled with rounded sand and gravel fluvial deposits, with a thickness that varies from 0.5 to 10 m. The colluvial deposits which are left by landslides can be observed in this study area.

Legend

Quaternary deposits

Discription

- Till deposit, thick cover
- Till deposit, thin cover
- Randmorene
- Glacio-fluvial deposits
- Marine and fjord deposit thick cover
- Marine deposits
- Marine and fjord deposit, thin cover
- Fluvial deposits
- Alterd bed rock
- Colluvial deposits
- Pit cover (organic material)
- Humus /pit cover (thin cover(
- Antropogenic deposits (flaying material)
- Exposed bedrock

Figure 2. Geology description of the study area

2.3. Geomorphology

Three morphology zones can be observed from north to south. Steep slope with its summit at the top, a quaternary deposit that ends in the E-14 road and the Stjørdalselva river valley. The quaternary deposit is susceptible to debris flow and avalanches that leads to road blockage. Several landslide reports and photographic evidence were found in the study area. landslide monitoring devices were installed in the four preferred areas (Depina & Oguz, 2021).
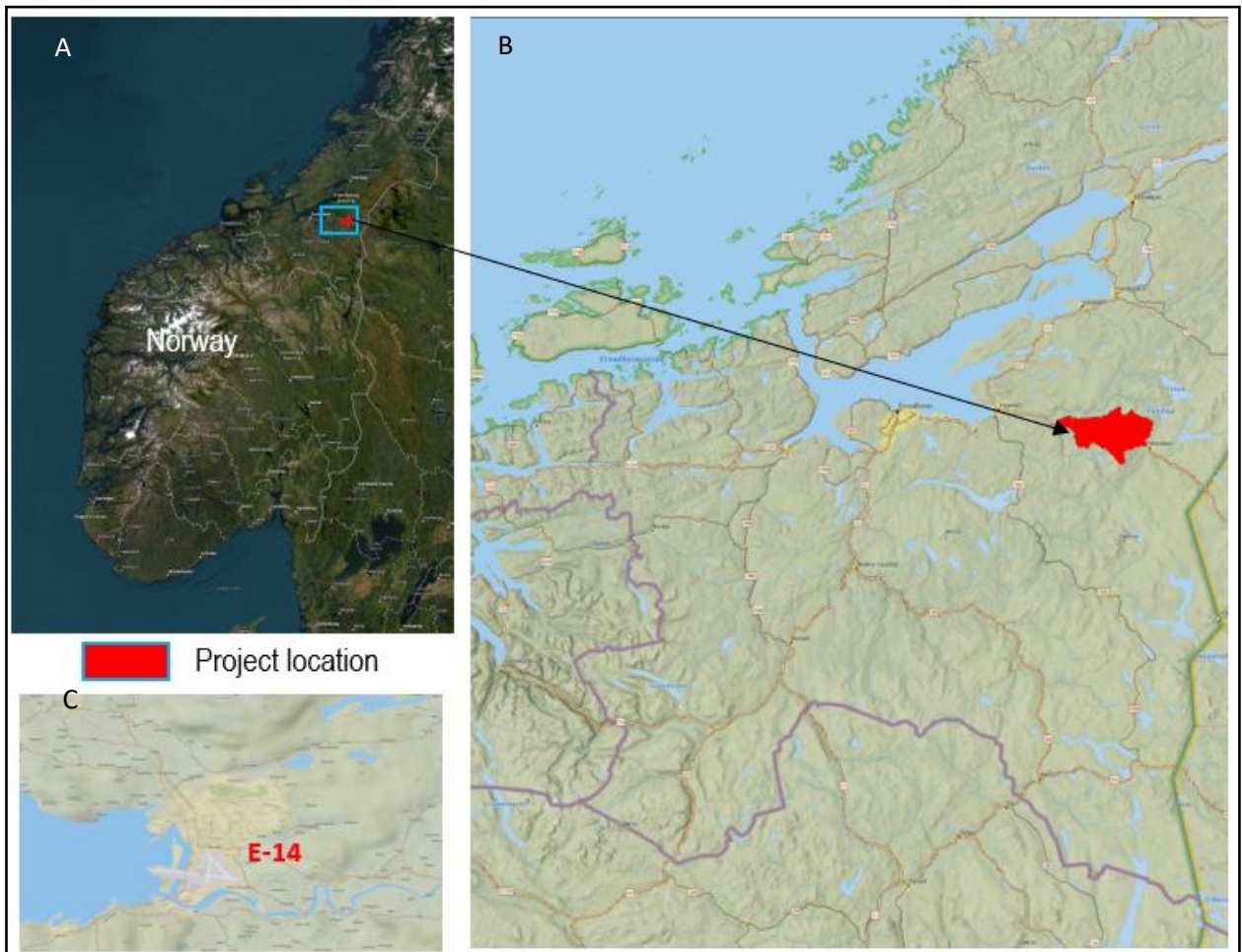
Figure 3. Study area location (A, B), E-14 road location on the study area(C)

2.4.   Climate

The average temperature of the study area ranges from -2.9^0 c to 12.6^0 c. In Meråker the summers are short, cool, wet, and mostly cloudy and the winters are long, freezing, snowy, and overcast. The precipitation in the study areas varies throughout the year. The month with the wettest days in Meråker is September. The dry season lasts 2.1 months, from March 21 to May 25. Rainfall is the most common for 8.6 months, from March 11 to November 28. The month with the most days of snow in Meråker is February, with an average of 5.6 days. (NVE., 2022)
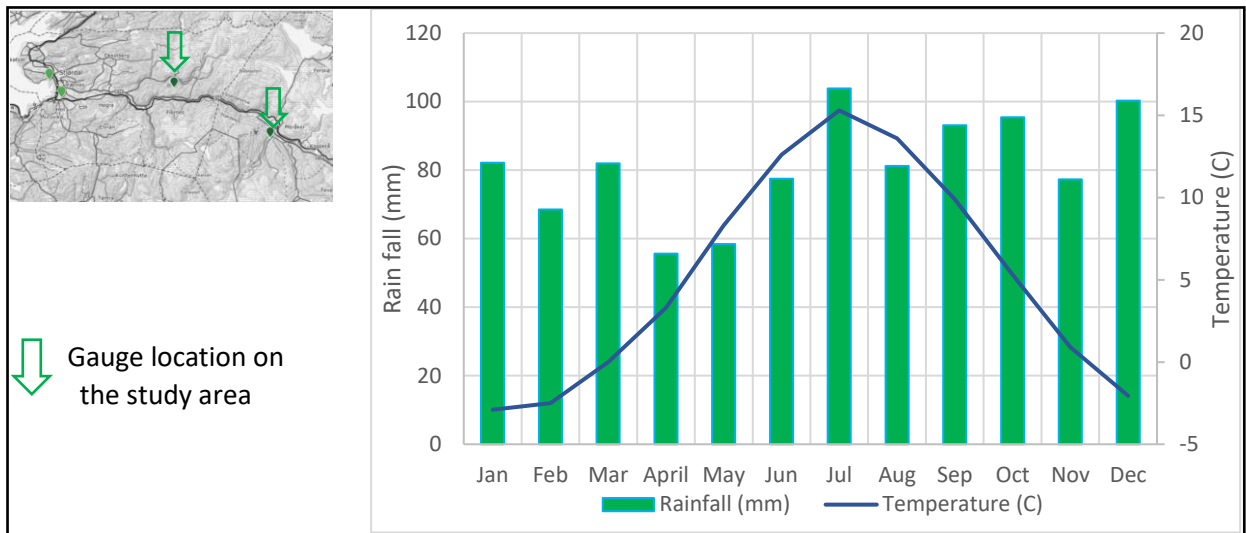
Figure 4. Average rainfall and temperature for the study area

2.4.1. Climate and geomorphological changes in the coming year

The climate change report ((IPCC), 2013) stated the projection of climate change which will be strongly affected by global warming in the coming year. The reason for this can be the melting of polar ice. According to the report, there is going to be more precipitation in Norway 10 to 20% of the global emission scenario. In addition, the amount of snow is going to decline during the century. The timing of this decrease is very dependent. The sea level is going to increase, with large regional variation The historic record of rainfall shows a clear pattern of increase in precipitation in InfraRisk in Norway (NGI, 2013) the rainfall history has been documented on daily extreme bases.
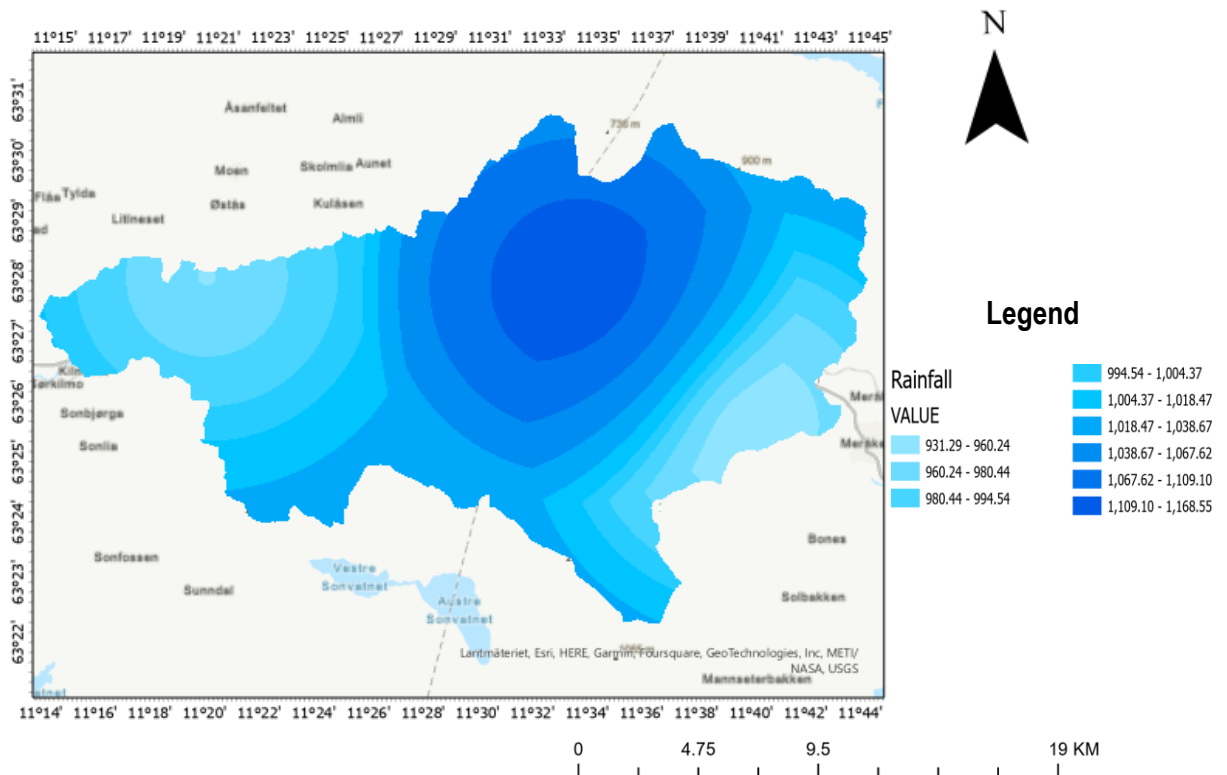
Figure 5. Average rainfall data in the study area.

2.5. Landslide inventory

Different types of landslides occurred in the study area. During a period of intense rainfall, shallow landslides in soils are the most frequent types of landslides because of the high amount of groundwater level and high soil saturation in the study area. Debris flows in the moraine deposits was observed. The historic landslide occurred along the slope and several damages were induced on the road, rail, and infrastructures (Depina & Oguz, 2021). According to (NVE, 1921) reported, 36 events were triggered by rainfall and snowmelt during the period 1750-2019. Among these events, 35 events are categorized as rock fall. The majority of landslides occurred after the year 2000 (Depina & Oguz, 2021). Grouping landslide inventory data are very important to map landslide susceptibility and categorize them on a spatial and temporal scale. To make a reliable map that predicts a landslide hazard in a certain area, it is important to have insight into the spatial and temporal frequency of landslides. Therefore, the susceptibility assessment should start by making a landslide inventory assessment that is as complete as possible in space and time (Safeland, 2011). However, for this case study, only a few amounts of data are of good quality. Most of the inventory data are still of poor quality.
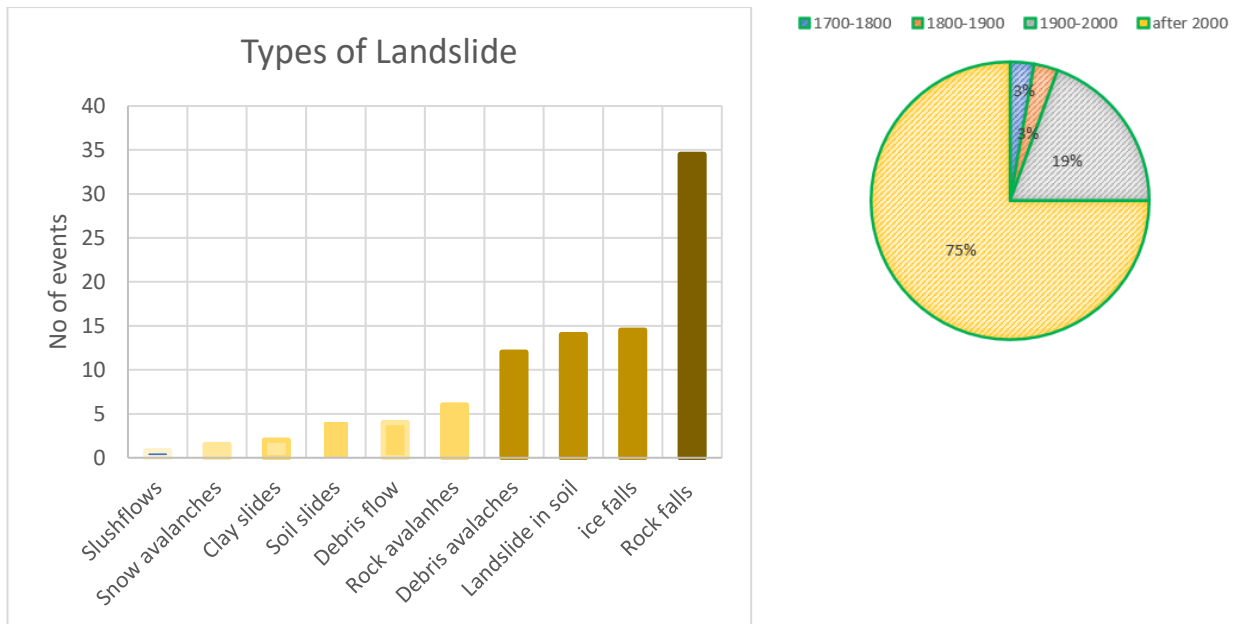
Figure 6. Types and number of landslides recorded from 1700 to 2000 in the study area (NVE, 1921) (Depina & Oguz, 2021)

Figure 7. Previous landslide occurred along the road E-14, rockfall (a), soilslides along the road(b),debris slide(c), debris flow(d (Depina & Oguz, 2021))

landslide events not registered in the database. The number of landslides per year from 2000 to 2019 can also be observed (Depina & Oguz, 2021). Around 27 events were recorded according to the NVE landslide inventory report.
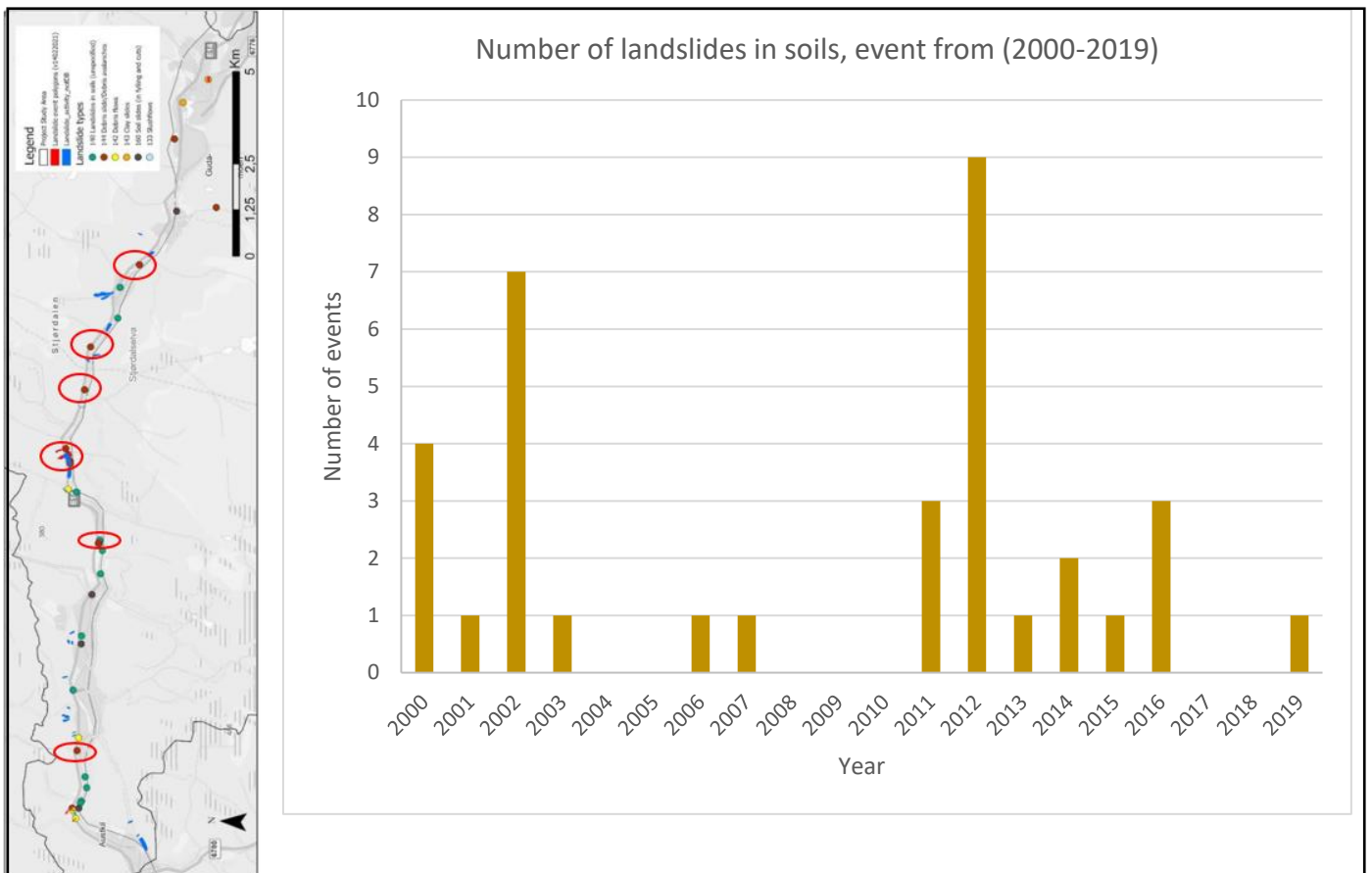
Figure 8. Landslide events recorded from 2000 to 2019 (NVE, Velkommen til skredregistrering, 1921)

3. Literature review

3.1. Landslide hazard assessment

A landslide is defined as a downslope ground movement such as rockfall, deep slope failure, shallow debris flow, and snow avalanches national park service (NPS, 2018). Landslides can be classified based on the type of movement and type of material. The type of material was divided into rock, earth, and debris and the type of movement was divided into fall, topple, slide, spread, and flow (Hungr et al., 2014). Landslides cause very significant loss of lives and damage to buildings, properties, and lifelines (Longoni, Scaioni, & Melillo, 2014).

Table 1. Landside classification is based on the type of movement and type of material(Hungr et al., 2014)

Type of Movement		Type of Material		
		Bedrock	Predominantly coarse	Predominantly fine
Falls		Rockfall	Debris fall	Earth fall
Topples		Rock topples	Debris topple	Earth topples
Slides		Rockslide	Debris slide	Earth slide
Rotational	Translational			
Lateral spreads				
Flows		Rock flow	Debris flow	Earth flow
		(Deep creep)	Soil creep	
Complex		Combination of two or more principal types of movement		

Landslide failure plane and runout distance are the most important when discussing landslide hazards. The failure plane defines the condition of failure both in the location and volume of slope failure. To study the potential damage that the landslide can cause, it is important to study the runout distance. Because it defines how far the material from the landslide reaches and if the damage is high or not.
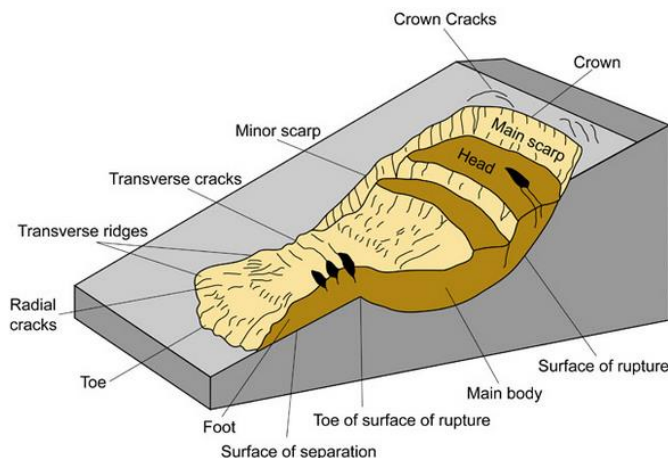
Figure 9. The schematization of a landslide and its topography (NPS, 2018)

Landslides are caused by an increase in the stresses acting on the slope or a decrease in the strength of the slope. When the stresses exceed the strength of the slope failure occurs at the failure plane and a landslide forms. The FOS determines the stability of the slope. When the FOS > 1, the slope exists in a stable situation, and when FOS < 1 the slope is unstable, and failure occurs.

$$FOS = \frac{Resisting\ stresses\ (shear\ strength)}{Driving\ stresses\ (shear\ stresses)}$$

Resistive force is the force that prevents the slope from falling which is governed by normal stresses and material properties of the soil or bedrock. The resistive force is also named shear strength. The shear strength of the slope is a function of soil cohesion, normal stress, and the internal friction angle. Cohesion is the force that bonds the soil together. The expression can be used from Mohr-Coulomb. C, cohesion (Kpa), σ, is the normal stress (Kpa), and ϕ is the internal friction angle.

$$\tau = c + \sigma tan\phi,$$

The resisting force is influenced by the existing moisture content. It increases the pore pressure which decreases the effective normal stress acting on the soil (Greco & Gargano, 2016). Water is incompressible like the grain in the soil, it can bear part of the normal stress, reducing the effective normal stress acting on the soil particles. The higher the pore pressure, the more normal stress the soil moisture carries. The effective normal stress is obtained by subtracting the pore pressure from the normal stress. Therefore, the soil moisture content influences the internal friction of the soil. An increase in soil moisture content can also decrease the apparent cohesion of the soil. This apparent cohesion consists of the cohesion defined by the soil properties and additional cohesion provided by soil suction and plant roots. Soil suction is the force of the soil particles that drag the water and other particles that are surrounded by water inside the soil. The moisture content influences the strength of the soil. The lower moisture content leads to an increase in the soil suction, thus also increasing the strength of the soil by creating a stronger bond between the grains (Dyf & Delwyn, 1982). Accordingly, the Mohor Columb criteria can be adjusted. c', is the apparent cohesion and σ' is the effective normal stress. and ϕ is the internal friction angle.

$$\tau = c' + \sigma' tan\phi,$$

The driving stresses are caused by the gravitational force acting on the slope, which depends on the weight of the soil. The soil weight is affected by the density of the soil particles, the weight of the water inside the soil, and the weight of vegetation and external factors. The driving stress is also affected by the slope angle (Lotte Ciska, 2018).

Slope stability is influenced by Slope angle, the weight of the soil, and moisture content. The most common triggering effects are seismic, long or short-term rainfall and human activity.

3.1.1. Definition of landside types

According to landslide classification and definition by Varnes (1978). The main types of landslides and their behaviour will be discussed in this topic.

3.1.1.1. *Falls and topples.*

1. **Rock/Icefall:** detachment, rolling, and bouncing may occur by a range of mechanisms, it may occur singly or in clusters, (sliding and toppling) categories, occurring at a limited scale. Rock avalanches move in a flow-like manner as masses of fragments. There is a transition between rock avalanching and rock fall or with the character of both (oldrich, Luciano, & serge, 2014). Rock material was realized by a medium-sized limestone rock wedge slide and several large fragments decoupled from the depositing mass and bounced and rolled in the manner of fragmental rock fall. Fragmental motion can be also called rock fall and it is appropriate to call the entire event rock fall. (Castelli et al., 2021)

2. **Boulder/debris/silt fall:** Detachment, fall, rolling, and bouncing of soil fragments such as large clasts in soil deposits, or blocks of cohesive soil (oldrich, Luciano, & serge, 2014). The failure mechanism is similar to a rock fall; However, the impacts are reduced by the weakness of the material. A special category of boulder falls involves the detachment of core stones separated from deeply weathered terrain.

3. **Rock blocks topple** separated by steeply dipping joints the rock is relatively massive, and rotation occurs on well-defined basal discontinuities. (oldrich, Luciano, & serge, 2014)The movement may begin slowly, but the last stage of failure can be extremely rapid. In block toppling, the Frictional forces are less important than the stabilizing stresses acting on the bases of the blocks (Goodman & Bray, 1976). Multiple block rotations can accompany sliding in large slopes of strong rock with several joint sets.

4. **Rock flexural topple:** Bending and forward rotation of a rock mass characterized by very closely spaced, steeply dipping joints, striking perpendicular to the fall line of the slope. The rock is relatively weak and fissile. (oldrich, Luciano, & serge, 2014)There are no well-defined basal joints, Therefore the rotation of the strata is defined by bending. Flexural toppling is a fundamentally different process. The major principal stress near the face surface of large slopes is oriented parallel with the slope face. (Goodman & Bray, 1976)

5. **Rock rotational slides:** Sliding of a mass of weak rock on a cylindrical or other rotational rupture surface. The morphology is characterized by a prominent main scarp, a characteristic back-titled

bench at the head, and limited internal deformation (oldrich, Luciano, & serge, 2014). These rotational slides occur only in very weak rock masses and move at slow or moderate velocities, partly because the rotational mechanism is self-stabilizing as gravitational driving forces diminish with increasing displacement(Hungr et al., 2014).

6. **Rock planar slide ("Block slide"):** Sliding of a mass of rock on a planner rupture surface. The surface may be stepped forward. The sliding head may be separating from stable rock along a deep, vertical tension crack. planar slides usually involve dip slopes that have been undercut by erosion or excavation (oldrich, Luciano, & serge, 2014).

7. **Rock wedge slide:** Sliding of a mass of rock on a rupture surface formed of two planes with a downslope-oriented intersection.(Hungr et al., 2014) No internal deformation. Wedge slides are translational slides exploiting favourably oriented intersecting discontinuities.

8. **Rock compound slide:** Sliding of a mass of rock on a rupture surface consisting of several planes, or a surface of uneven curvature, so that motion is kinematically possible only if accompanied by significant internal distortion of the moving mass. Compound rockslide has a rupture surface following a horizontal, or gently inclined plane of weakness such as a bedding plane or weak layer in the stratigraphy, daylighting at the toe.

9. **Rock irregular slide:** Sliding of a rock mass on an irregular rupture surface consisting of several randomly oriented joints, separated by a segment of intact rock ("rock bridges") occurs in strong rocks with non-systematic structure. The failure mechanism is sudden and extremely rapid.

3.1.1.2.   Slides in soil.

10. **Clay silt rotational slide ("soil slump):** Sliding of a mass of homogeneous and usually cohesive soil on a rotational rupture surface. The failure mode is usually Slow to rapid soil collapse. Deep-seated rotational motion is favoured by undrained failures and is most common in saturated soils of low permeability (clay or silts). Under special circumstances, undrained failure can occur in granular soils, particularly if rapid motion is triggered by liquefaction (oldrich, Luciano, & serge, 2014).

11. **Clay/silt planar slide:** Sliding of a block of cohesive soil on an inclined planar rupture surface, formed by a weak layer (often pre-sheared). The head of the slide mass separates from stable soil along a deep tension crack. (oldrich, Luciano, & serge, 2014)Shearing failure in cohesive material prefers curved rotational or compound sliding surfaces. If a planar slide occurs, it is likely controlled by a weak layer or a discontinuity, inclined at an angle exceeding the friction angle.

12. **Gravel/sand/debris slide:** Sliding of a mass of granular material on a shallow, planar surface parallel to the ground. Usually, the sliding mass is weathered soil. Many debris slides become flow-like after moving a short distance and transform into extremely rapid debris avalanches.

13. **Clay/silt compound slide:** Sliding of a mass of soil on a rupture surface consisting of several planes, or a surface of uneven curvature, so that motion is kinematically possible only if accompanied by significant internal distortion of the moving mass. Compound soils slide from where a weak horizon attracts the major distal part of the rupture surface.

14. **Rock slope spread:** Near-horizontal stretching (elongation) of a mass of coherent blocks of rock because of intensive deformation of an underlying weak material, or by multiple retrogressive sliding controlled by a weak basal surface. Usually with limited total displacement and slow movement.

15. **Sand silt liquefaction spread:** The extremely rapid lateral spreading of a series of soil blocks, floating on a layer of saturated (loose) granular soil, liquefied by earthquake shaking or spontaneous liquefaction.

16. **Sensitive clay spread** extremely rapid lateral spreading of a series of coherent clay blocks, floating on a layer of remoulded sensitive clay. (Hungr et al., 2014)

17. **Flow-like landslides:** rock/ice avalanche: Extremely rapid, massive, the flow-like motion of fragmented rock from a large rockslide or rock fall. Large rockslides disintegrate rapidly during motion down mountain slopes and travel as extremely rapid flows of fragmented rock.

18. **Dry (non-liquefied) sand/silt/gravel/debris flow** Slow or rapid flow-like movement of loose dry, moist sorted or unsorted granular material, without excess pore pressure.

19. **Sand/silt/debris flow side:** Very rapid to the extremely rapid flow of sorted or unsorted saturated granular material on moderate slopes, involving saturated granular material on moderate slopes, involving excess pore-pressure or liquefaction of material originating from the landslide source. This material usually ranges from loose sand to loose debris (fill or waste, usually originates as multiple retrogressive failures) (oldrich, Luciano, & serge, 2014)

20. **Sensitive clay flow slide:** Very rapid to the extremely rapid flow of liquified sensitive clay, due to remoulding during a multiple retrogressive slide failure at, or close to the original water content. Rapid strength loss because of sudden remoulding during failure at natural moisture content, a behaviour similar in its effect to liquefaction, also occurs in very sensitive, so-called "quick" clays, often leached marine clays in terraces created by isostatic uplift. As the behaviour involves a sudden "phase change" of the material from solid to liquid, triggered by shear failure, the traditional geotechnical term "clay flow slide" has long been applied to such landslides.

21. **Debris flow:** Very rapid to the extremely rapid surging flow of saturated debris in a steep channel entrainment of material and water from the flow path. The term "debris flow" is a widespread hazardous phenomenon in mountainous terrain. It is distinct from other types of landslides in that it occurs periodically on established paths, usually gullies and first -or second-order drainage channels. Thus, debris flow hazard is specific to a given path and deposition area ("debris fan"). (oldrich, Luciano, & serge, 2014) Debris flow events often occur simultaneously with floods. The flow may be initiated by a slide, debris avalanche, or rock fall from a steep bank, or by spontaneous instability of the steep stream bed. Once soil material begins to remove in a steep stream channel, the bed becomes subject to rapid undrained loading, often so sudden that it could be characterized as impact loading. Under such conditions, even coarse material can liquefy, or at least suffer a significant increase in pore pressure(Hungr et al., 2014).

22. **Earthflow:** Rapid or slower, intermittent flow-like movement of plastic, clayey soil, facilitated by a combination of sliding along multiple discrete shear surfaces, and internal shear strains. Earth flows occur in plastic, distributed, and mixed soils, whose consistency lies close to the plastic limit. Such material deforms easily but is essentially ductile and does not significantly lose strength during deformation. As a result, earth flows move slowly and intermittently.

23. **Soil creep** Extremely slow movement of surficial soil layer on a slope (typically less than 1m Deep). As a result of climate-driven cyclical volume changes (wetting and drying frost heave). Soil and weak rock layer within one meter, approximately, of the ground surface, are subject to cylindrical volume change due to swelling and shrinkage with moisture changes, freezing and thawing, and plant and animal activity (oldrich, Luciano, & serge, 2014).

3.2. Landslide susceptibility assessment

Landslide susceptibility is defined as the probability of a landslide occurring in an area on the bases of local terrain and hydrological conditions. Landslide susceptibility is the most commonly used statistical approach in which landslide inventories are used to produce maps for the prediction of landslide events. Method of assessment can be classified mainly into deterministic and probability methods. The deterministic method often assumes the slope surface to be infinite slope and the method can be used in predicting landslides by a specific rainfall event. The probability method requires long-period observations and multi-event landslide inventories as basic samples for probability analysis. A landslide susceptibility map requires data such as DTM, geological map, Rainfall data, and land use map. DTM and geological/land use data are the basic data to acquire landslide susceptibility factors, which include geological, topographic, hydrological, human activity, and triggering factors (rainfall data). Landslide

susceptibility maps can provide references for estimating unstable zones to reduce losses of life and damage to properties and infrastructures (Chin-Tung Cheng, 2013).

3.3. Methods of Landslide susceptibility assessment

The approaches to landslide susceptibility or hazard assessment depend on the objectives of the project, the scale, the physical environment, the geographical coverage, and the availability of input data to the possible models (Peter T, 2016). Several methods and approaches exist for landslide hazard assessment. The general classification is qualitative and quantitative approaches. Qualitative methods mainly include heuristic methods. Whereas quantitative methods use a numerical assessment of the relationship between slope instability and other controlling factors. The method includes landslide inventories, statistical models, and physical-based models.

3.3.1. Qualitative approaches

Qualitative or heuristic approaches include mainly direct (geomorphological) and weighting indexing approaches. geomorphological mapping, susceptibility is assessed by professionals directly in the field and with the aid of aerial photography and satellite image analysis and interpretation. The concept of a mapping unit is central to the generation of landslide susceptibility, hazard, and risk maps. The method can be fast and cost-effective for producing landslide susceptibility maps. GIS is mainly used for mapping DEM-derived products and additional interpretation purposes (Peter T, 2016). Weighting approaches combine maps of factors associated with landslide occurrence such as (slope, land use, geology, aspect, rainfall, etc.) and factor maps based on an estimate of their relative influences on the landslide. The weights are assigned based on professional engineering judgment then, susceptibility is derived for each mapping unit (Peter T, 2016).

3.3.2. Statistical approaches

Statistical (probabilistic) analysis models allow for quantitative correlates of geo-environmental factors that may influence slope stability with the occurrence of past and current landslides. Statistical approaches generally require the collection of large amounts of data. Statistical approaches can be used to map landslide susceptibility using the necessary input data. Further the statistical method can be classified into bivariate and multivariate. In bivariate statistical analysis each factor map, lithology, slope angle, and land use are combined with the landside distribution map, and weighing values based on densities are calculated for each factor class. Another approach in this bivariate analysis is the matrix approach, whereby the landslide susceptibility map is created by constructing and analysing cross tables between the different types of landslides with their conditioning factor. Multivariate allows one to

determine the relative contribution of each slope instability factor to the total susceptibility of a mapping unit.

3.3.3. Physical based model

The physical-based model also called relays on physical laws influencing slope stability analysis. The model is developed to investigate a particular type of landslide (Guzzetti, 2005). For rainfall-induced landslides, the required input data are soil cohesion, Internal friction angle, Soil depth, Soil unit weight, and groundwater depth. In the physical-based model, the susceptibility assessment is expressed by the factor of safety. The factor of safety can be calculated using a simple infinite slope model. Physical-based modelling can also be used for the numerical modelling of rockfall. Because of the association of pore water pressure with landslide triggers such as rainfall, a physically based model can be appropriate for evaluating and mapping landslide susceptibility (Peter T, 2016).

Prediction of landslide runout behaviour is a fundamental tool for risk assessment. Landslide runout behaviour is a set of qualitative and quantitative spatially distributed parameters that determine the destructive potential of a landslide. The parameters considered for the risk assessment from the physical-based model of landslide mainly include (Runout distance, damage corridor width, Velocity, Depth of moving mass, and Depth of deposits)

Physical-based modelling methods use terrain data, soil parameters (Soil cohesion, internal friction angle, bulk density, soil depth), and Hydrological parameters (saturated hydraulic conductivity, infiltration capacity). Physically based models consider the underground surface condition. Based on the simulated underground situations, the model can estimate the unstable slope and the potential failure surface by analysing slope stabilities.

There are two basic principles to analyse slope stability. The limit equilibrium model (LEM), and numerical model are finite element models (FEM). FEM split the model into a finite number of elements, then the force and strain for each element can be calculated using constitutive law. The limit equilibrium models predefine potential failure surfaces and investigate the equilibrium state. The equilibrium state is expressed by a ratio, FOS between the upslope stabilizing force R and the downslope destabilizing force T. For FOS > 1 Indicates stable condition, FOS = 1 indicates critical condition and, FOS < 1 indicates unstable condition Factor of Safety (FOS)

$$FOS = \frac{R}{T}$$

The instability occurs due to external factors. The result can be obtained by modelling different soil parameters with the possible triggering factors. The limit equilibrium model's assumptions are.

- Failure mass consists of rigid materials and slides along a single failure plane(Mergili et al., 2014)
- There is no progressive mass movement along the slip surface, failure occurs simultaneously, this means the Factor of safety result is uniform along the predefined slip surface.
- Deformation and strain of failure mass are neglected.

3.4. Description of open LISEM and method of analysis

Open LISEM is the abbreviation of the open-source Limburg Soil Erosion Model. It is a physically based soil erosion model (De Roo et al, 1996). A series of dynamic hydrologic processes including rainfall infiltration, surface flow, and interception are included in Open LISEM. Considering this infinite slope model was implemented into the model for obtaining an iterative slope failure and factor of safety result. (van den Bout, 2017).

The Main Components of LISEM models are (soil water balance, overland flow, channel flow, channel flooding, Erosion, sediment transport in all flows, and multiclass sediment). After a new hazard model component is added the model starts simulating slope failure and debris flows. This makes the model one of the few multi-hazard models that model debris flow, landslide, and flooding in one model. The main objective of the model is to improve the understanding, and analysis and to predict the behavior of land surface processes. (van den Bout, 2017). According to the modeler's objectives, the model is still under development for better development of an integrated, universal, and fundamental modelling tool for the numerical simulation of land surface processes.

Using the terrain, soil parameters physical and chemical properties of soil (soil cohesion, soil internal friction angle, bulk density), and hydrological parameters (infiltration, porosity, initial and residual soil moisture, hydraulic conductivity) the potential failure surface and failure depth can be estimated.

3.4.1. The main component of the LISEM model

3.4.1.1. Hydrology component

LISEM model provides dynamic rainfall input options. Rainfall is modelled from rainfall intensity, which can be spatially and temporally dependent. the spread amount of rainfall in the steeper area is less, the model corrects the width and length of each cell that receives rainfall and changes based on the slope of their local topography. Therefore, the surface area of the cells with steeper slopes enlarged.

Interception

In LISEM the interception of the rainfall accounted for vegetation and buildings. That means the water captured by the plant canopies and buildings before it reaches the soil surface. Evaporation is not modelled in LISEM because the event-based nature of the model allows for the assumption that slows the processes such as evaporation can be neglected (van den Bout, 2017)

$$IC = S\_max \left(1 - e^{-k\frac{Pcum}{Smax}}\right)$$

$$k = 1 - e^{-(co\ LAI)}$$

Where Ic is the total intercepted storage at a given time (mm), S_{max} is the maximum canopy storage, P_{cum} is the total precipitation in (mm), co is the canopy openness, and LAI is the leaf area index.

Infiltration

Infiltration is a process where water is transferred downwards from the surface to the subsurface. Several infiltration models are included in the LISEM model: For this project, the GreenAndAmpt equation is used for the infiltration model. This infiltration method assumes a wetting front moves downward into the soil layer parallel to the soil surface. Above this front, the soil is saturated, while beneath this front the soil is dry (Green&Ampt, 1911). The method assumes that the wetting front parallel to the surface is moving downward into the soil during infiltration. Following this, a simplified Darcy equation for vertical water flow can be used.

$$f = Ks \left(\frac{hf - ho}{zf}\right) = Ks \left(\frac{\psi}{zf} + 1\right)$$

Where: -

f =	The infiltration rate (ms^{-1})
hf=	The hydraulic head at the wetting front (m)
ho=	The hydraulic head at the soil surface
Zf=	The depth of the wetting front (m) = $zf = \frac{F}{\theta s - \theta i}$
F=	Cumulative infiltrated water (m),
$\theta s, \theta i =$	Porosity and initial soil moisture (m^3, m^{-3}
$\psi=$	The matric pressure at the wetting front (h=ψ+Z) m
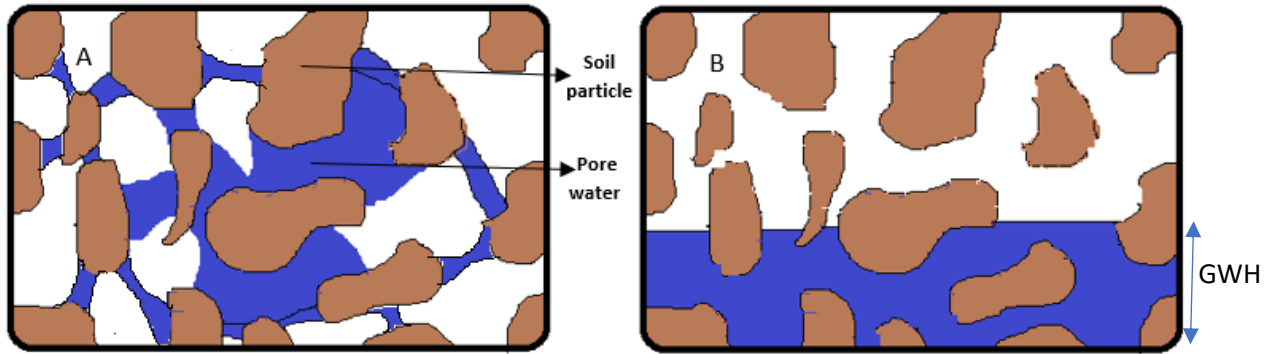
Figure 10. A Soil with initial moisture, B, assumed ground water table in LISEM (Chiyang, 2018)

3.4.1.2.　　Slope Process (Iterative Methods)

The conventional infinite slope model predefines the bottom of the soil layer as the potential slip surface. whereas the iterative method iteratively searches the potential slip surface. The factor of safety can be calculated using the equation to calculate FOS (Van Beek , 2002). The Slope process considers soil cohesion, soil depth, IFA, and soil density using elevation data. LISEM is a dynamic model which means the calculation is performed every time a step can be defined by the users.

$$FOS = \frac{c + \Delta c + [\{z - zw\} * Y + zw * Y']cos^2\Theta tan\o'}{[\{-zw\} * Y + zwYs]sin\Theta cos\Theta}$$

Where: -

c' and Δc (kpa)=	Effective soil cohesion and root cohesion
z=	Soil depth (m)
zw=	The depth of the "groundwater level"
Y, Y' and Ys(kN/m³) =	Soil unit, buoyant unit weight, and saturated unit weight
Θ (⁰) and ø (⁰) =	Slope angle and IFA

The iterative methods calculate the stability of each pixel over the entire DEM map using the FOS equation and the unstable pixels with FOS less than 1 will be picked out. For unstable pixels, the stabilizing force R is less than the destabilizing force T. Therefore, the iterative method calculates the failure depths and removes the unstable part then the pixel experienced a decrease in depth. Therefore, the rest of the pixel becomes greater than 1. This procedure repeatedly calculates all the unstable pixels. Due to the removal of failure depth for unstable pixels, the slope between the cantered unstable pixel and the surrounding pixel will be increased at the same time, this process leads to slope failure for the previous stable pixels.
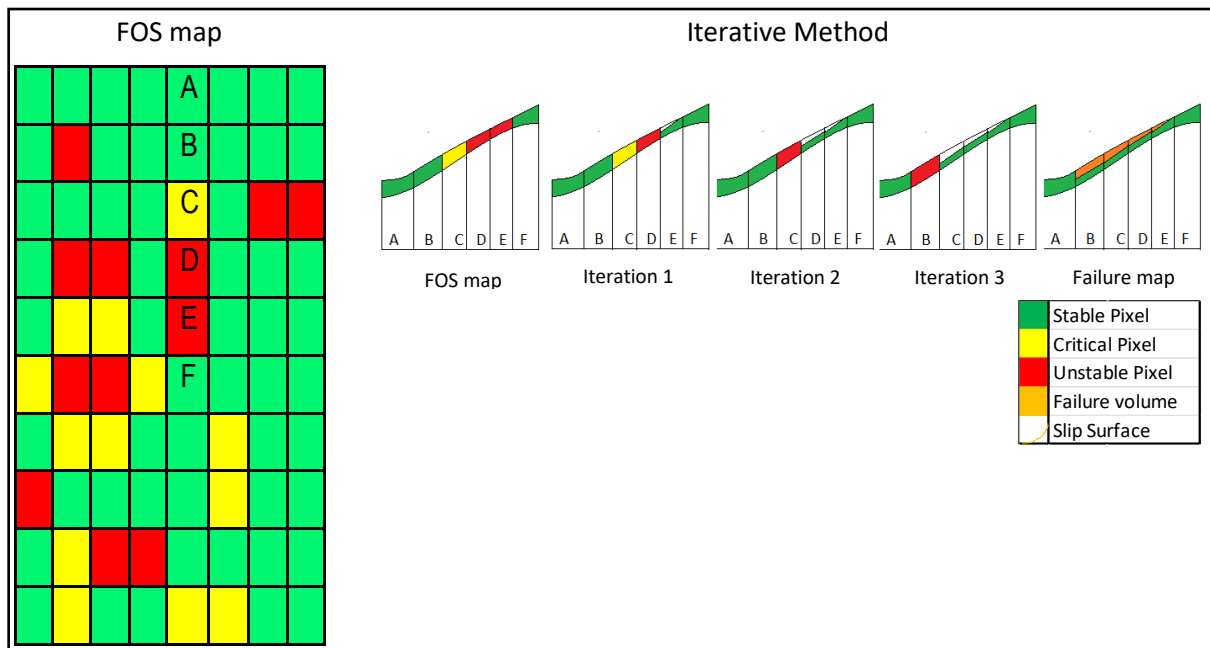
Figure 11. Iterative method to calculate potential landslide slip surface.

The FOS map Indicates the overall stability of all pixels, for group A-F, Slope failure starts from pixel E then failure is calculated using the FOS equation and the unstable part of the pixel is removed. Due to this, the slope between E and D is changed and pixel D becomes unstable. Based on the new slope the failure depth for pixel D is calculated and removed the unstable part. After pixel D become stable the stability of pixel C changed then the failure depth was removed. Finally, after all the pixels are calculated and removed the failure part of the slip surface can be formed.

3.5. Landslide risk mapping

Landslide risk refers to the expected damage or losses caused by landslides, including damage to property and infrastructures. Landslide risk mapping is quite difficult, especially because of the information needed for a precise estimate of hazard and vulnerability. Landslide risk maps are essential for land use and risk management regulations plans. Risk assessment involves hazard, exposure, and vulnerability assessment) (Peter T, 2016). The element at risk involves population, properties, and infrastructures., in the area that are potentially affected by the landslide.

Risk = Hazard X Exposure X Vulnerability.

Hazard is expressed in terms of the probability of occurrence, exposure expresses in terms of the element at risk based on their amount and value, and vulnerability (the element's degree of losses) is expressed on a scale. Landslide risk assessment and management comprises the estimation of the level of risk, deciding whether or not it is acceptable, and exercising appropriate control measures to reduce the risk. Risk assessment requires the following assets to be addressed probability of landslides, runout behaviour of landslide debris, Vulnerability of property, landslide risk to property and people, management

strategies, and decision-making. The probability of a landslide shall be assessed in detail while performing a risk assessment. The preparatory variable makes the slope susceptible to failures such as geology, slope gradient, aspect, elevation, soil geotechnical properties, vegetation cover, and long-term drainage patterns and weathering; and triggering factors that make the unstable slope marginally fails such as rainfall and earthquake. Therefore, the probability of a landslide depends on the preparatory and triggering effects.

3.6.   Case study on Landslide hazard assessment using LISEM.
3.6.1.   Mapping and modelling of landslides on St. Eustatius with LISEM

The objective of this study is to create a multi-hazard landslide map of the St. Eustatius area. The study analyses the historical occurrence of the landslide and estimates the hazard for different return periods. St.Eustatius is a small volcanic island located in the northern part of the Lesser Antilles in the Caribbean. The island consists of three geological units: the quill volcano, the northern hills, and a limestone formation in the south. The climate of the island is tropical. The average temperature varies between 22.3^0c and 25.0^0c (Lotte Ciska, 2018). LISEM was the only available model that met all the set requirements for this project. The storm-based approach of the model also makes it possible to model long-term precipitation effects. Assuming the input rainfall events during wet seasons, this could be solved by using a higher initial soil moisture content value (Lotte Ciska, 2018). To calculate the return period of the landslide and flood hazards on the island, the model was run with several scenarios. The scenarios were limited to a 10-year return period. A 50-year design storm was chosen to represent an extreme weather event. DEM was constructed from aerial photographs taken in 1991. Since the model needed a map of the leaf area index (LAI), vegetation cover, and vegetation height. Land-use data also consisted of vegetation-related maps (Lotte Ciska, 2018). For slope stability and debris simulation, the parameters related to soil density, apparent cohesion, soil internal friction angle, rock size, and soil depth were calibrated. Insitu and laboratory measurements were reported in the research paper. According to the field observation report, the occurrence of landslides seems to be focused on cliffs at the coast and around the main volcano. A sensitivity analysis was performed by changing the soil parameters. Cohesion, internal friction angle, soil depth, and initial soil moisture content were the most sensitive parameters (Lotte Ciska, 2018). Accordingly, a maximum slope failure depth value of 5.0 was obtained. Further, the study showed that soil depth and initial moisture content have the largest effect on the model results. The soil depth influences the amount of slope failure positively, an increase in soil depth leads to an increase in slope failure (Lotte Ciska, 2018). In addition, cohesion and IFA showed high sensitivity. It was concluded that an increase in cohesion leads to a decrease in the amount of slope failure and a delay in the timing of slope failure (Lotte Ciska, 2018). Four design storm data were used to observe the slope stability of the study area for different rainfall return periods. Accordingly, the 1-year design storm

did not result in any failures, however, the 5 -year, 10-year, and 50-year return periods showed a significant amount of slope failure (Lotte Ciska, 2018). This case study concluded cohesion, IFA, soil depth, and initial soil moisture content had the largest impact on the model results. It is also recommended additional field observation and sufficient landslide inventory data for the validation of the model (Lotte Ciska, 2018).

3.6.2. An integrated, modelling method for shallow landslides and debris flows catchment hydrology in Norther-Eastern Sicily, Italy.

The LISEM model was used to investigate the initial runout of the debris flows that were caused by a storm hitting the north-eastern part of Sicily, Italy in October 2009. The event had a maximum rainfall intensity of 120mm/hr and a return of 1 in 30 years (Bout, 2018). The event caused a landslide, debris flows, and flash flooding in the area between St. Stefano Briga and Fiumedinisi. Most of the required input parameters were estimated based on the digital elevation model (DEM), land use map, and soil texture map.   LAI and NDVI were calculated. A method that relates slope, profile curvature, distance from channels, and wetness index is used to calculate soil depth. For comparing the model, the full method was used, simulating slope failure locations timing and runout, together with catchment hydrology. And landslide inventories were used to provide a predefined failure volume. Accordingly, the depth of failure was varied to be between 50,70, and 90 percent of the soil depth (Bout, 2018). Soil parameters were calibrated such as (soil cohesion, IFA, infiltration rate, and initial moisture). The resulting slope failure patterns show a good match with the highest 20 percent of elevation for each landslide impact polygon. General landslide patterns and areas of high hazard are well estimated. The number of landslides predicted was 341 out of the 395 landslides, however, the modelled slope failures are over-estimated with 591 predicted landslide locations (Bout, 2018). The paper concluded that slope failure prediction is not accurate in both spatial and temporal locations. The lack of available data limits the prediction of slope failure. However, the model can be applied for the investigation into the physical processes that lead to and cause hazardous processes in a catchment is the first and primary usage (Bout, 2018).

3.6.3. Landslide early warning runout modelling case study in Norway.
The thesis investigates the potential of integrating rainfall-induced failure and runout physically based modelling to predict local landslide impact areas using forecast precipitation. The event simulated is a rainfall-induced landslide that occurred on August 16 /2011, in kjellberget. The LISEM model was chosen because it allows the construction of a multi-process model capable of simulating slope stability to obtain failure depth (Fernanda, 2022). The calibration was based on slope stability and the calibrated parameters were soil depth, cohesion, and IFA. Accordingly, the result gives information about the

variation of the Factor of safety (FS), Failure Depth (FD). Data related to Terrain, ground truth, and Rainfall were collected. Soil depth, cohesion, and internal friction angle (IFA) were selected for the calibration because these parameters influence the FS (Fernanda, 2022). The soil depth model was built using the Steady State Soil. The model is based on the dynamics of erosion and deposition governed by elevation and slope. erosion is active in a shallow soil depth. The soil depth model was calibrated with drilling depth measurements found in a geotechnical report (NADAG) database at ngu.no (Fernanda, 2022). The calibration process consisted of varying the soil depth model by iterating two parameters within the Steady State Soil tool. Soil production from rock weathering and speed of soil movement. Soil hydraulic properties were determined by (Saxton & Rawls,2006). The study area was classified into three zones (1) a steep slope, (2), a quaternary deposit, and (3) the Stjordalselva river valley. Laboratory test results from the Klima Digital project were collected. Direct shear laboratory tests were performed to obtain cohesion and IFA values of the Quaternary deposit and the moraine. Following that, a cohesion map was created with two zones. However, the IFA value reported on Klima Digital (Depina et al,2021) was applied to the entire area (Fernanda, 2022). Precipitation recorded was rainfall and snowmelt, rainfall that triggered the landslide in the study area presented. Landslide on August 16, 2011, a landslide on March 22, 2012, and a landslide on November 23, 2021. Slope stability (IS) was implemented for slope stability assessment. Range of values related to soil depth, cohesion, and IFA iterated during calibration. A confusion matrix was created considering the predicted and observed landslides. True positive where FD > 0 in the observed landslide on August 16, 2011, and False positive (FP) where FD > 0 in the outside observed landslide area. The result showed that the heavier soils with less cohesion and lower IFA exhibited failures more frequently (Fernanda, 2022). Runout model results were reported using the observed precipitation. Accordingly, an hs_max (maximum solid hight) value of 1.38m was obtained for the combination of soil parameters, Maximum soil depth = 5.88m, cohesion =3450 [pa], and IFA = 0.577 [rad]. Further, it was decided to observe the runout with increased soil depth and reduced IFA. Thus, the hs_max value of 2.22m was obtained (Fernanda, 2022). It was concluded that soil depth, cohesion, and IFA, were selected because these directly influence the magnitude of FS and therefore, the occurrence of failures. In addition, it was reported that the failure frequency changed linearly with the changed soil parameters (Fernanda, 2022).

3.7.   Rainfall-induced landslide assessment in Norway

Many different methods have been used to produce landslide susceptibility maps for rainfall-induced landside in Norway. The choice depends on the purpose of the work, the extension of the area, the work scale, and the data available. The methods are classified as qualitative (inventory-based and knowledge-driven method) and quantitative (data-driven methods and physically based models) (NVE, Norwegian

Water Resources and Energy Directorate, 1921). The Norwegian landslide forecasting and warning service use rainfall thresholds to forecast the temporal occurrence of a landslide triggered by rainfall and snowmelt. (Krøgli et al., 2018)

Rainfall thresholds relate landslide initiation with the main triggering factor of rainfall. They are used for temporal forecasting and for warning purposes by the national and regional forecasting services to predict the temporal resolution. However, they do not provide detailed information about where the landside might take place (NVE, Velkommen til skredregistrering, 1921). In Norway, the necessity to combine the spatial landslide probabilities and landside thresholds was evident already in 2012. The project carried out in 2011-2012 by NVE and NGI to improve landslide thresholds in Norway suggested that the landslide dataset used in the thresholds analysis will benefits from additional features for their characterization qualitatively. Landslide susceptibility, magnitude (volume or area), and intensity (depth and velocity).

In the report by (Graziella Devoli (NVE), 2019) it is shown that the national susceptibility map for landslides at the catchment level is being used to improve the forecasting of rainfall-induced landslides. The first susceptibility model was tested in the region of western Norway (Cepda, 2012). Following this, the susceptibility analysis was performed separately for five regions eastern Norway (Østlandet), western Norway (Vestlandet), Southern Norway (Agder), Central Norway (Trøndelag), and Northern Norway (Nord Norge). To develop the landslide susceptibility map of Norway, catchment units, historical landslide events, the quaternary map, land cover, average annual rainfall, and various water runoff available data were collected and analysed.

Historical landslide events were obtained from the national database for all types of landslide movements www.skredregistrering.no;www.skrednett.no more than 60,000 events recorded from the last 500 years that covering the whole country. The most common types are rockfalls, slides, snow avalanches, and debris flow followed by soil slides. According to the reports the landslide occurrence is placed at the location where the landslide hit the road or railway, and this introduces large inaccuracies when landslide susceptibility models are developed and calibrated. The landslide susceptibility was modelled at the regional unit (catchment) level because this scale is sufficient for the regional nature of the landslide early warning system. The Norwegian landslide forecasting and warning service operating at NVEs use rainfall and soil saturation thresholds to forecast the temporal occurrence of landslides triggered by rainfall and snowmelt. The threshold map predicts where and when the landslide thresholds will be exceeded (Graziella Devoli (NVE), 2019). The produced map does not show the presence of a steep slope or the availability of loose or quaternary deposits. To resolve this issue, they have combined the national susceptibility in the soil at the catchment level with thresholds using a pixel-based approach. Therefore,

the landslide susceptibility map was converted into a 1km x 1km grid Subsequently, the raster of the Hydmet map and susceptibility map are combined. Matrix approaches have been used for landslide susceptibility hazard and risk assessment in various applications. The national susceptibility map for landslides in the soil at the catchment level and the national susceptibility map for debris avalanches and small debris flows have been prepared for different purposes and several types of landslides using different methods and work scales. The national susceptibility map for landslides at the catchment level was prepared in the last five years as part of a collaborative effort between NVE, and NGI to improve the landslide early warning system at NVE. The map shows the susceptibility level of 1st order catchment to landslides. (Graziella Devoli (NVE), 2019). The paper recommended that the matrix approach is very useful for the combination of spatial and temporal landslide properties. However, the method is extremely sensitive to the classification of the input data.

3.7.1. Susceptibility assessment of rainfall-induced landslides case study: Hegra-Meråker

The study presents the methodology to assess the susceptibility of rainfall-induced landslides using TRIGRS. Several data gathering and assumptions on the study area were made for the assessment. The assessment of rainfall-induced landslide hazard was applied in four stages definition of the study area, Selection, and evaluation of input data, calibration of model parameters, and susceptibility assessment of rainfall-induced landslides. Landslide inventory data were collected from NVE (Norges vassdrags- og energidirektorat, 2019),
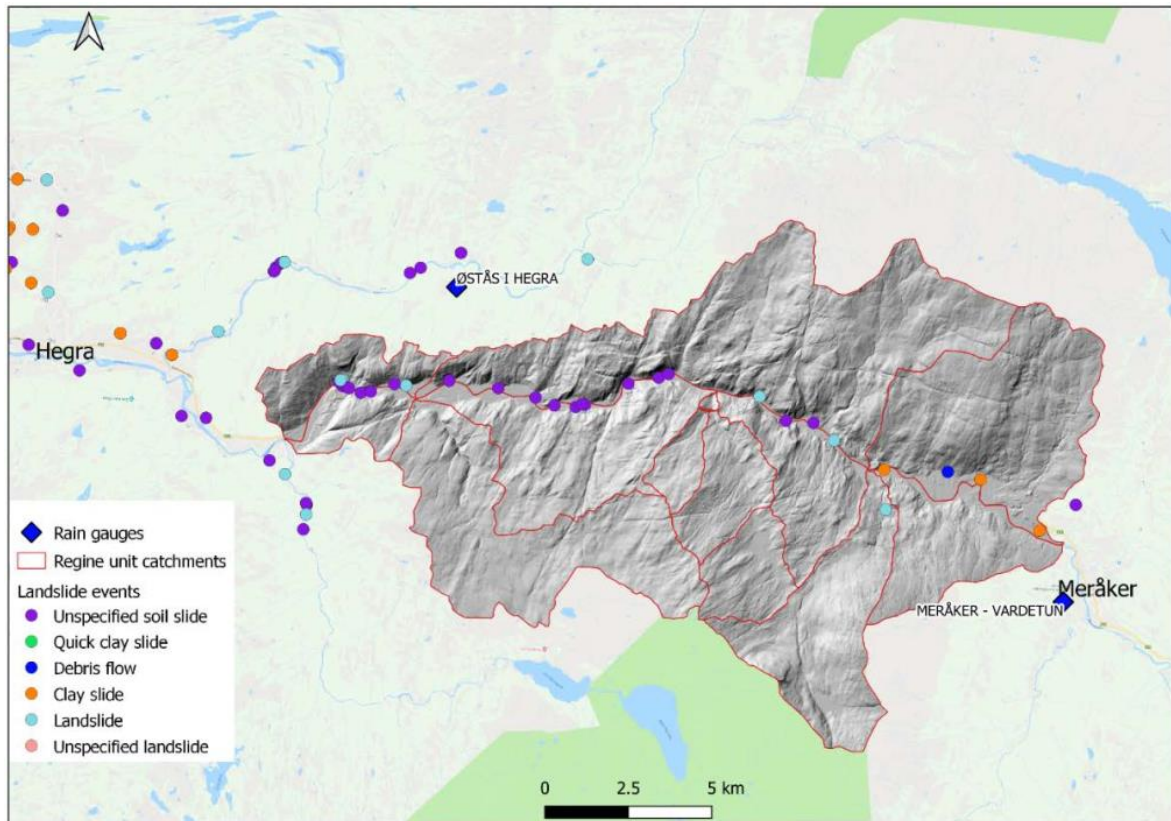
Figure 12. Landslide inventory (NVE, Norges vassdrags- og energidirektorat, 2019)

The geotechnical properties of the study area were selected according to the literature values (Melchiorre & Frattini, 2010).

Table 2. Geotechnical property of study area

Soil type	Cohesion (Pa)	IFA (^{0})	Saturated Permeability, ks (M/S)	Soil Unit weight (KN/m^3)
Organic	20000	0	1.10^{-6}	15
Rock	100000	44	1.10^{-6}	25
Sedimentary	Calibration			19

The thickness of the soil is modelled through a correlation with the slope angle. (Godoy Leiva, 2019). The model which relates the slope with the bedrock was found to be fitted to the available data. Several historic rainfall-induced landslides were reported from NVE. Among the 22 recorded data from (1964 – 2016), 16 data were found to be unspecified landslides in the study area. Geotechnical properties of sedimentary soil types were presented with the value of cohesion = 5 (Kpa), internal friction angle = 0.3 (rad), soil density = 1900(kg/m3), saturated permeability, Ks = 1.10^{-4}.

Slope stability assessments were done by considering the FOS value. Calibration of sedimentary properties was done to calculate FOS that best fit the inventory data. Slope stability conditions were checked before the rainfall (primary condition) and after the rainfall. The result showed Instability of the slope increased after the rainfall (Godoy Leiva, 2019). The average probability of failure on a slope steeper than 20 degrees on the sedimentary zone was found to be 5.8% and 6.9%, for 5-year and 1000-year return periods, respectively. The report indicated that the area between Hegra and Meråker is highly susceptible to rainfall-induced landslides. A constant relationship between the water table and the depth of the bedrock was assumed. The model is sensitive to the initial water table accordingly, the height of the water table is considered to follow a beta distribution whose mean is close to the saturated case which is more critical for the stability of the slopes (Godoy Leiva, 2019).

4. Methodology

The assessment methods depend on the objectives of the project, topography coverage, the physical environment, the land sliding process, and the availability of input data to the possible methods. For this project, the assessment methodology mainly focused on data gathering, processing available data, slope stability assessment, calibration of the parameters, and sensitivity analysis of the input parameters. Considering the objective and the available data the statistical approach is better suited for this case study because the model enables quantitatively relating geo-environmental factors that may cause slope failure considering past and current landslide data.

The landslide runout model for risk assessment is modelled using the physical-based model that relies on physical law influencing slope instability. Rainfall-induced landslide susceptibility assessment requires input data, which are (cohesion, IFA, soil depth, density, and groundwater depth). (Bobrowsky, 2009). In the physical-based model, the landslide susceptibility is expressed by the FOS. The safety factor can be calculated using the infinite slope stability model.

4.1. Data gathering

4.1.1. Study main input parameters for the physical base model

4.1.1.1. Soil hydraulic properties

Saturated hydraulic conductivity depends on the size of soil particles, porosity, and soil moisture whereas water potential varies with the water content. Laboratory tests and field measurements should be well known to determine the soil's hydraulic properties. Otherwise, a literature value can be used for the well-known type of soil. If parameters like soil porosity and saturated hydraulic conductivity, are not known from the laboratory an empirical model named soil water characteristic can be used (Saxton & J. Rawls, 2006). To study the soil hydraulic property of the project site, laboratory test results reported by NTNU and SINTEF were used (Depina & Emir, 2022).
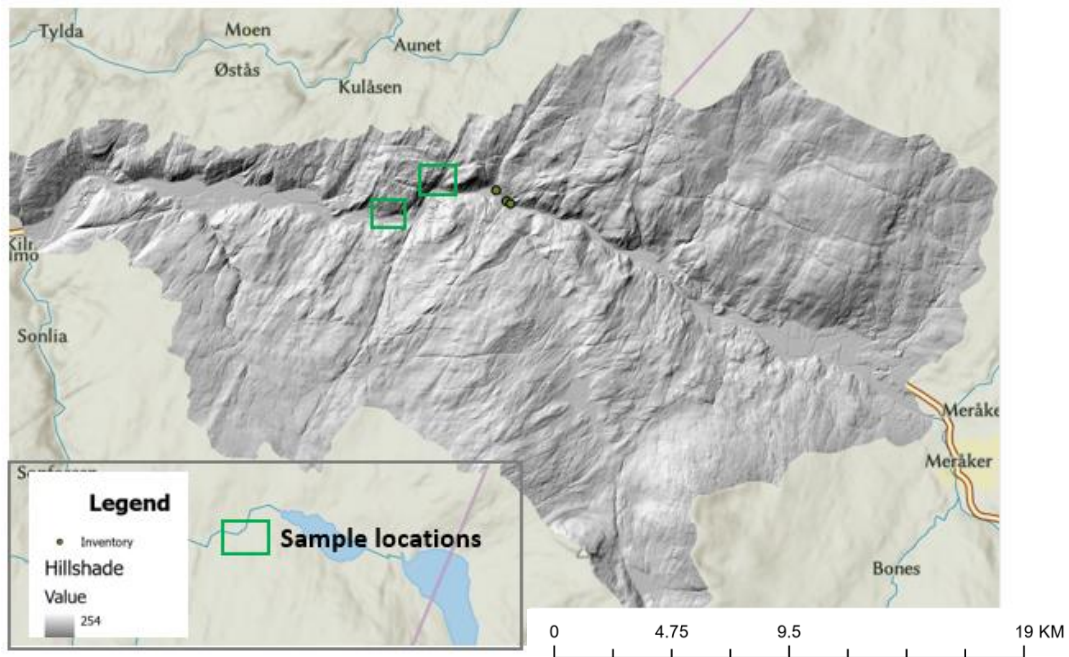
Figure 13. Recent laboratory sample location

A laboratory test including methods for water content and organic content determination, sieve analysis, and hydrometer test for soil classification has been performed. According to the laboratory result at location 1, the wet-in-situ density resulted in around 18 kg/m^3 at 0.9 m depth of soil. The top 20 -30 cm has much higher organic content than deeper depths at both locations.

4.1.1.2.   Geotechnical parameters

The geotechnical property of the soil is studied based on the laboratory and field measurement results. Geotechnics describes the physical and chemical properties of soil from an engineering perspective. Soil investigation mostly includes geotechnical drilling and laboratory sampling. For this project laboratory, sample results and field measurements were studied in the study area. In 2013 the geological survey of Norway launched a national database for soil investigation which is known as NAGAD, where the public and private sector share data from their projects. For the LISEM physical base model assessment of landslide prior information about soil parameters such as (soil depth, soil cohesion, IFA, soil density, and particle size distribution of sand, gravel, and clay content are needed).

From (NAGAD, 2016) geotechnics reports of the soil in different locations of the study area were found. Grain size distribution curves for fluvial and moraine deposits from the laboratory report were used as reference values.
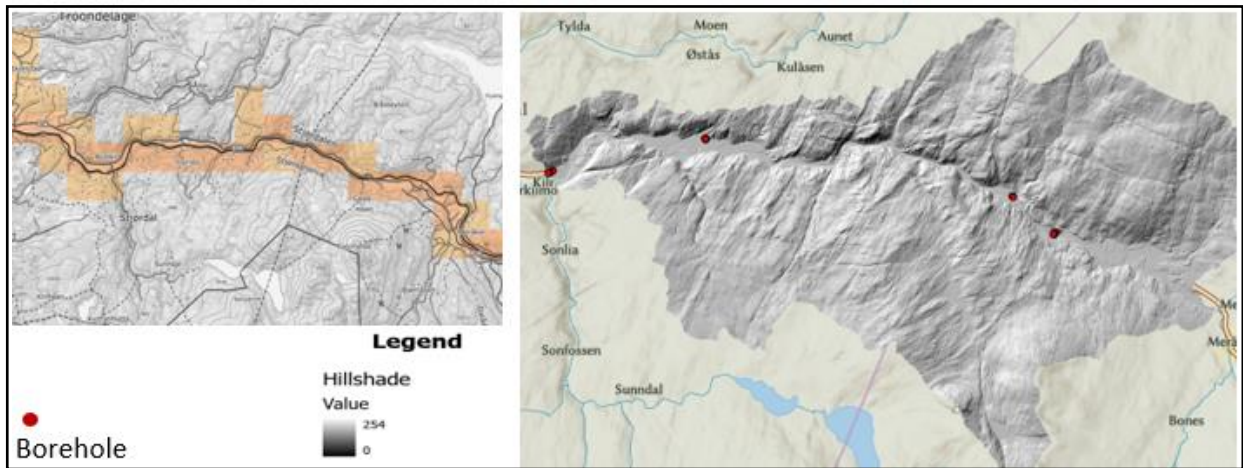
Figure 14.NADAG sampling data and borehole location in the study area
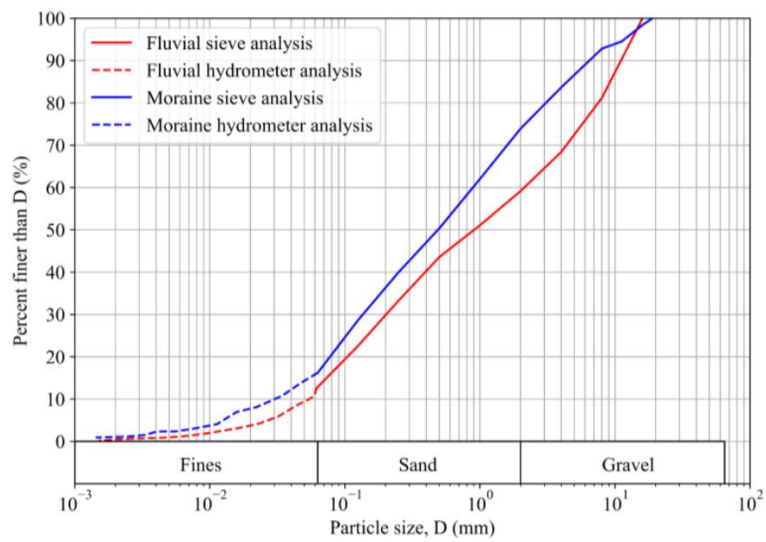
Figure 15. Grainsize distribution of moraine and fluvial deposits. (Depina & Emir, 2022)

4.2. Processing available data

LISEM needs rainfall data, land-use data, Geotechnical data, hydrological data, Infiltration parameters, and topographic data as input.

4.2.1. Morphology data

The digital elevation model (DEM) was taken from ((Kartverket), 2021). The DTM was constructed from aerial photographs. The DEM has an x and y resolution of 5 m.
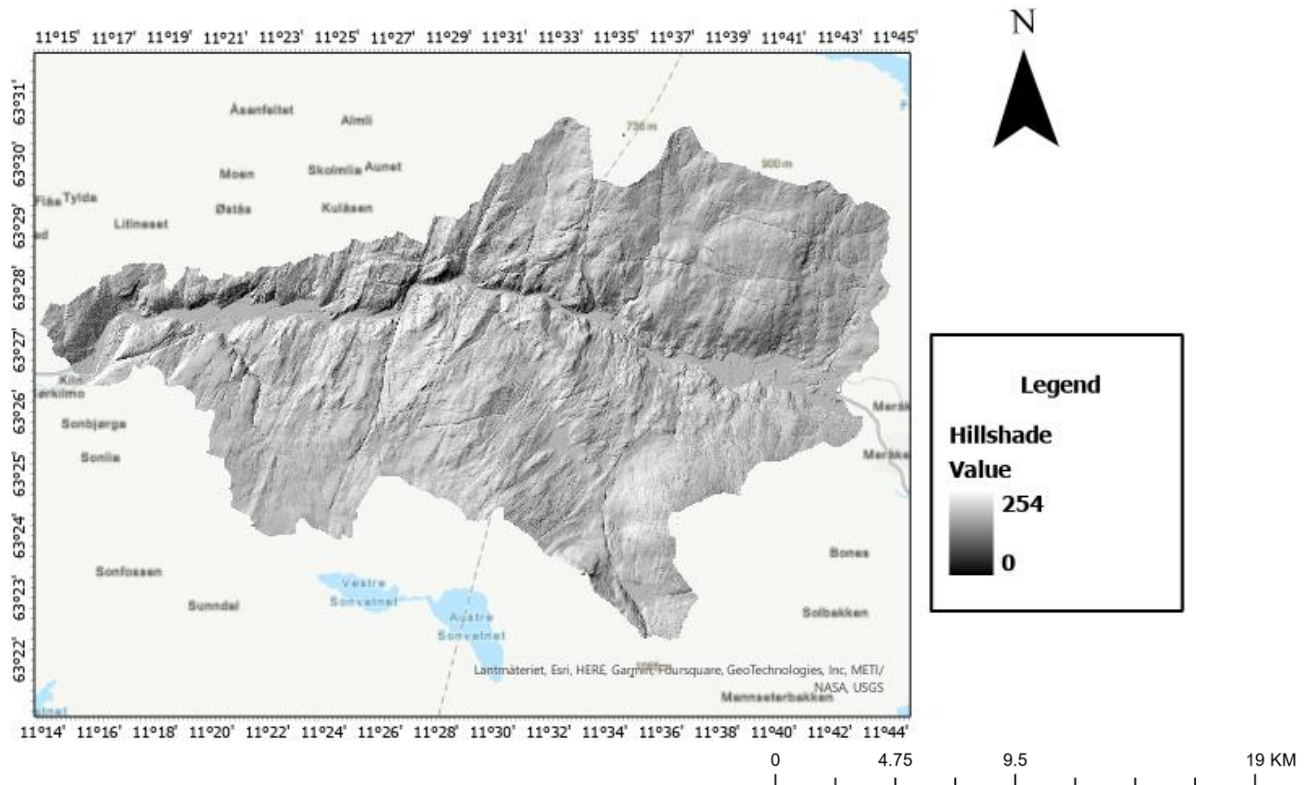
Figure 16: Hillshade of the DTM

The DEM map was used to produce several maps that were needed as input for the model: a slope map, aspect map, local drainage direction map (LDD), and catchment characteristics. This map gives detailed information about the topography of the study area. ArcGIS (ArcGIS Pro) environment is used for mapping topographic information data.

Figure 17. Aspect map of the study area

Figure 18. Slope map of the study area

4.2.2. Catchment characteristics and land use and surface data of the study area

The LDD gives for each cell the direction in which a substance would drain to another cell.
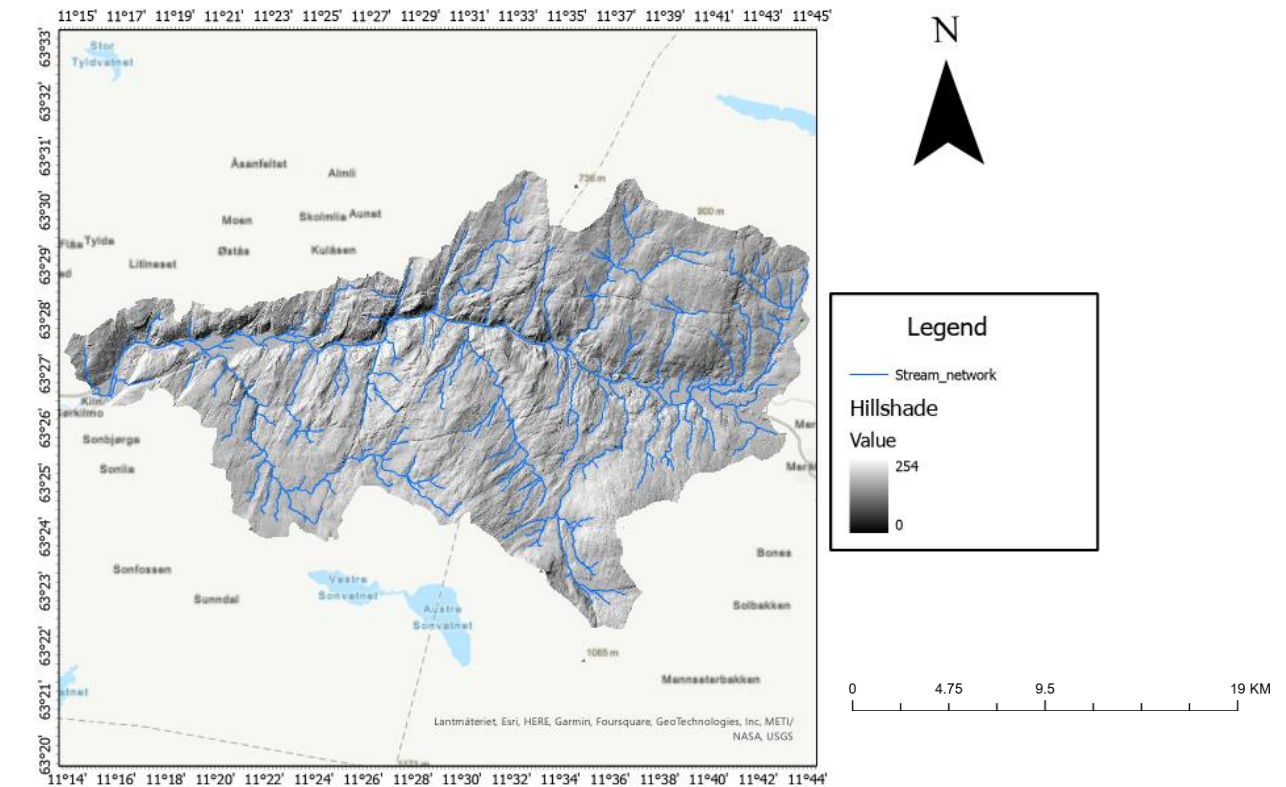
Figure 19. stream order map
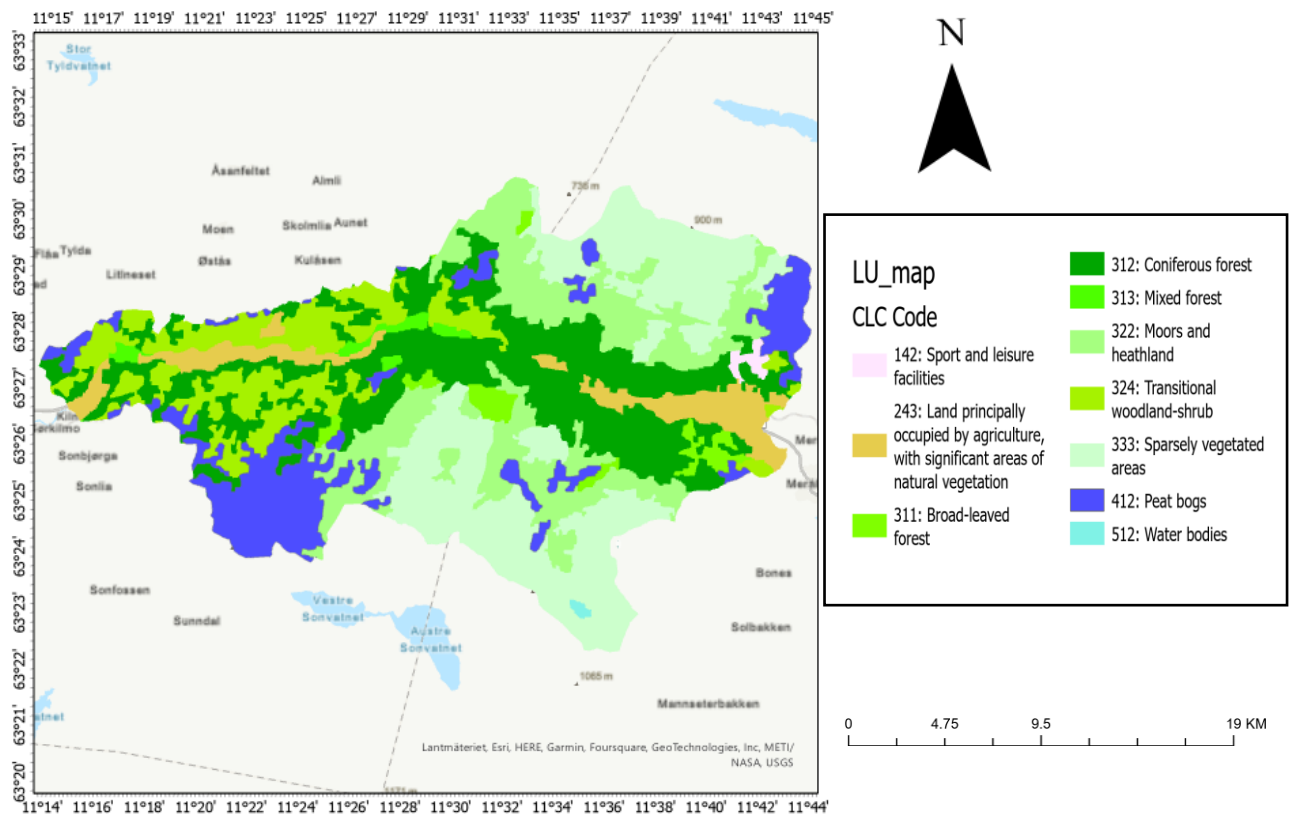
Figure 20. landcover map

The land cover data was obtained from the Copernicus land monitoring system ((CLC), 2018). From the land cover data, the surface property can be defined. Such as (Manning's n, LAI, Vegetation height, Vegetation cover, SMax_Surface, and SMax_Canopy) can be obtained. The LAI was calculated from the enhanced vegetation index (EVI), and the EVI was chosen over the normalized vegetation index (NDVI), Building map, road map, and railway map used to investigate elements at risk in the study area.
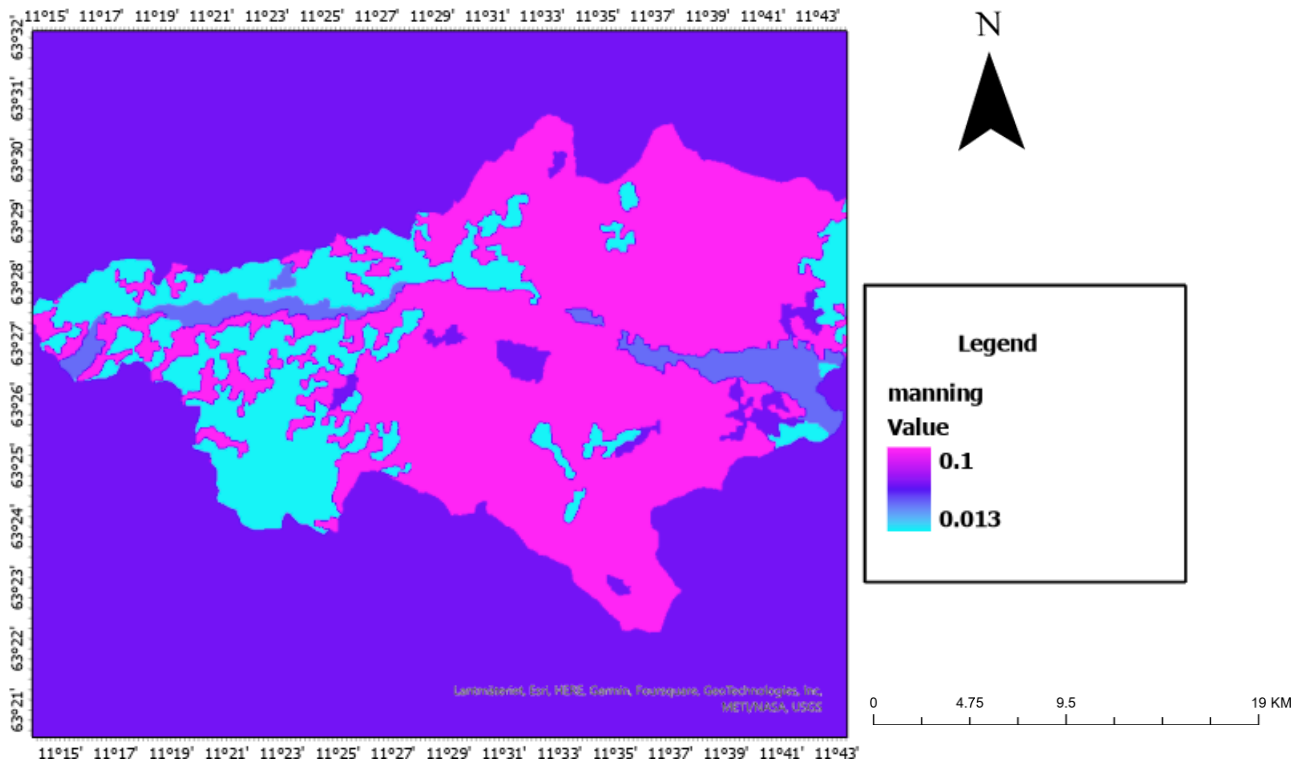
Figure 21. Manning Map
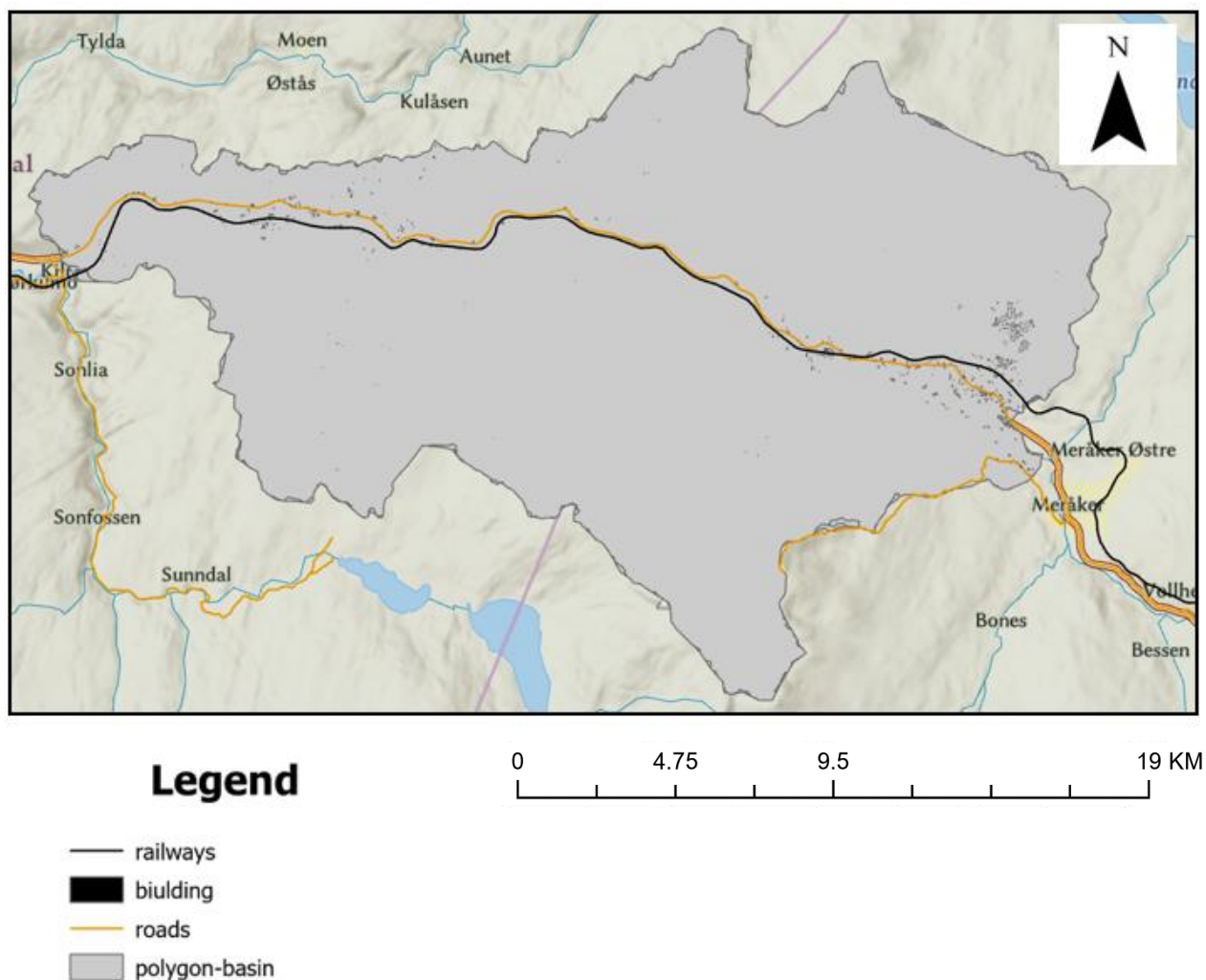
Figure 22. Building a map of the study area

4.2.3. Precipitation data

Precipitation data for the four previous landslide events are presented below. To investigate the rainfall scenario before, after, and during the occurrence of a landslide, daily precipitation data were collected from http://skima.met.no/observations/ (Norwegian Center for climate , 2022). This data is collected to have prior information about the maximum amount of rainfall that triggered the landslide in the study area.

 ➢ **Landslide on August 16, 2011**

The landslide was documented at 8:00 am. The maximum amount of precipitation recorded in that area was 69 mm. The rainfall value before the event was constant. However, some peak values were obtained before the event and after the event. The landslide was triggered due to the rainfall event and the high amount of soil saturation.
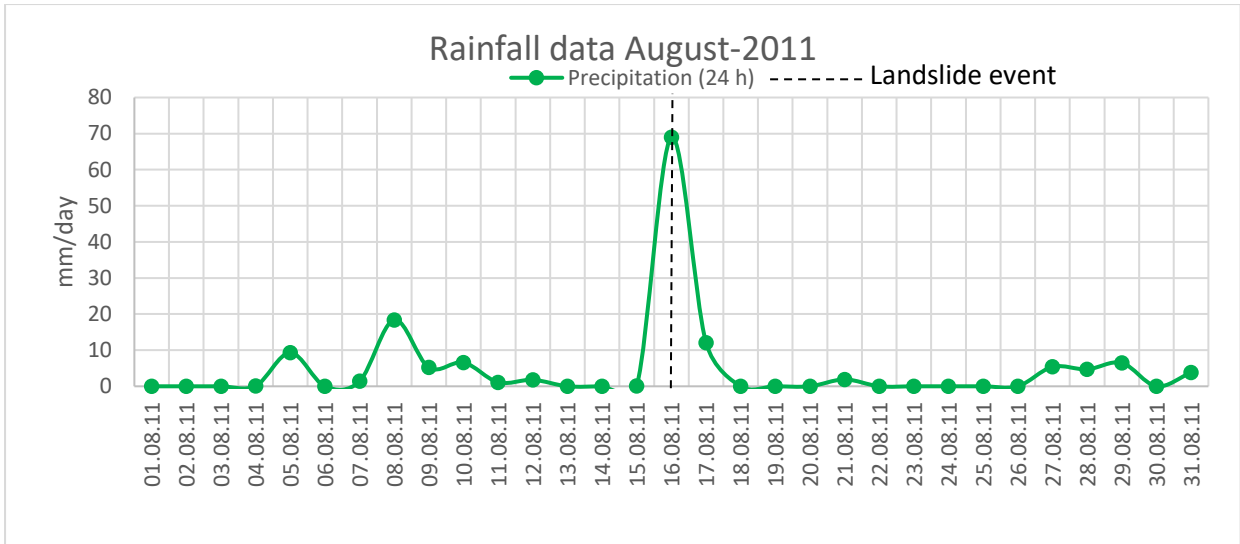
Figure 23. Rainfall event August-2011

> **Landslide on March 22, 2012:**

In this case, the precipitation was high on the first day of the month. Then, it gradually decreases until March 4. After March 4 the result shows there is a constant perception amount for the constitutive 4 days. On March 13 the rainfall suddenly reaches a peak amount of 38 mm. The next day again suddenly drops to the value of 1.6 mm. The landslide occurred on March 22 at 1 pm, and the amount of rainfall was 11.6 mm. The amount of rainfall was less compared with the other days. However, the possible reason could be the amount of soil saturation was already high.
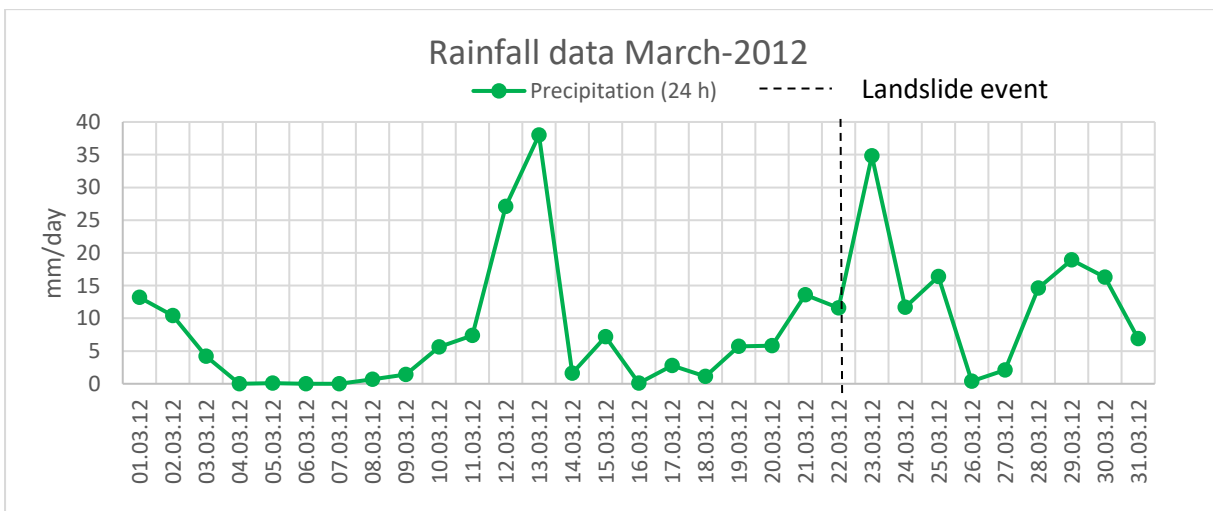
Figure 24. Rainfall event March-2012

➢ Landslide on November 23, 2021

In November there is only small amount of rain comparatively. This is because the temperature in this season is very low in Norway which causes the water to freeze. The rainfall amount was very low until November 19, 2021. Later there was a significant change in the rainfall amount. The rainfall-triggered landslide occurred on November 23 this is also because of the high amount of soil saturation.
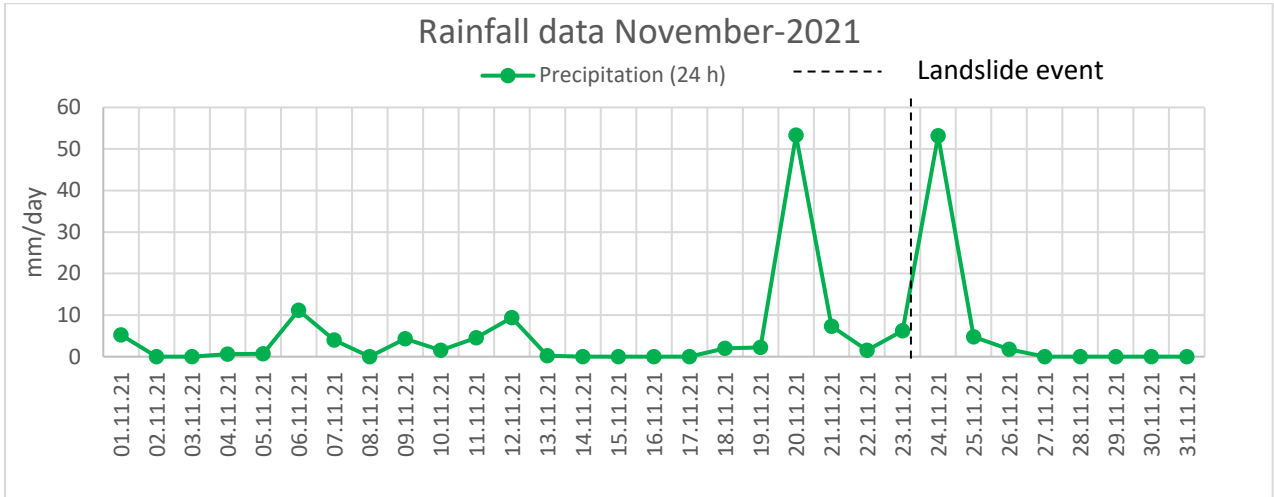
Figure 25. Rainfall event November-2021

➢ Landslide on January 13, 2022

The rainfall registered on January 13 was very high. The landslide occurred at 1:40 pm. The peak rainfall occurred suddenly. Before January 13 the rainfall amount was almost uniform throughout the day. After the event, most of the perception amount was in the range of 10-14 mm.
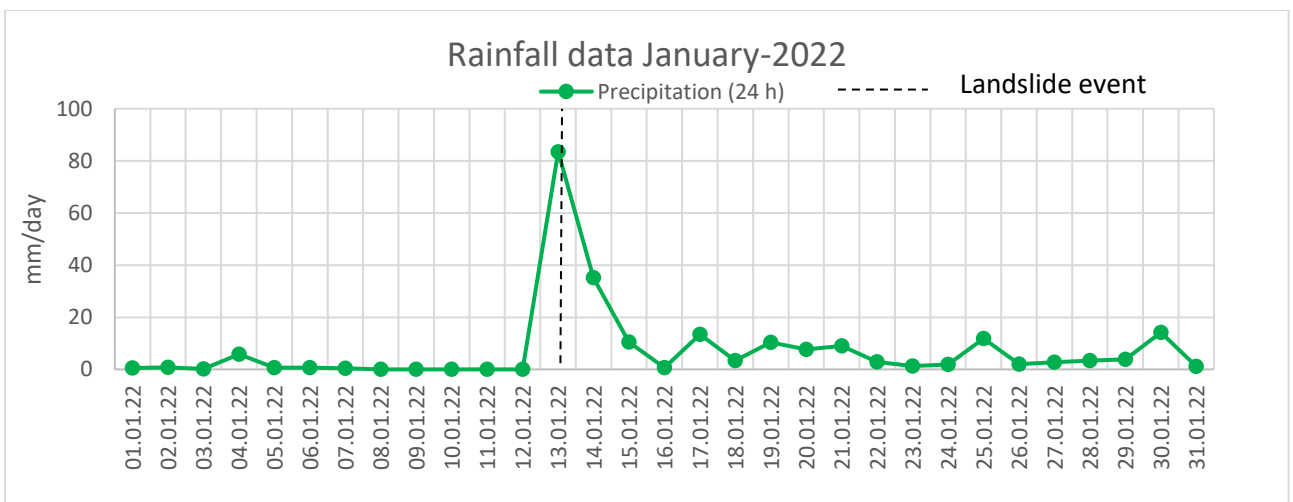
Figure 26. Rainfall event January -2022

30 years of rainfall precipitation data were used to calculate different return periods in the study area. The precipitation data were collected from (Norwegian Center for climate , 2022) and the maximum 24hr rainfall was extracted from the available data. This data is collected to perform sensitivity analysis for a different return period of rainfall data on slope failure assessment. LISEM needs precipitation in mm/hr and time in minutes.
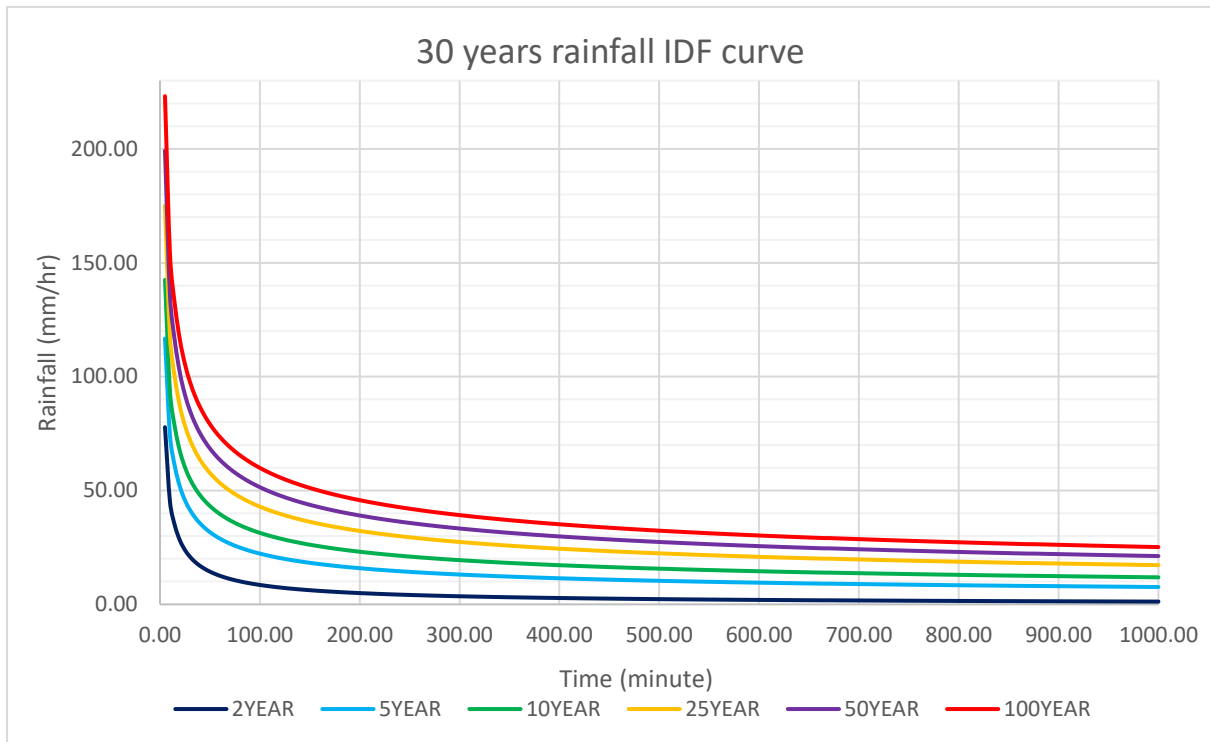
Figure 27. Rainfall IDF curve

4.2.4. Geotechnical and hydrological parameters

The geotechnical and hydrological parameters were obtained from literature values, laboratory tests, and field measurements. An empirical model is developed by (Saxton & J. Rawls, 2006) and used to develop statical relationships between soil water characteristics, soil texture, and Organic matter (OM).

Several soil hydrological parameters are required when simulating hydrology. The infiltration and groundwater flow require Soil depth (m), Hydraulic saturated conductivity (m/time), porosity (-), and initial moisture content (-). All these values are determined from measurements. Besides measurements, there are other ways to approximate these values. The soil texture can also be obtained from national/regional soil classification maps or the SOILGRIDS statistical model https://soilgrids.org/.

4.2.4.1. Slope Stability and debris flow data

For slope stability, the model needed the following parameters as input: Soil density, apparent soil cohesion, soil internal friction angle, rock size, and soil depth. For the first simulation of slope stability in

the study area, constant values of soil parameters from laboratory results were used. which are (sand, silt, gravel proportion, bulk soil density, soil cohesion, and IFA).

To determine slope failure of the surface it is usually very important to have reasonable soil depth data. According to many different authors' findings, it's troublesome o find accurate soil depth data neither from field measurement nor from modelling. Even though, field measurement always depends on accurate results. It is very labour and cost-intensive to perform a borehole measurement in several locations. Therefore, some kind of interpolation or modelling is required. For this project, borehole data recorded in different locations of the areas were collected. Some studies in the literature proposed that soil depth data can be obtained by using different topography, slope, and land cover or geology and interpolating the soil depth value collected from the site (T.K. & David G., 2009). However, this requires a high level of data accuracy. As shown in figure (28), the average borehole measurement data is in the range of 10-20 m. Therefore, it was necessary to visualize the interpolated actual measured values of borehole data in the ArcGIS environment. This helps to make a clear visualization of interpolated results and to compare If the results are acceptable for slope stability assessments. Typically soil depth is a product of all previous instabilities in the landscape. Therefore, as soon as soil reaches too high of a depth, starts to become unstable during an extreme rainfall event and starts to fill some steeper slopes, and all the accumulation of those failures and erosion processes typically accumulate in the deeper soils. The interpolation result from borehole data does not give reasonable soil depth data for slope stability assessment, because it does not reflect the topography or geomorphology of the area. Therefore, to run a sufficient soil depth model the dependency of the model on the slope, topography, geomorphology, and some soil properties is important.

BH-no	Average Borehole data(m)
1	21.46
2	8.10
3	26.00
4	22.50
5	20.17
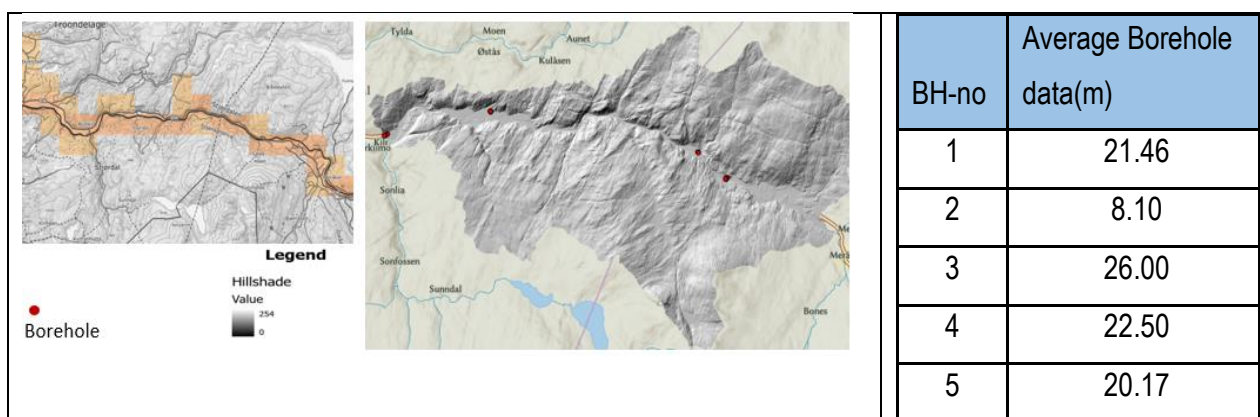
Figure 28. Borehole data location and average depth result.

The soil depth map was determined from DEM. Several research studies were applied to calculate soil depth from the DEM map. On the LISEM model, the **SteadyStateSoil** model was adopted. This model comes from a paper (Von Ruette & Lehmann, 2013). The model assumes steady-state conditions

between soil production rate and erosive processes. According to the author's statement, Soil depth is solved through a routing algorithm starting with the soil column with the highest elevation denoted as z and progressively going downslope.
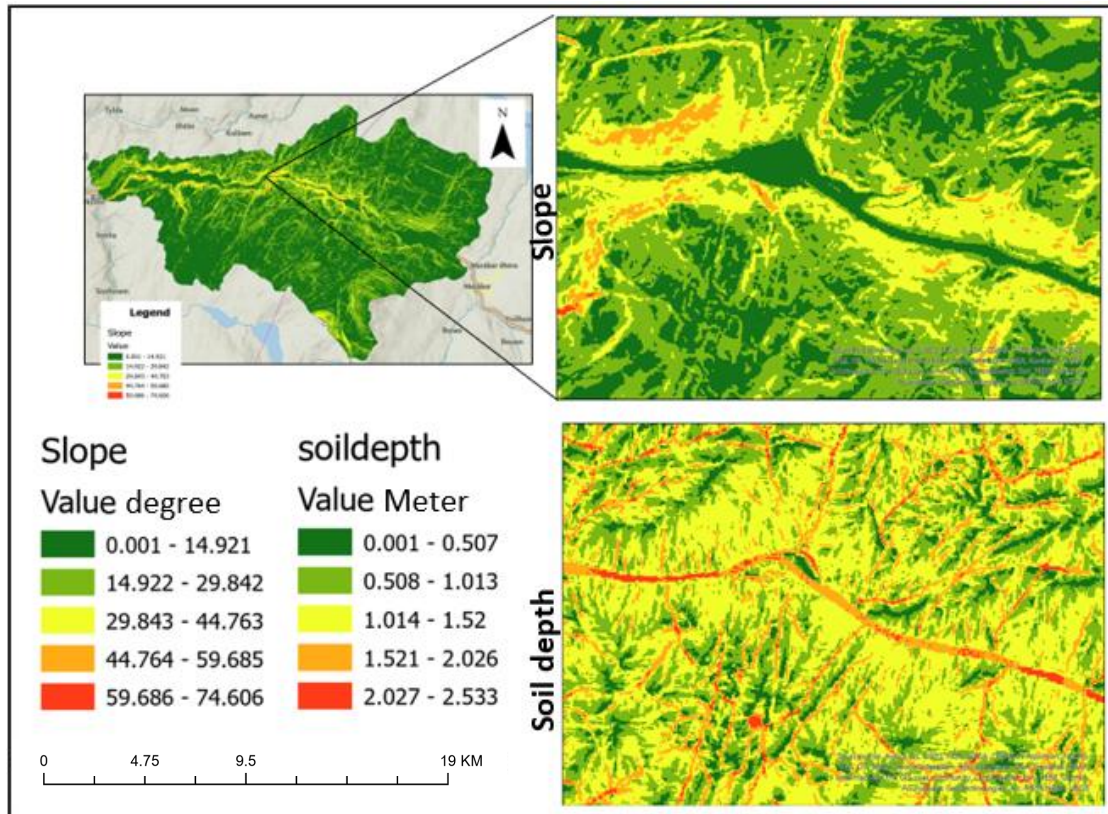
Figure 29. Soil depth map

4.2.4.2. Physical and chemical properties of soil parameters used in the model.

Generally, soil characteristics have a significant influence on landslide occurrence. For this study, soil properties such as grain-size distribution, soil cohesion, Internal friction angle (IFA), soil density, hydraulic conductivity of soil, soil organic content, and surface manning coefficient values were presented. The values were taken from laboratory test results reported by (Depina & Oguz, 2021) .

4.2.5. Input for LISEM

The Input data of LISEM for landslide simulation is described as follows.
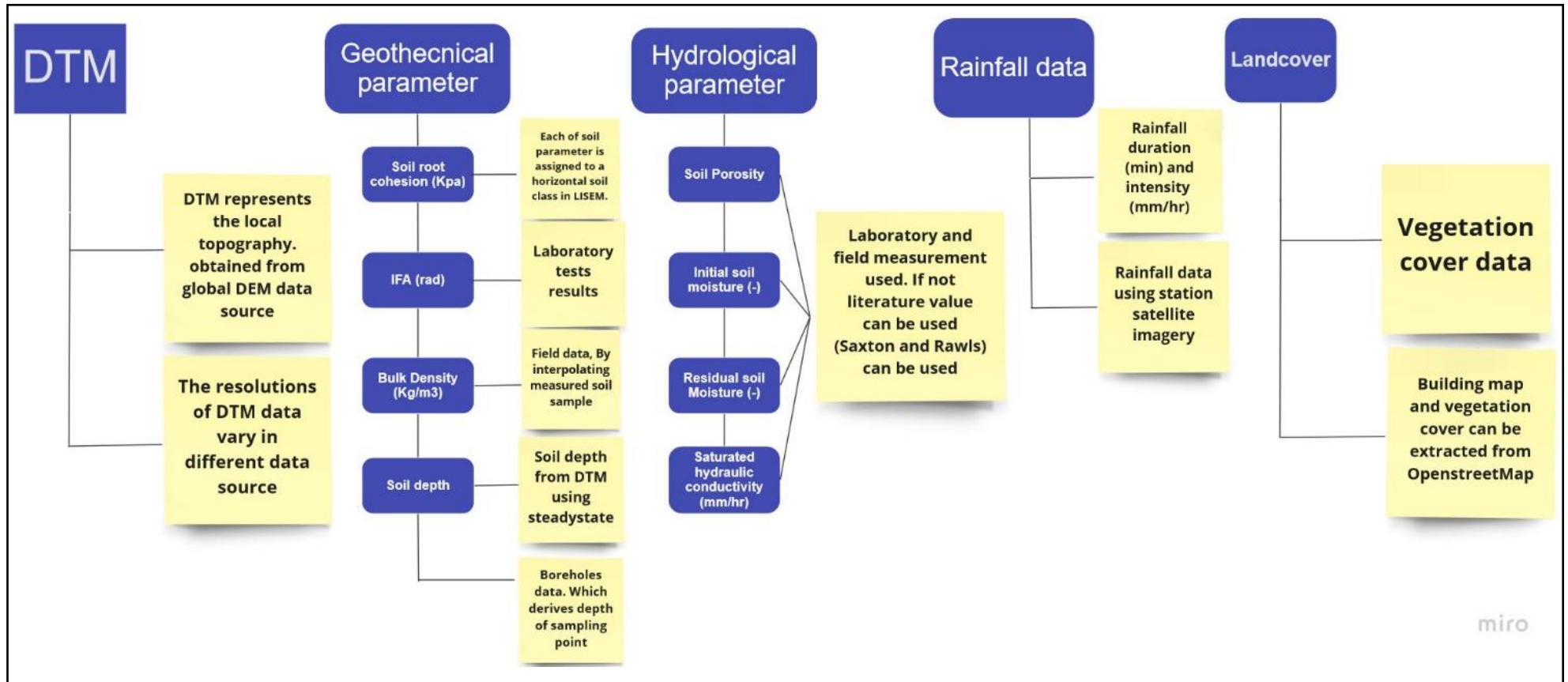
Figure 30. Input for LISEM can be classified into two five main parts as shown in the chart above. The geotechnical and hydrological parameters can be used from laboratory and field reports. Otherwise, an empirical model can be adopted. Rainfall data in LISEM is the duration (minutes) and intensity (mm/hr).

4.2.6. Model assumptions and Suitability.

LISEM model assumptions for landslide volume simulation can be summarised as follows.

➢ Assumptions related to the infiltration process.
➢ Assumptions related to slope stability analysis.
➢ Assumptions related to triggering mechanisms.

Several assumptions and input parameters are needed in the model. During the rainfall process, evaporation is not included. Moreover, since the model is storm-based, evaporation is neglected. In the infiltration process, the GreenAndAmpt model is a simplistic infiltration model which considers a vertical infiltration, and it disregards a horizontal subsurface flow. This is because of the limitation of the available data and for the storm-based approach, it is impossible to model long-term precipitation effects.

Slope stability analysis in the LISEM model is based on the infinite slope model. LISEM adopts an iterative method to calculate slope failure. which assumes that the slope failure is caused by the change in the surrounding slope. However, slope failure is caused by the change of force propagation in the subsurface.

The LISEM model considers different hydrological and geotechnical parameters of the study area to obtain slope stability of the surface in dry conditions and due to rainfall conditions. During a rainfall event, the groundwater level is not changed until the wetting front reaches the groundwater level. After the wetting front reaches the groundwater level, the level of the groundwater will be increased due to the supplied amount of wetting front (Chiyang, 2018). However, the assumptions result in completely dry soil above the groundwater level. This is also different from the real condition; the soil can be partially saturated everywhere above the groundwater level during a rainfall event. The model allows to perform of a sensitivity analysis on slope stability assessment. This analysis helps to observe which parameter triggers failure. The software has a tool to calculate landslide failure location and failure depth. These values can be used to find the initial volume for the runout model following that, solid height and fluid height obtained from the runout model. LISEM is an available deterministic model that meets all the set requirements of the needed physical model.

4.2.7. LISEM model calibration

For physically based modelling, all models need to be calibrated to improve the results and predictions based on the reference values. Calibration means finding a set of parameters that result in optimal accurate simulations. LISEM is user-friendly for performing calibration and sensitivity analysis. In the LISEM model, the calibration is done mostly using the measured landslide inventory data.

Table 3. Input soil property parameter for LISEM

Parameters		
Geotechnical Parameters	C' (Pa)	2500
	Φ (^{0})	32
	ρ (kg/m^3)	1900
	Sand	0.463
	Silt	0.162
	Gravel	0.261
Hydrological Parameters	Ksat(mm/hr)	29
Initial saturation	Ɵi(-)	0.3
Residual saturation	Ɵs(-)	0.4

5.   Slope stability assessment
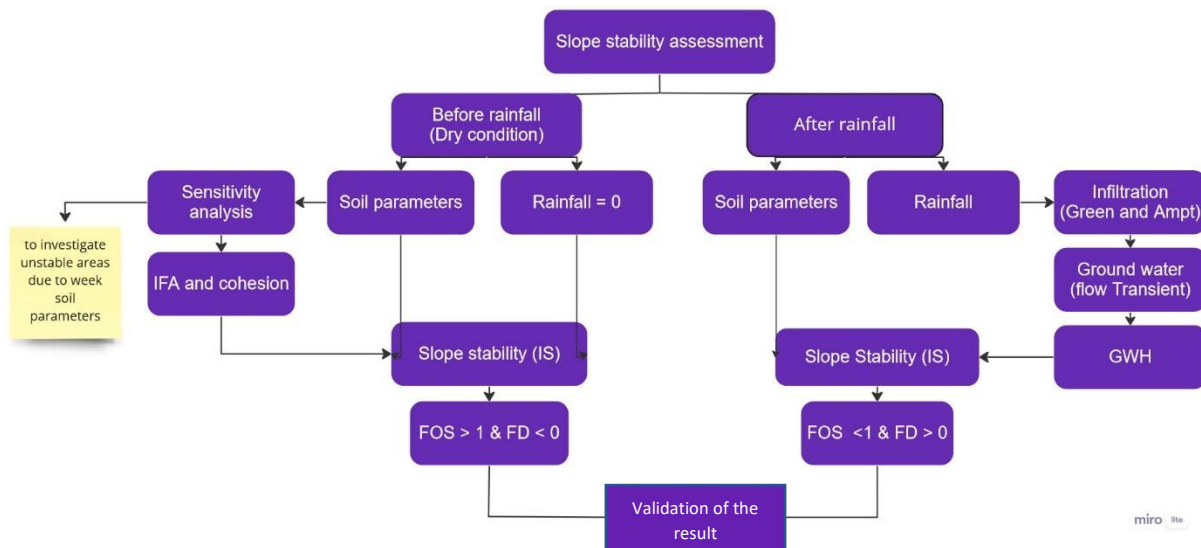
Figure 31. slope stability assessment approach before rainfall (Dry condition) and after rainfall. Sensitivity analysis is used in dry condition slope stability assessment to investigate unstable areas due to weak soil parameters. Rainfall conditions in the model consider (Green and Ampt) and flow transient to obtain GWH. The result from the two-condition calibrated using an inventory map.

slope stability assessment was performed with LISEM using the Slope Stability (IS) model as specified in the methodology. Geotechnical parameters of the soil such as soil cohesion, IFA, soil depth, and soil density, and hydrological parameters such as groundwater height, initial saturation, and porosity of the soil were used for the calculation. From the analysis of slope stability, the FOS and failure depth at the same time were obtained. Calibration of input parameters was done to highlight the more sensitive parameter for the slope process. It was decided to perform the analysis before the rainfall in dry conditions and after the rainfall. To perform a slope stability assessment, it was necessary to select a reference value of the input geological and hydrological parameters of the soil. Therefore, the reference values were taken from table 3.

5.1. slope stability assessment before the rainfall (Dry condition)
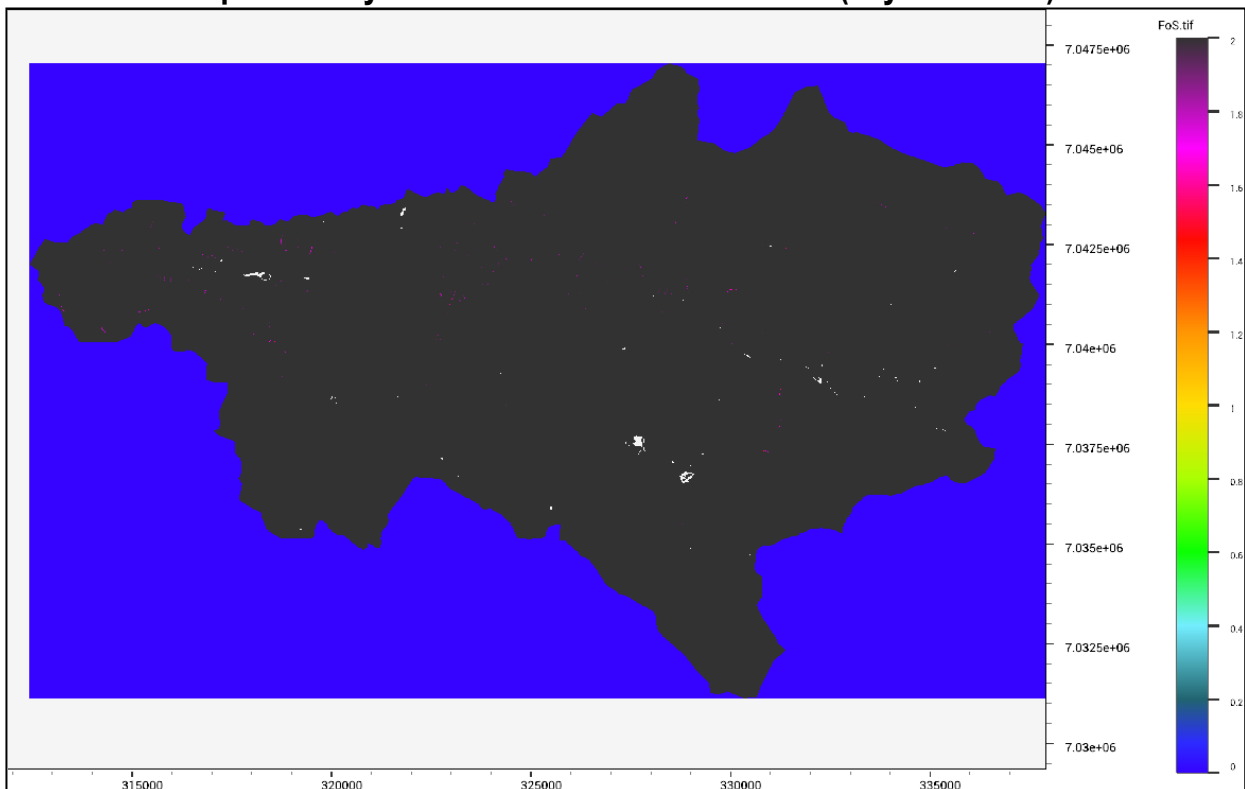
Figure 32. FOS map for the dry condition using a cohesion value of 2500(Pa), IFA of 0.57(rad), and soil density of 1900(kg/m³)

The FOS map presented in the figure above showed the stability of the terrain due to dry conditions. For that reason, most of the area showed black which means the FOS value is above 2 as shown in the legend. This result is expected in the sense that, the terrain is assumed to be stable before the rainfall event. If FOS>1 the failure depth value is 0. Considering several unstable factors of the slope, the stability was assessed by changing the soil depth and cohesion for sensitivity analysis as explained in figure (30). This is to observe the unstable area of the terrain due to weak soil parameters.
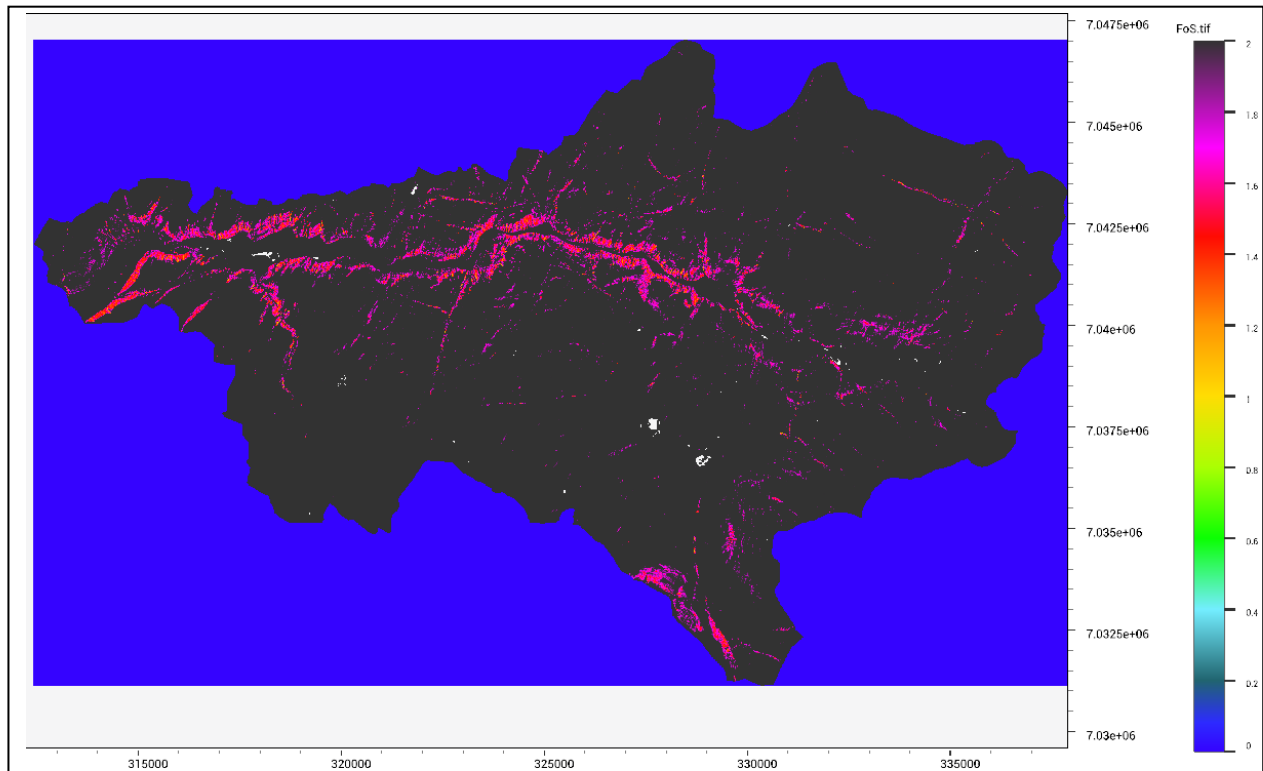
Figure 33. FOS map for dry conditions using cohesion 1500(Pa), IFA 0.57(rad).

Comparing the map presented in figure (32) and figure (33), FOS is greater than 1 for both maps. However, it is possible to detect some parts of the area are changed due to the assumed weak soil parameters. Consequently, these areas are assumed to be unstable due to rainfall events.

5.2.   Slope stability assessment after rainfall events.

The rainfall effect in the model accounted for the rise of GWH. The GWH is calculated from the transient flow condition. The rainfall value was taken from the back analysis of the landslide events that were triggered by heavy rainfall. A maximum rainfall value of 85 mm/hr was used for the simulation. This value is taken considering the January 13, 2022, landslide event from figure (26). The methodology to account for the rise of GWH from the infiltration process is explained in the description of the LISEM model.
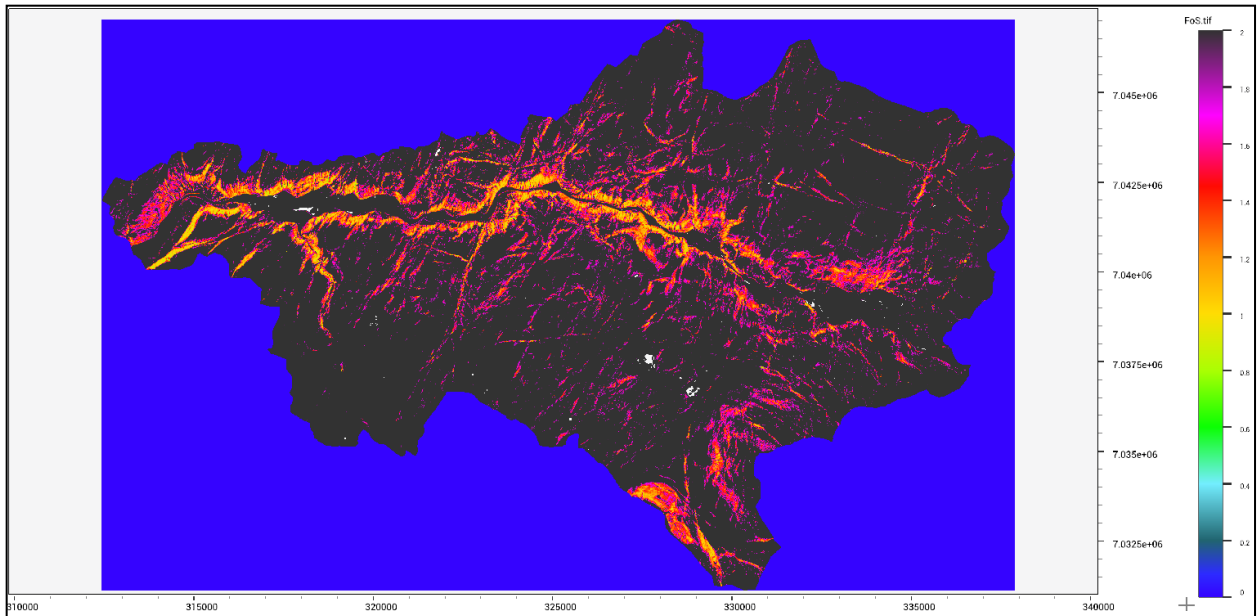
Figure 34. FOS map after the rainfall event cohesion 1500(Pa), IFA of 0.57(rad)
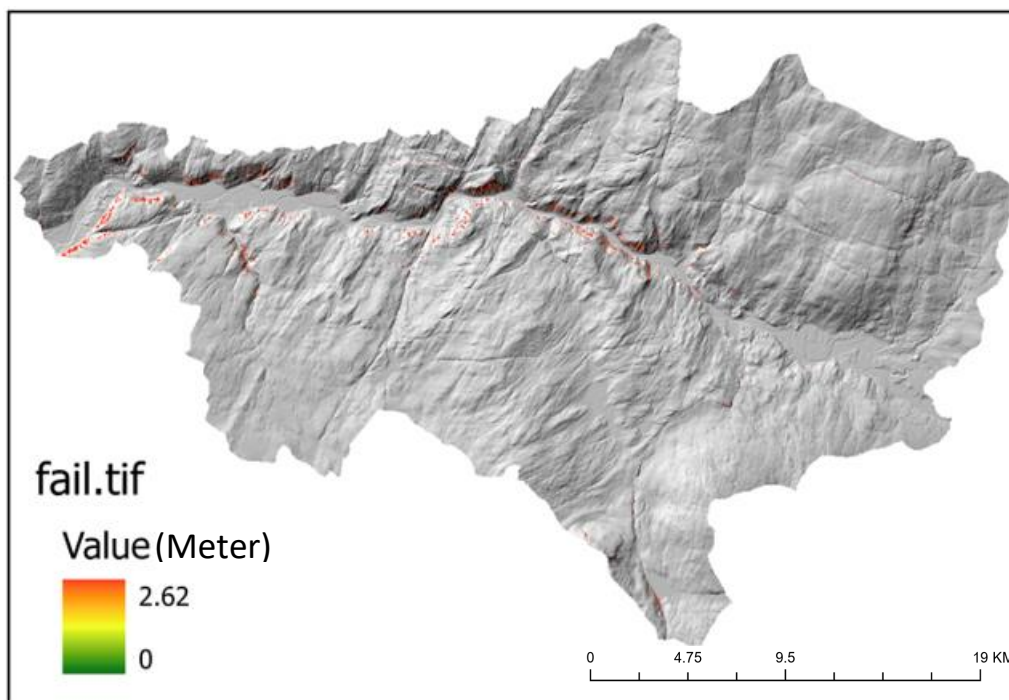
Figure 35. Failure depth map after the rainfall event

Slope stability assessment after the rainfall resulted a failure depth value of up to 2.62 m. This time the FOS map showed areas that are lower than 1. These areas were detected to fail from the sensitivity analysis result of the dry condition slope stability assessment. However, this result needs to be validated from the inventory maps. Accurate inventory maps were impossible to obtain since data were not accurately recorded in the study area as specified in the literature review section. Therefore, shapefiles

were extracted from ArcGIS using the inventory map obtained from the figure (12).
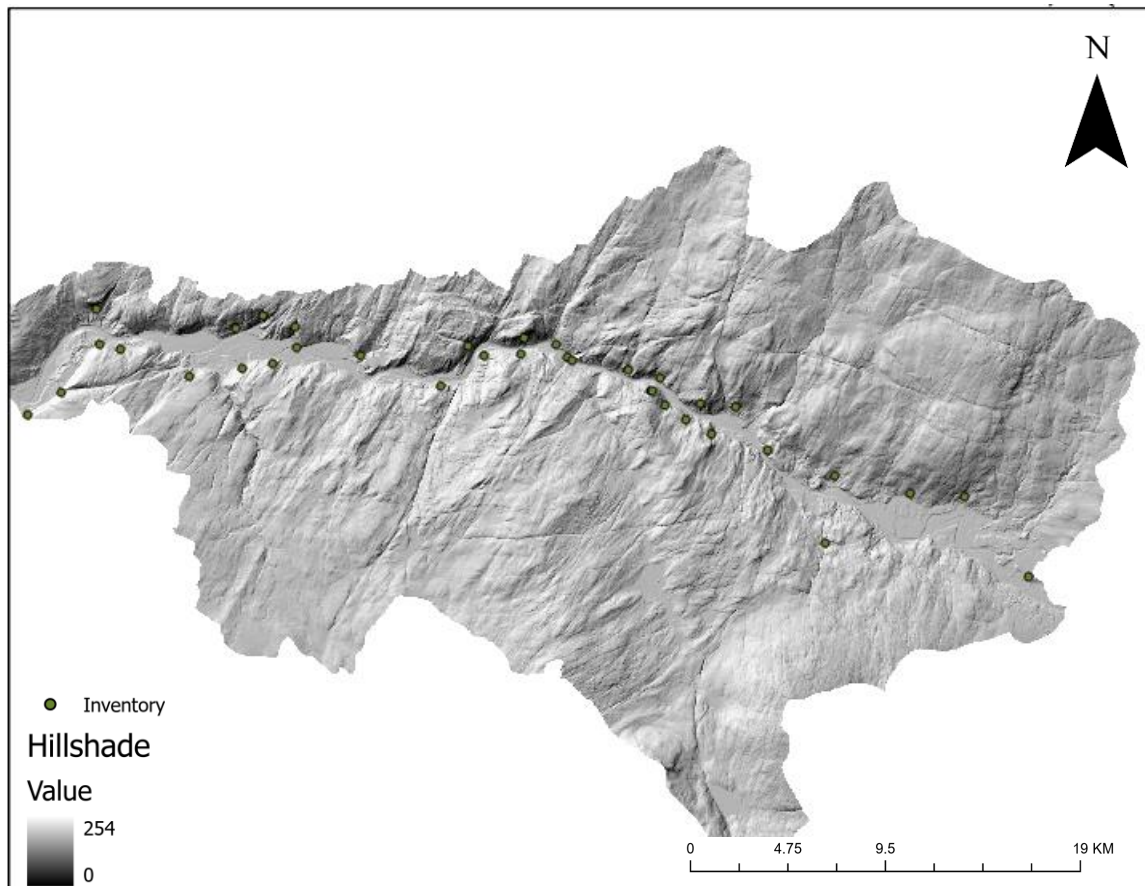
Figure 36. Inventory map (landslide recorded after 2005)

The inventory map showed that most of the landslides were in the fluvial deposit. landslide susceptibility map usually requires calibration and validations of results with the inventory map.

5.3. Calibration of the slope stability assessment

Calibration means finding the set of input parameters that results in an optimally accurate simulation in reference to real landslide events. This requires accurate inventory data. Validation of the model with the real event is not an easy task since the accuracy of the data is mostly the problem. In LISEM for landslide runout model calibration is an option to calculate the error of the predicted landslide model. The Cohens Kappa metric provides an iterative method to calibrate the model (van den Bout, 2017).

According to the methodology adopted in LISEM, the inventory map and impact map (FOS map) are used for calculating the error and the parameters used for calibration were IFA and cohesion. The value 1.0 indicates the critical threshold for defining impact. The iteration is done by changing the IFA and cohesion from the input parameter. Inventory shapefiles were changed to the "Tiff" file in ArcGIS and imported into LISEM. The impact map (FOS map) is adjusted with the calibrated parameter and the iteration stops when the error becomes too small. In addition to this, the FOS map and failure depth for

the three different soil parameters were presented, and three different IFA and cohesion values were chosen for calibration.
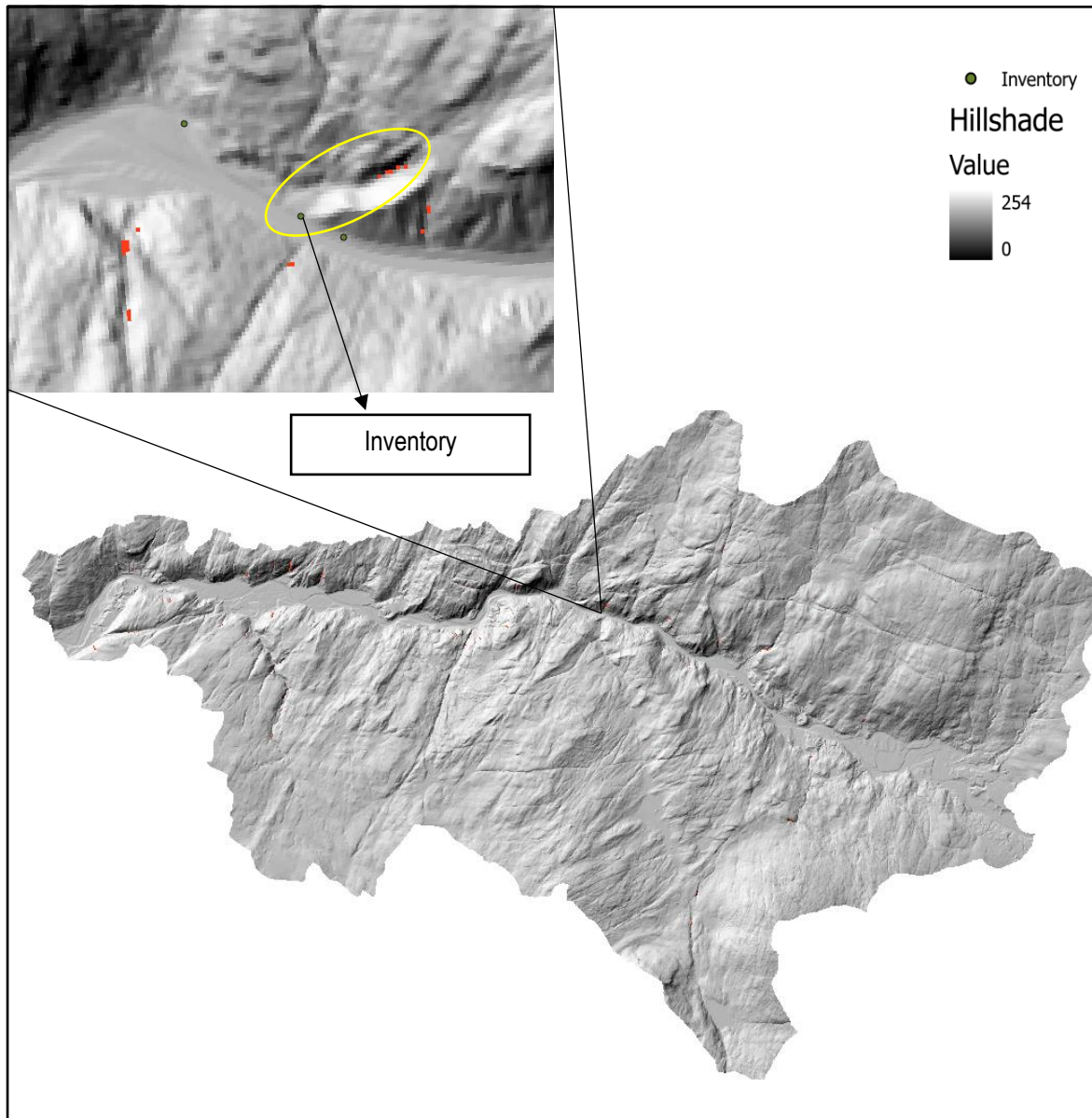
Figure 37. failure result for cohesion 2500(Pa), IFA =0.57(rad)
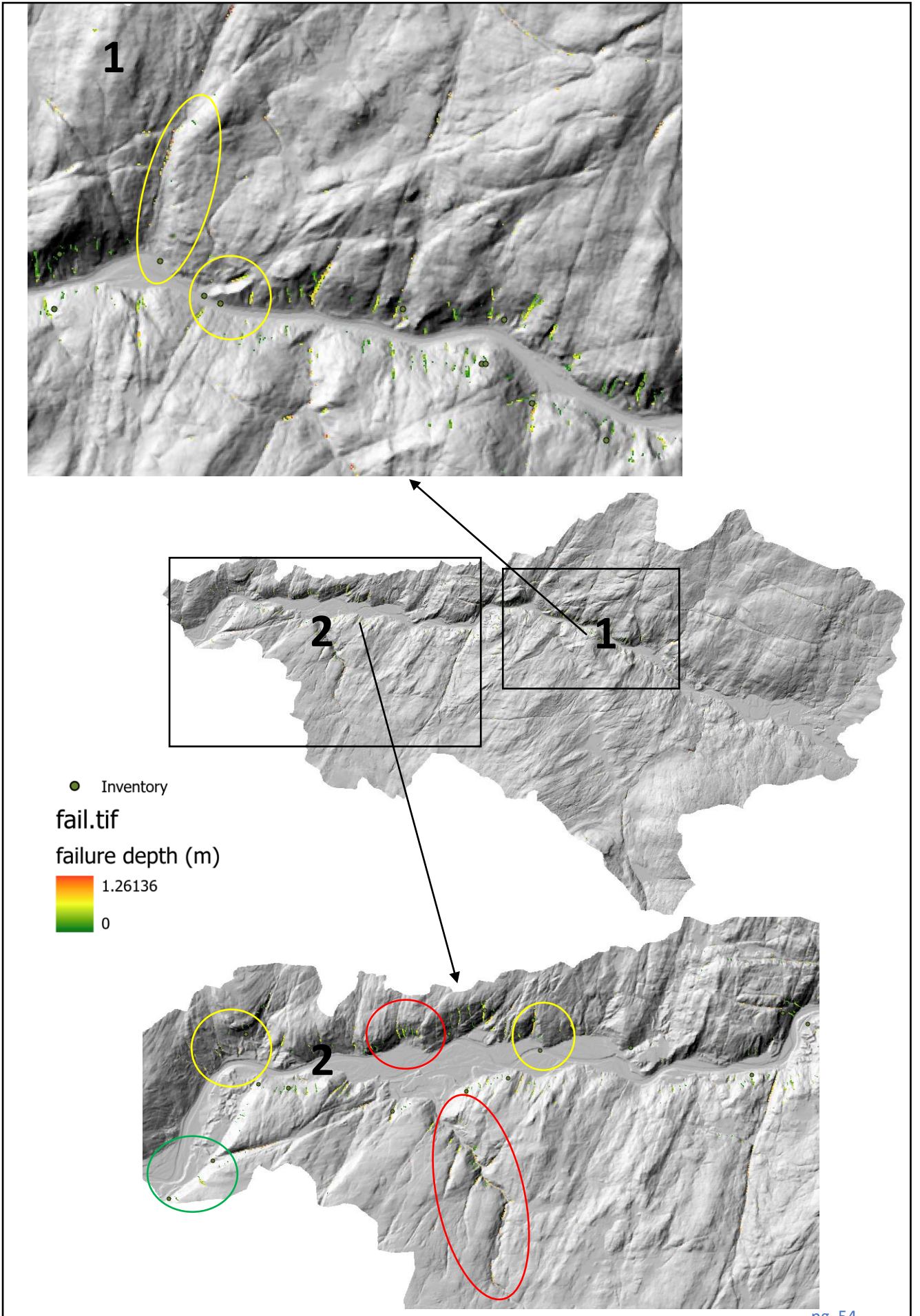
Figure 38. failure result cohesion 2800(Pa), IFA 0.3(rad)

Figure 38 showed the validation of the failure result using inventory maps. Two locations were selected for calibration of the predicted unstable area. From location 1 it is possible to understand that the predicted failure result is in the location where the landslide inventories are located. The failure depth map indicated the initiation of unstable areas. The observed maximum failure depth value is 1.26 m. location 2 presented clear validation of the result. For that reason, the yellow circle indicated the predicted landslide is almost comparable with the inventory. The red circle indicated the predicted unstable location however, the result is not comparable to the inventory. On the contrary, the green circle indicated no failure prediction in the observed landslide. Having this in mind, the parameter selected for calibration can be adjusted to obtain a better result. The failure location is now studied considering the inventory and model result. The calibration approaches adopted in LISEM used cohesion and IFA for calibrating the result. The calibration is done by iterating the input parameters of cohesion and IFA. The parameter was selected by considering the most comparable result of failure result and observed landslide. The calibration described in figure (38) illustrates the location of landslides which are predicted but not observed, predicted and observed, observed but not predicted. soil parameters can easily be calibrated using this observation. Thus, a reference value of soil parameters can be selected considering the inventory map. This reference value is considered to be the applicable result for the slope stability assessment. The calibration was done considering the maximum rainfall recorded on January 13, 2022.
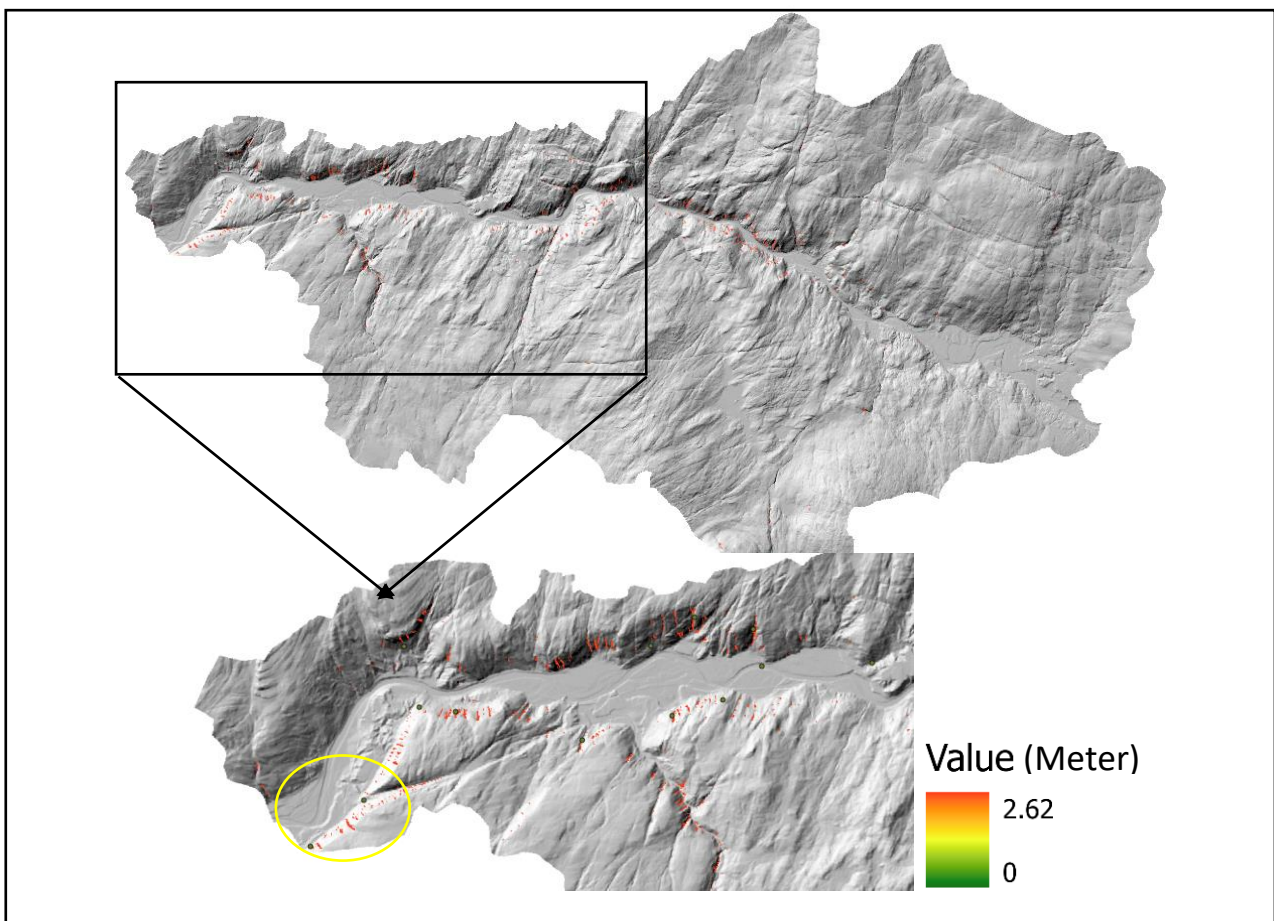
Figure 39. Failure depth result cohesion 1500(Pa), IFA 0.57(rad)

The failure depth map using cohesion = 1500 Pa and IFA = 0.57 (rad) showed more comparable results with the inventory shapefile. Location 1 which was selected in figure (38) was assessed with the newly selected soil parameter. From this result, new failure prediction is observed that is more comparable with the inventory. This result can be selected as a reference soil parameter value for sensitivity analysis. Increased soil depth gives higher failure depth but not a new location for slope failure.

From the inventory data, 12% of the area was covered by the landslide. Following that, the three cases were calibrated according to the inventory data. Case 1, case 2, and case 3 covered 7%, 8%, and 14% of the area by the predicted landslide respectively. To measure the significance of LISEM outcomes and to determine the slope failure triggering condition that gives the best prediction, four different errors can be determined which are "True positive (TP)", prediction of a landslide where one occurred, "False positive (FP)", prediction of a landslide where no landslide has occurred, and "False negative (FN)", non-prediction of a landslide where one occurred, and "True negative (TN)", or non-prediction of a landslide where no landslide occurred (Salciarini, 2007). Further, predicted and observed landslides were studied by considering a failure map and constructing a confusion matrix. They are classified as TP, FP, TN, and FN.

- ➢ TP (True positive) if the FD > 0 in the observed landslide
- ➢ FP (False positive) if the FD > 0 outside observed landslide
- ➢ TN (True negative) if the FD = 0 outside observed landslide
- ➢ FN (False negative) if the FD = 0 In the observed landslide

The area of predicted landslide polygons was computed and compared with the area of the observed landslide. Using ArcGIS, a polygon was created and the area of predicted and observed landslide was compared with the total study area. For better validation of the result, the landslide in the study area was assessed and a polygon was created from the satellite image using "Finn kart" map source (FINN, 2019) and ArcGIS pro. This is because various landslides were observed from satellite images that are not recorded in the inventory data. Thus, several landsides were selected from the image for the calibration process. Landslide Image analysis was performed based on the Finn kart map source on events that occurred in 2019 or before. The landslides can easily be detected from this satellite image. Landslides that were observed during the image analysis and polygons that show the inventory and the predicted landslide from LISEM are presented below for a qualitative calibration process.
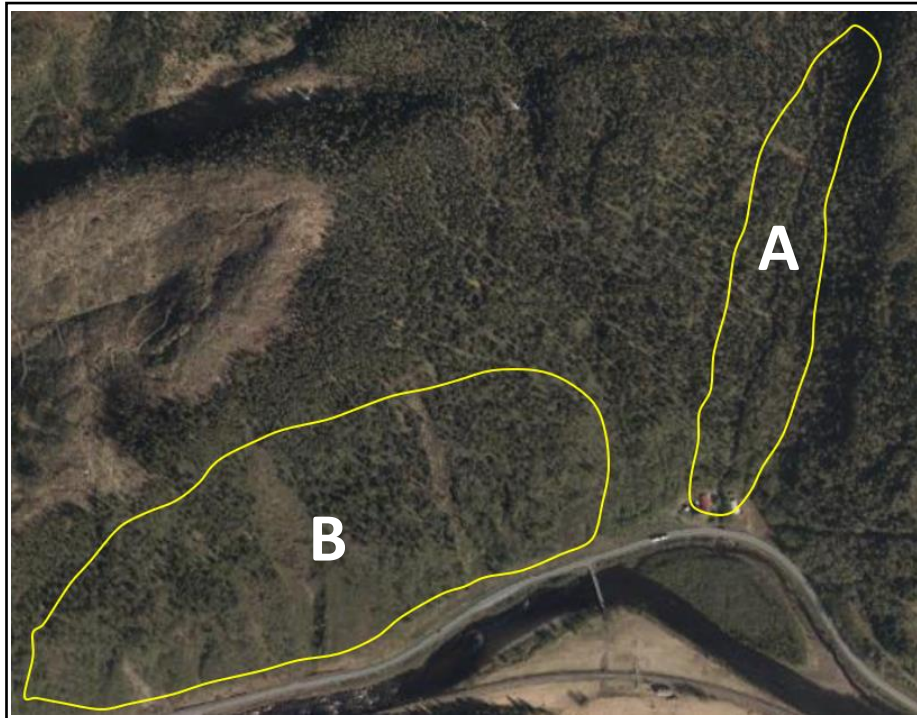
Figure 40. Image analysis for landslide inventory assessment

Polygon A and Polygon B showed the scarp of the landslide. In polygon B several scarps were observed, and these image results were assessed using ArcGIS by applying the LISEM failure result. hence, polygons for both results are applied in figure (41).
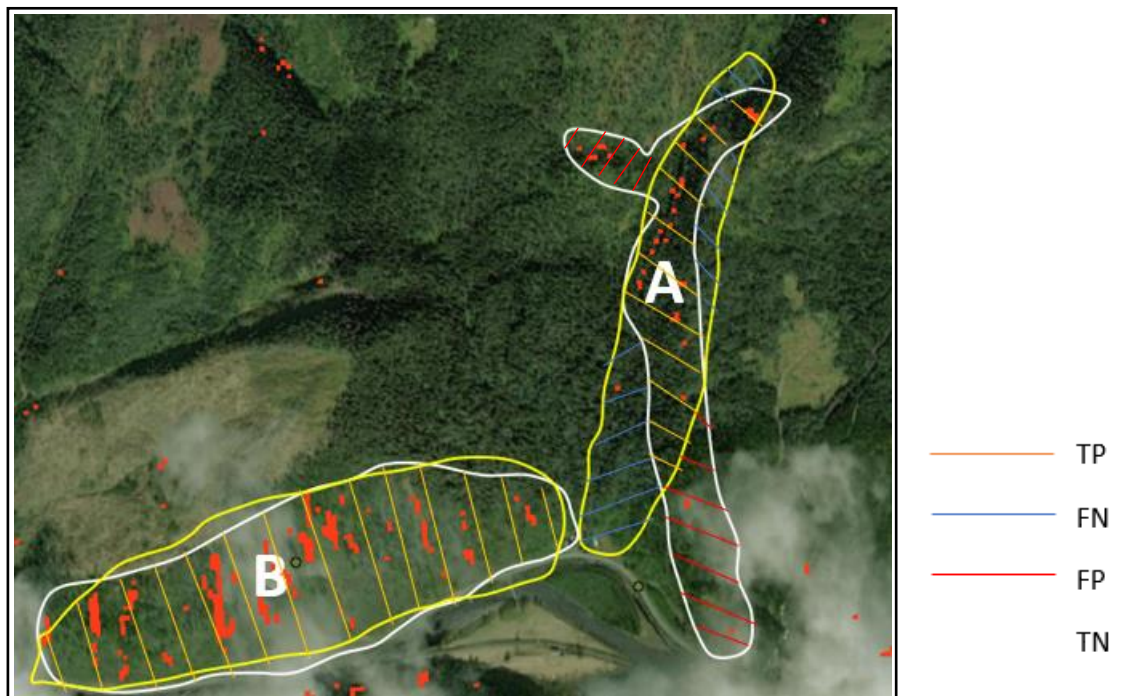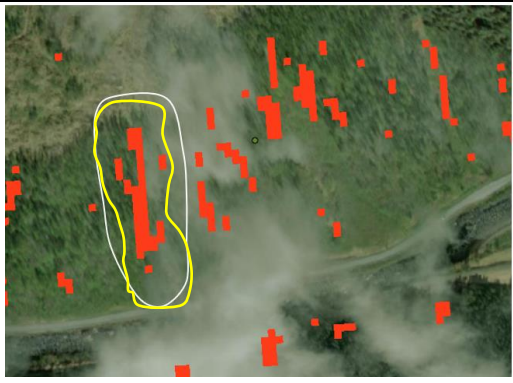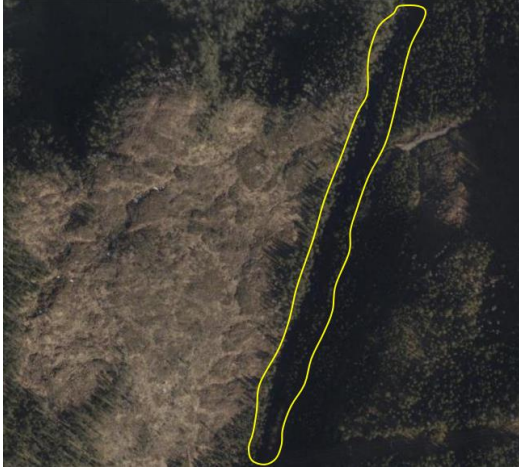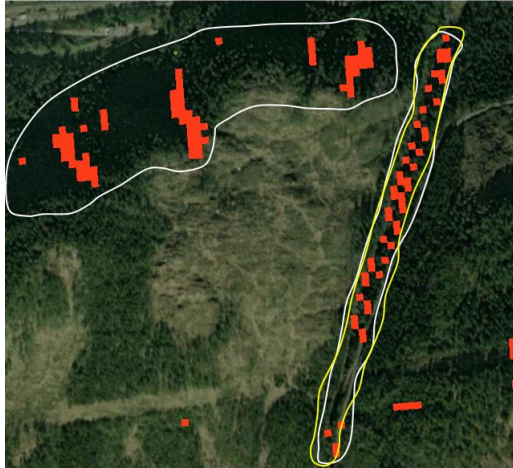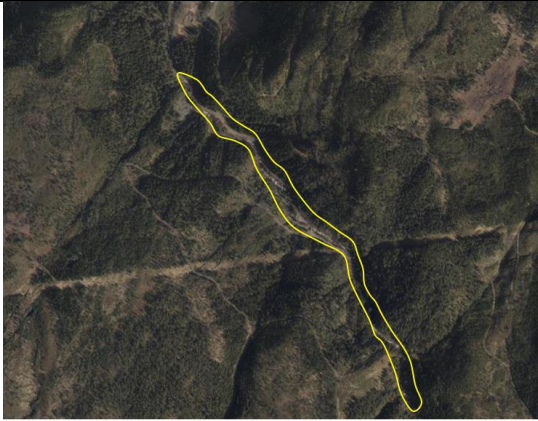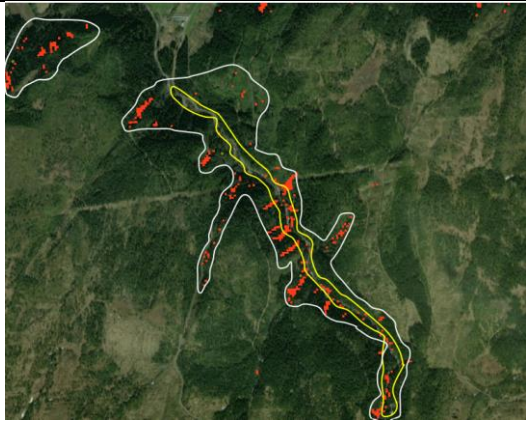
Figure 41. white polygon predicted landslide from LISEM and yellow polygon landslide inventory from image analysis.

Landslide polygons from the LISEM model and inventory are drawn to perform a qualitative landslide calibration assessment. The area of the yellow polygon for A and B is 241,187 m² and 156,942 m²

respectively. Consequently, the area of the white polygon for A is 266,362m^2, and for B is 156,008m^2. The true positive is considered in the location where the two polygons overlap. FN and FP are indicated with the blue and red lines respectively in figure (41). TN is the area outside of the two polygons. Accordingly, several landslide inventories from the satellite image were selected for further qualitative calibration. The figure below shows the selected inventory and its calibration of failure results.

Landslide inventory from Satellite Imagery (2019)	Failure results from LISEM
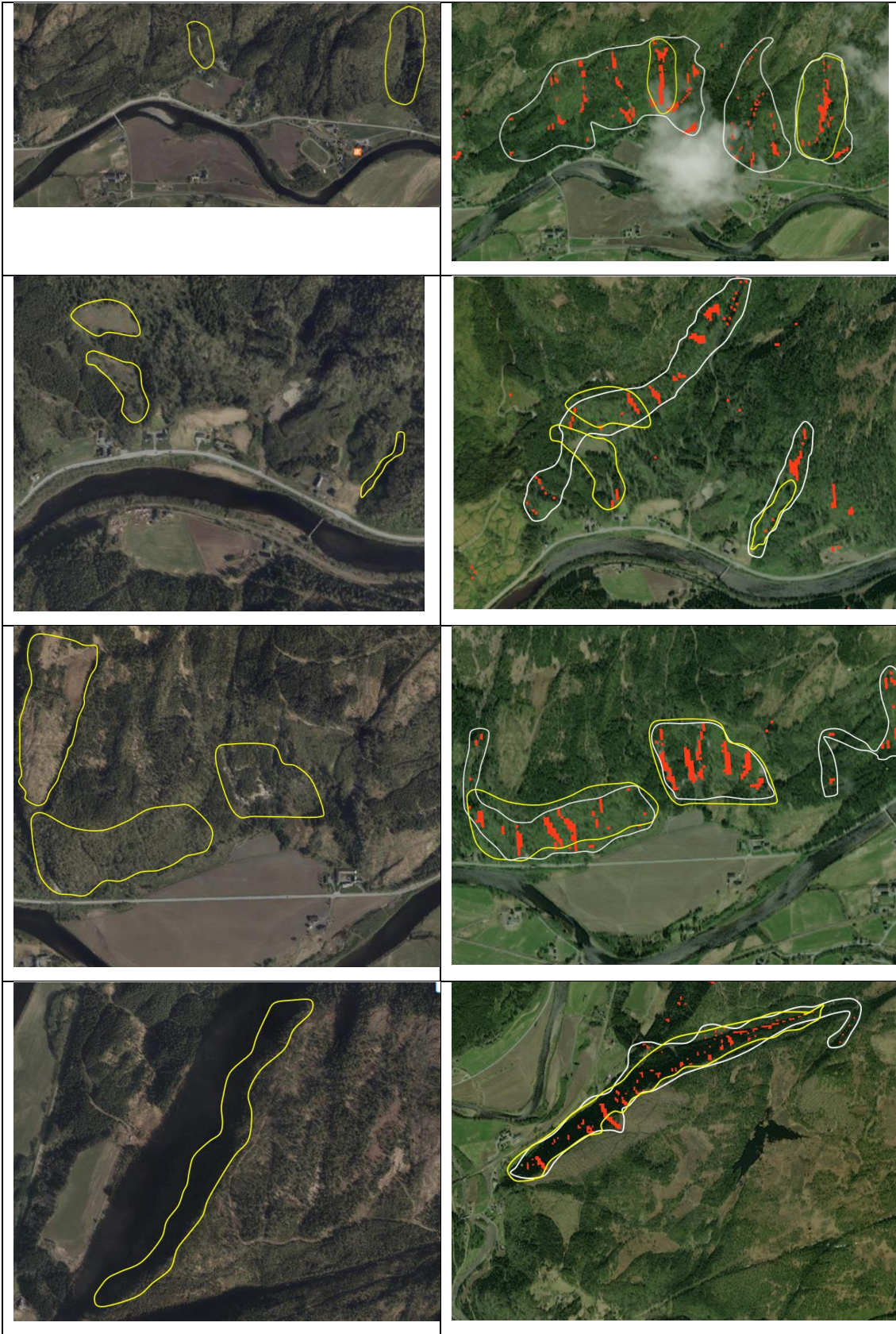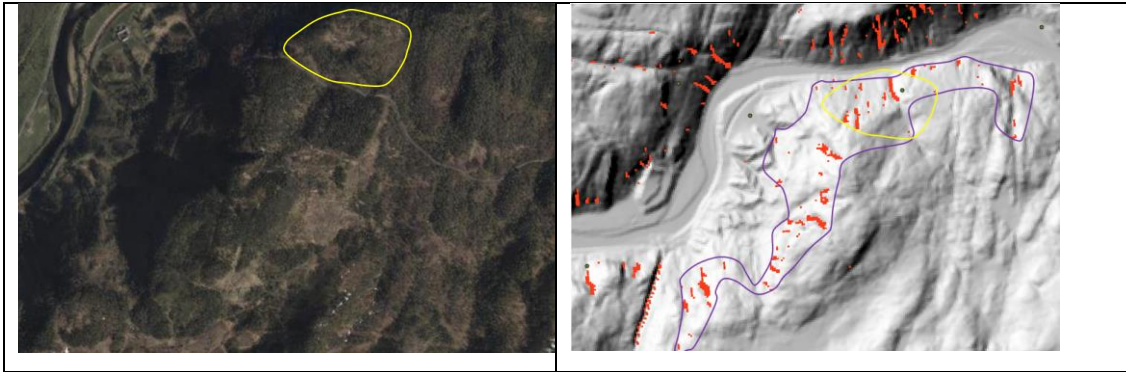
Figure 42. landslide inventory from satellite imagery and LISEM failure calibration. The yellow polygon is for inventory and the white polygon is for the LISEM failure result. The satellite image of inventory taken from data recorded in 2019. The base map used in ArcGis is the recent image.

15 landslide polygons were selected for calibration from the satellite image. Among the 15 selected landslide areas, landslides were predicted in 10 of the areas, and no landslides were predicted in 3 of the areas. Consequently, 6 landslides predicted from LISEM were not found in the inventory (satellite image). From image analysis, it was possible to observe landslides that were not recorded in the inventory data. The polygons from satellite images don't precisely show the landslide inventory. In another word, one cannot surely define the initiation zone of the landslide from the satellite image. The reason for this is that the images are not recent and there are some zones where the vegetation is removed and there are some areas where the landslides occurred in previous years but now seams vegetated. However, these areas are susceptible to landslides due to the presence of loose material and its topography observed from the site visit. Therefore, the polygons were drawn considering the possibility of landslide occurrence in the area from the discussion.

From the preliminary slope process assessment, it was possible to understand the sensitive soil parameters which cause slope failure for the LISEM model. Therefore, soil depth, soil cohesion, IFA, and groundwater values were changed using the reference value from table 3. Thus, data calibration can be approached. It is clear to understand from the IS model formula that cohesion and internal friction angle influence the slope stability of the soil. Soil depth directly influences slope stability, the higher the soil depth the higher the amount of soil that will fail. This statement can be further studied in the sensitivity analysis. Soil saturation is affected by rainfall infiltration. Shallow soil cover can easily be infiltrated by rainfall and cause shallow slope failure. However, the infiltration process is longer for deeper soil depths, and the soil is assumed to be fully saturated by the rise of groundwater because of the wetting front. This is also one of the reasons for deep slope failure in deep soil depth (Dibaba, 2019). Sensitivity analysis is performed for a better understanding of each soil parameter's influence on slope instability. The parameters were changed independently, and a range of values was used by multiplying the parameters with a factor. The table below shows more detailed soil parameters selected for the sensitivity analysis.

The maximum soil depth obtained from the model is 2.53m and this value is multiplied with varied factors for sensitivity analysis as presented in the table below. To save computation time, it was necessary to clip the DEM to a smaller extent. This area is clipped considering the inventory data from the figure (36). This area is selected since the inventory is almost comparable with the predicted failure result. Different values of soil depth, cohesion, and IFA were selected to observe the effect of these parameters on failure results. Ten different parameters are presented in the table below and the corresponding failure map is presented. The FOS map and the failure depth map for parameters 1,5, and 10 are presented as follows.

Table 4. Soil parameters were used for assessing the increased situation of each parameter value on slope stability analysis using LISEM.

No	Maximum Soil depth (m)	Cohesion (Pa)	IFA (rad)
1	1.52	1000	0.21
2	2.03	1200	0.23
3	2.28	1250	0.29
4	3.17	1500	0.34
5	3.60	1750	0.40
6	4.18	2000	0.43
7	5.07	2100	0.45
8	6.33	2300	0.46
9	10.13	2500	0.48
10	12.16	2600	0.60
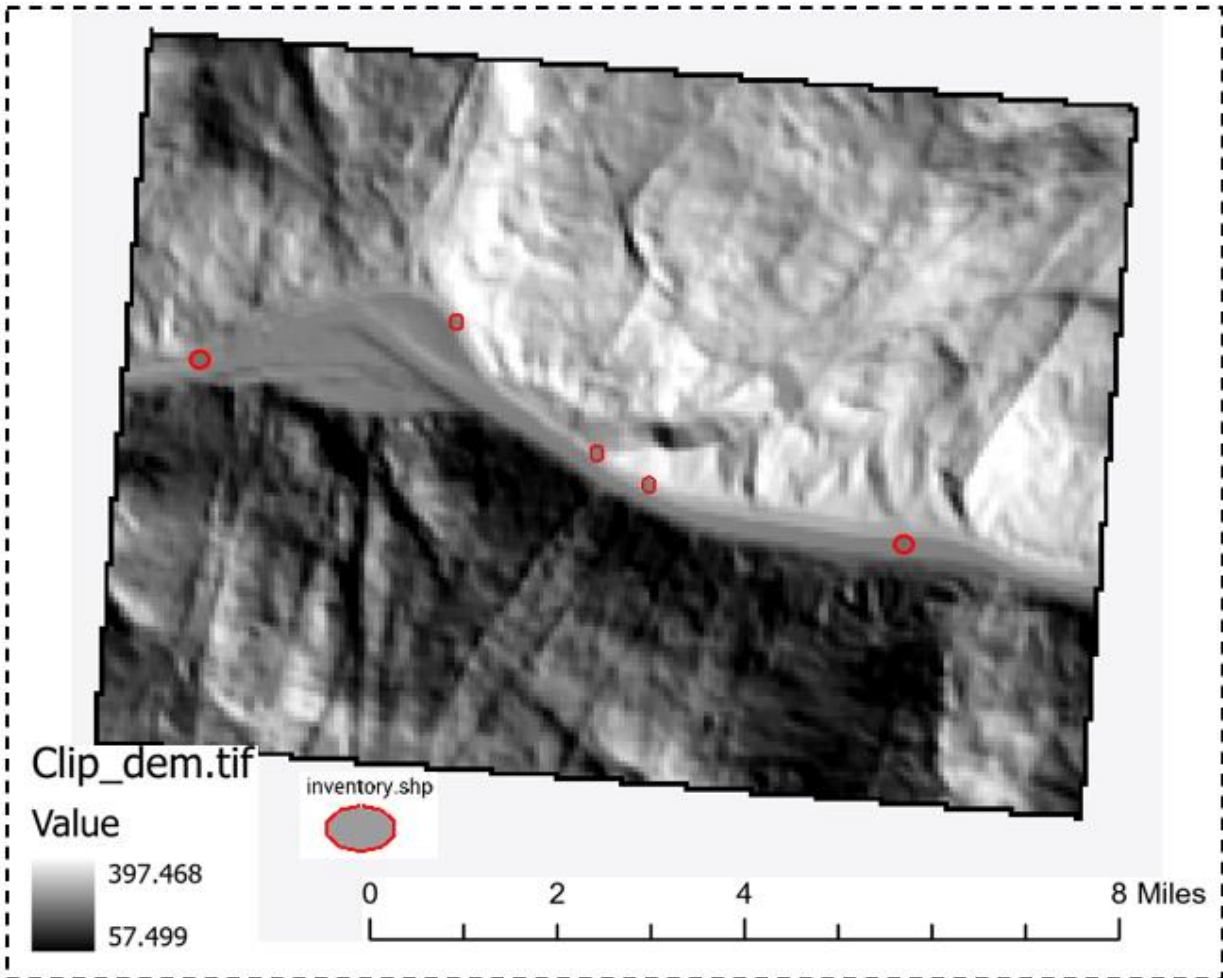
Figure 43. Clipped DTM for the sensitivity analysis
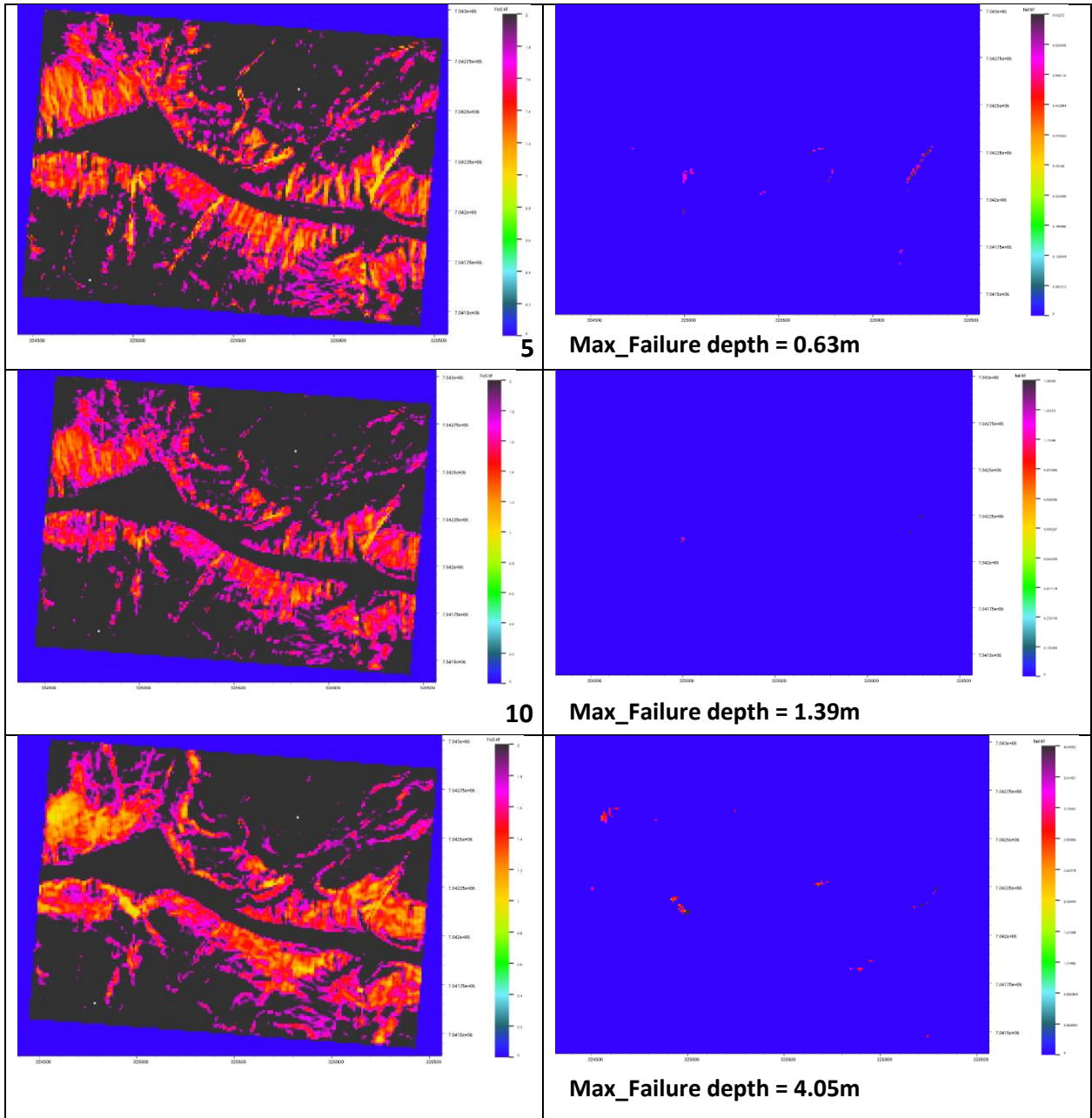
Figure 44. Slope failure results from table 4 input soil parameter.

The result indicated that slope failure is sensitive to soil parameters. To be more consistent, the increasing situations of soil parameters were considered. Consequently, the failure result can easily be assessed due to the increasing effect of these parameters on the failure. Soil depth directly affects the failure depth. The result indicated a direct relationship with the failure depth. However, the increased IFA and cohesion positively affect the failure result or reduced the size of the failed area. The graph below shows a better illustration of the result and the effect of parameters for the corresponding failure result.
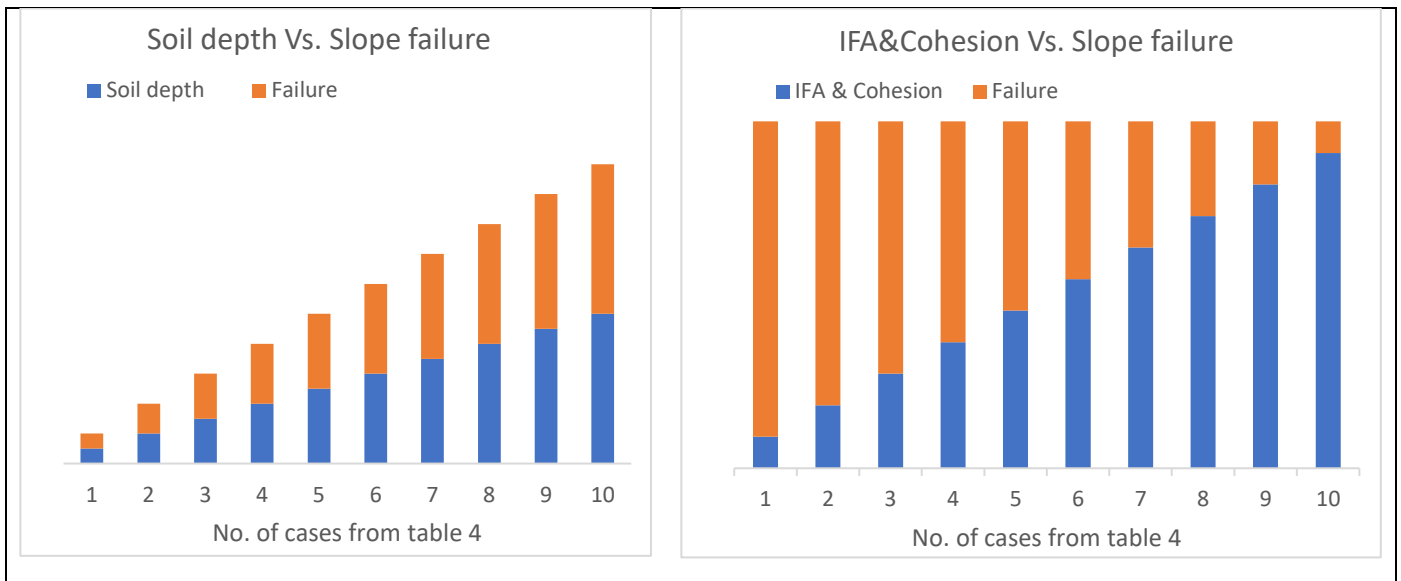
Figure 45. Impact of soil parameter for slope failure

The graph shows a rough estimation of the relationship between slope failure and soil parameters. Slope failure increase when the soil depth increase. IFA and cohesion have an inverse relationship with failure. Even though the failure value is not precisely consistent with the value of increased parameters a relationship can be drawn from the observed result. Detailed investigation of each parameter and their influence on the slope failure result needs to be assessed.

It is now possible to further study which parameter is more sensitive to failure depth (amount) and which parameter is sensitive to failure area or failure extent. In addition, it is possible to recognize that the slope is sensitive to higher soil depth, lower soil cohesion, and lower IFA. The higher failure depth is obtained from the higher soil depth. Having this in mind, further sensitivity analysis is done to assess the influence of each parameter and their combination on slope failure.

5.4. Sensitivity analysis

Three main soil parameters were selected for the sensitivity analysis which are soil depth, soil cohesion, and IFA. After a clear observation of failure conditions due to the input parameters. Suitable reference values were selected using the combination of higher soil depth, lower soil cohesion, and lower value of IFA. Engineering assumption and inventory data were considered to select the value of the soil parameter for the reference value that best represents the possible slope failure.
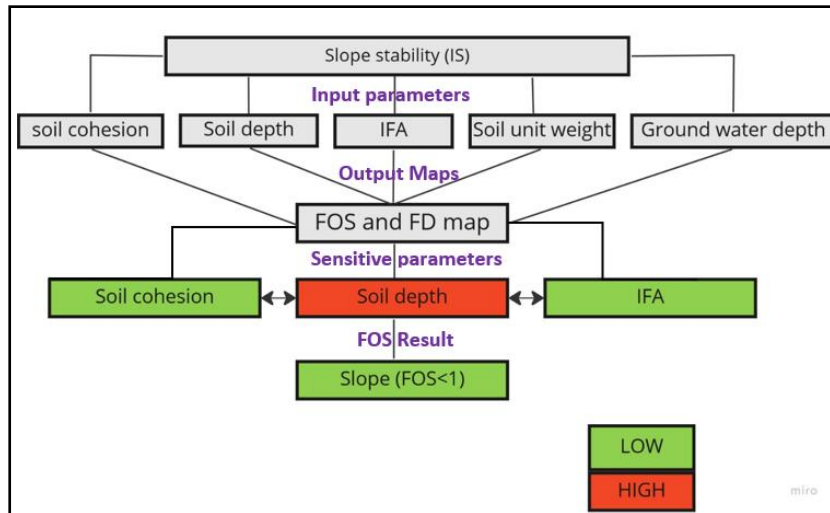
Figure 46. Sensitivity analysis for slope stability assessment

Three main input parameters were selected after the preliminary assessment of slope stability using the LISEM software. For a better interpretation of the sensitivity analysis on slope failure, the three selected soil parameters from the calibration result were changed by a common multiplication factor. Accordingly, the slope failure result is affected by the changed soil parameters. By using site investigation and inventory maps, a reference value for the soil parameters was selected. To represent the possible failure condition of the slope. Then, the slope failure results from the changed parameters were compared with the reference value. The motive here is to investigate the effect of soil depth and cohesion on failure depth. From the preliminary assessment, it was possible to observe that IFA doesn't affect the failure depth, only soil depth and cohesion significantly affect the failure depth. Therefore, these two soil parameters are considered for sensitivity analysis on failure depth. The table and the figure below indicate the selected reference value and the corresponding FOS and FD map. The reference value is selected from the model calibration.

Table 5. selected reference value (RV) for Slope stability assessment

Max_Soildepth (m)	Cohesion (Pa)	IFA (rad)	Max_FD (m)
5.22	1500	0.57	2.44
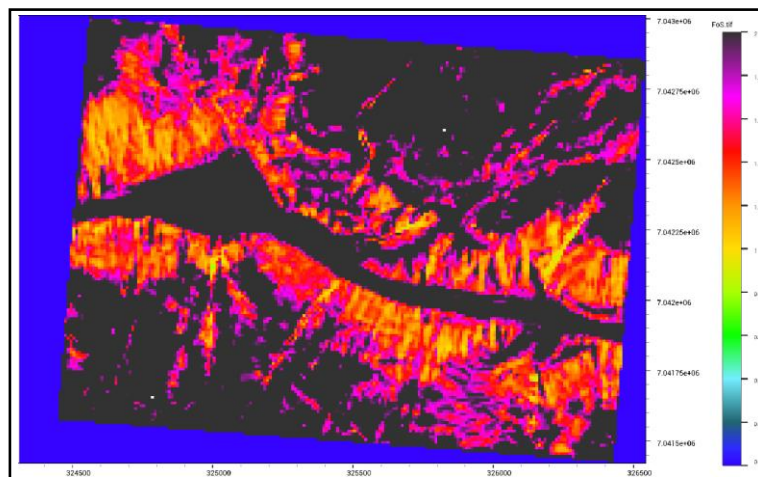
Figure 47. FOS map for the RV (reference value)
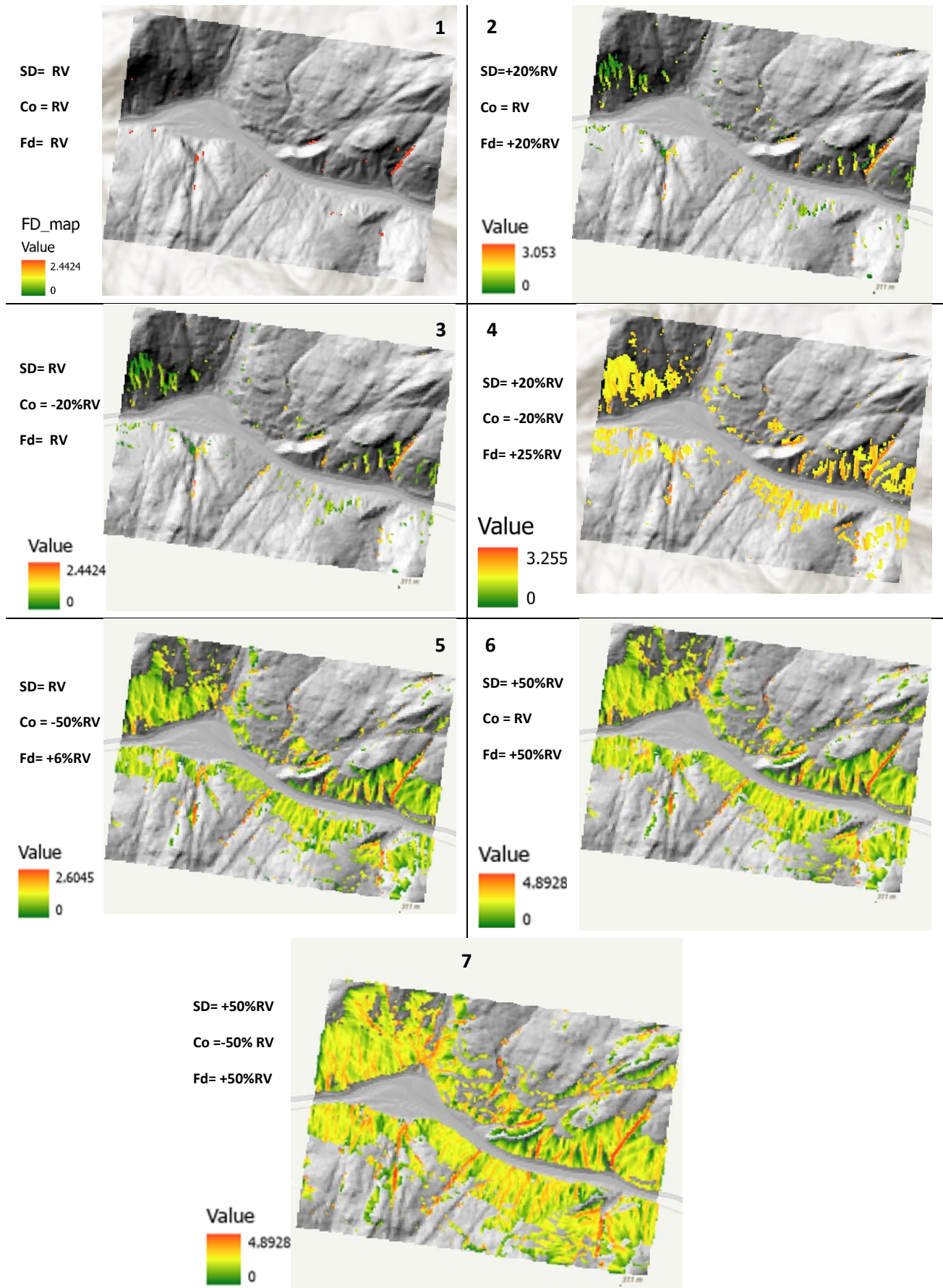
Figure 48. sensitivity analysis for slope failure using LISEM.

The sensitivity result shows that the failure depth is very much sensitive to the soil depth value. As shown in figure (48) Failure results are presented for each combination of soil parameters. Soil failure depth (amount of slope failure) has a direct relationship with soil depth. The result is changed from the reference value with approximately the same amount of soil depth variation. To illustrate these findings a graphical representation is presented below to observe the effect of soil property variation and its failure condition according to the reference value.
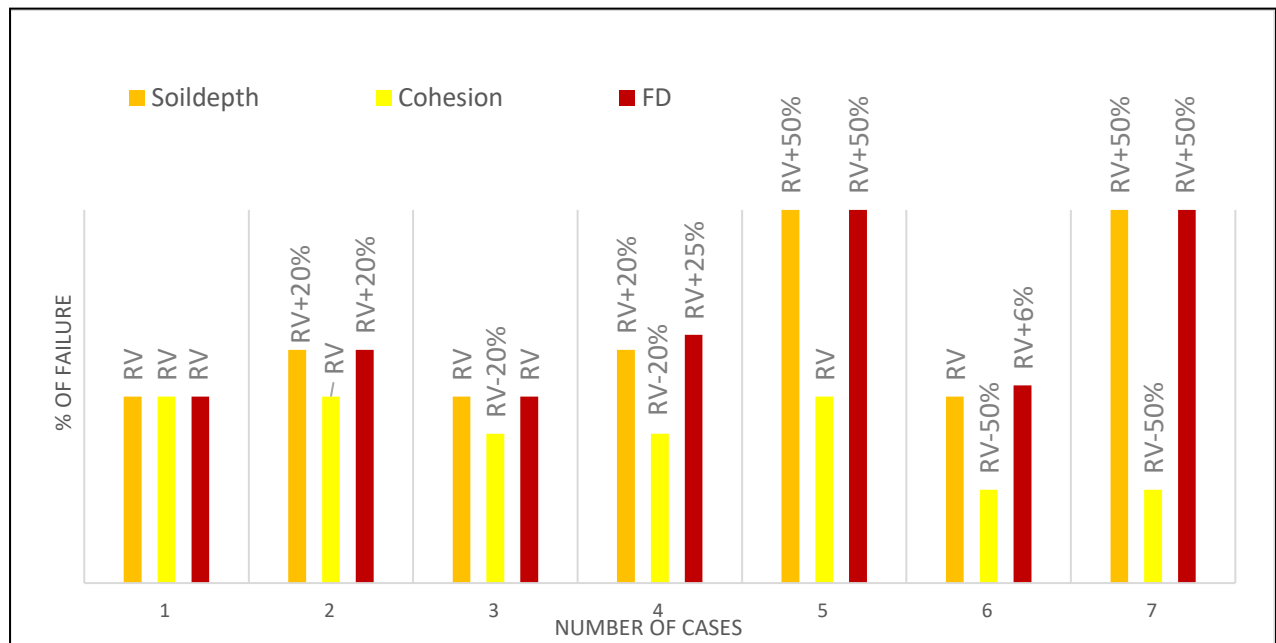
Figure 49. Failure depth results according to the changed soil property from the reference value

From this result, it was possible to observe that soil depth has a higher impact on the amount of slope failure compared to soil cohesion and IFA. Soil cohesion and IFA also showed higher sensitivity to slope failure. However, the results indicated that the soil cohesion value is very much sensitive to the extent of slope failure rather than the depth of slope failure. An increase in IFA leads to less slope failure. Even though, Cohesion and soil depth were found to be the most sensitive parameters in this model.

Further sensitivity analysis has been done to investigate the magnitude of failure on the surface due to the groundwater saturation effect along with the sensitive soil parameters. As discussed in the literature review section, most of the previous landslides that occurred in the study area were due to the high groundwater saturation of the soil. Therefore, it was decided to analyse the slope failure condition due to high initial water saturation. The groundwater height was calculated from the tool employed on LISEM (Flow transient). The model gives the height of the groundwater but not the evolution of the groundwater level inside the soil. Therefore, the initial groundwater level is assumed to be 80% of the soil depth and the failure result is compared with the reference value.
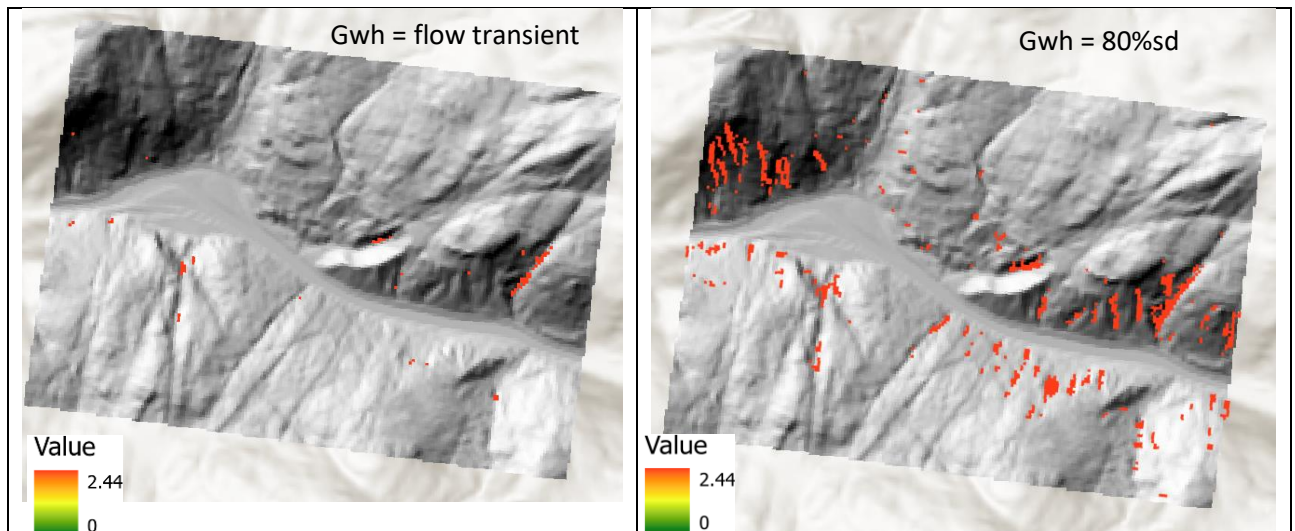
Figure 50. sensitivity analysis of slope failure for the GWH condition

As shown in figure (50) the groundwater height or initial saturation is sensitive for the slope stability model. The failure depth for both conditions is the same. However, the failure extent or magnitude of failure is high for higher initial water saturation. This result motivates to investigate the parameters that trigger more failure extent or more pixels failure on the slope stability model. For that reason, sensitivity analysis is done by changing the parameters that are sensitive to the number of pixel failures or the extent of the failure. A graphical representation is presented below to illustrate the slope failure condition due to the variation of susceptible input parameters.

The graph below shows the different sensitivity analysis results. Four sensitive parameters were selected which are groundwater, soil depth, soil cohesion, and IFA, (1), RV (reference value) of all sensitive parameters was selected and the corresponding failure results were used as a reference value for comparison purposes. The number of failures is the counted failure pixels and failure depth is the depth to the failure surface. (2), only the soil cohesion value was reduced by 20% from the RV (reference value) and the corresponding failure increased by 65% from the reference value of the failure result. However, the failure depth doesn't change when the cohesion value changes. (3), only the soil depth value was increased by 20% from RV and the failure depth increased by 20%. The number of failures doesn't show a huge difference in this case. (4), the combination of increased soil depth and decreased soil cohesion results in a huge number of failures. The number of failures increased by 80% from the RV. (5), soil initial saturation is now increased by 30% from the initial value, and as was expected the failure depth is not affected by the groundwater height. However, the number of failures is now increased by 90% from the RV. It was possible to observe that the initial saturation of the soil has a huge factor in the magnitude of slope failure. (6), IFA (internal friction angle) was reduced by 20% from the RV and the result showed a high number of slope failures. This is also to observe the effect of IFA on slope failure. As indicated the

failure depth is not sensitive but the number of failures increased by 80% which is the same result from the case (4) due to the effect of soil cohesion and soil depth. The last case (7) is to observe the worst-case scenario due to the worst combination of all sensitive parameters. GWH=RV+30%, SD=RV+20%, Cohesion=RV-20%, and constant IFA. The result indicated that the number of failures increased by 90% from the RV and a 23% increase in soil depth.

The two graphical representations in figure (49) and figure (51) represent the impact of input parameters for the slope stability model. Detail investigation of each parameter's contribution is very important for a better understanding of the slope stability model. The slope failure is triggered by the loss of materials in the soil. The effect of huge failure depth and failure extent on the slope can trigger a massive debris flow during heavy rainfall.
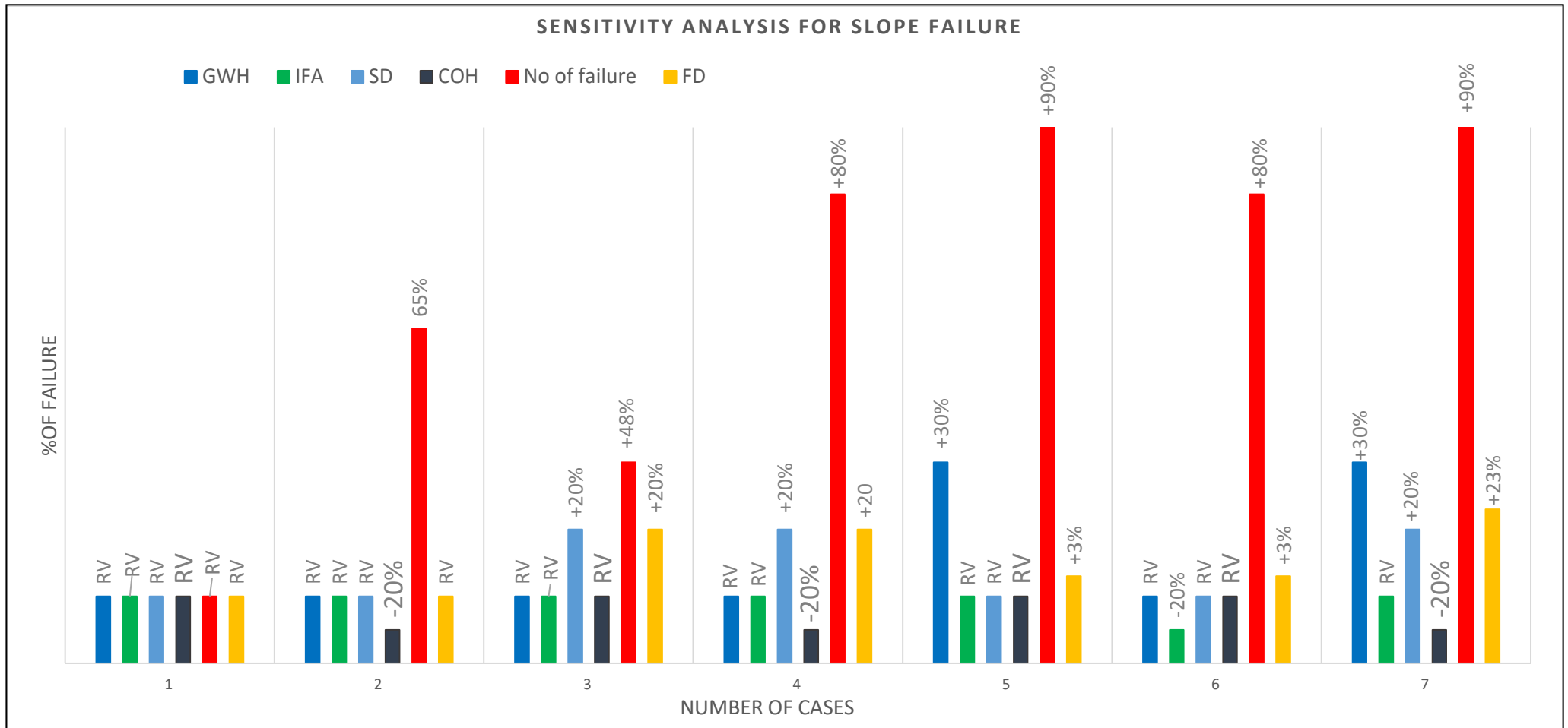
Figure 51. Sensitivity analysis of slope failure

The slope failure results using the reference value from calibration and using the triggering effect of rainfall from the January 2022 landslide event. The slope failure result is presented for the bigger scale.

Table 6. Soil parameters selected for the slope stability assessment.

Maximum soil depth (m)	Cohesion (pa)	IFA (rad)	Maximum failure depth (m)
5.22	1500	0.57	2.44
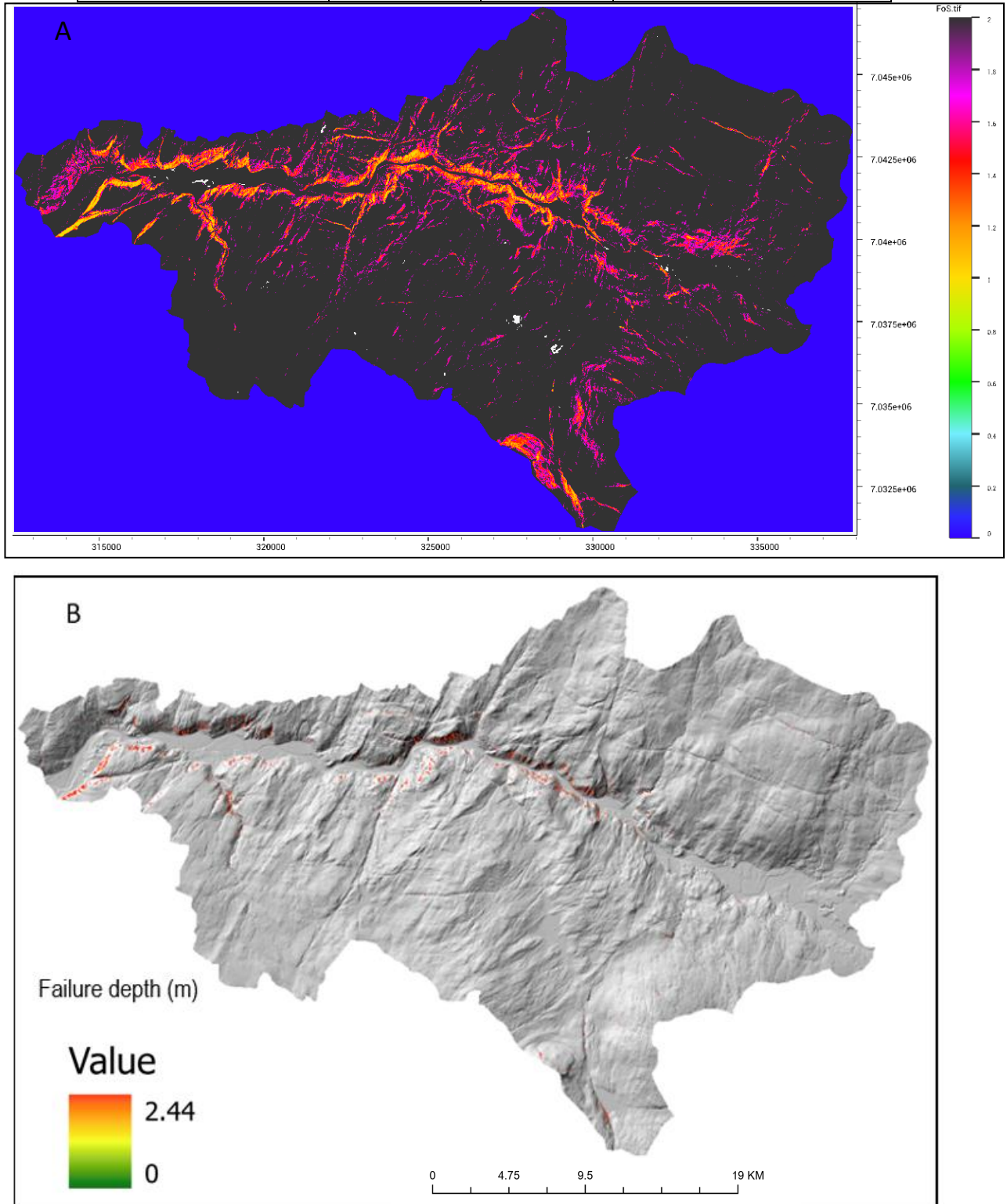
Figure 52. slope stability maps. A, FOS and B, FD map

5.5. Effect of different rainfall return periods on slope stability assessment.

As discussed in the methodology section, LISEM assumes Groundwater level is a function of initial and residual soil moisture, porosity, and soil depth. Therefore, during a rainfall event, the groundwater level will increase when the wetting front reached the groundwater level. Therefore, a series of 16 hours of rainfall data, duration (minute) Vs Intensity(mm/hr) were imported into the model. The effect of rainfall in LISEM accounted due to the increase in the GWH level. The comparison is done to investigate the effect of different rainfall return periods on the slope model. Additional rainfall events of different return periods might lead to different estimates of the failure probabilities, and it could provide insight into the landslide-triggering conditions (Godoy Leiva, 2019). However, greater variability of estimated failure is expected due to a variation in the initial groundwater condition. Moreover, LISEM is more sensitive to the groundwater flow conditions thus, the rainfall saturates the surface of the soil above the wetting front, then the Green&Ampt model (Green&Ampt, 1911) is used to simulate the wetting front infiltration. Therefore, the model assumes the wetting front moves downward into the soil and creates a connection with the groundwater. Due to the connection between the wetting front and the initial groundwater table, the groundwater table will increase. This assumption could give insights that the different amounts of rainfall may not give significant differences in slope failure results. For a further interpretation of this assumption, the slope failure condition for different rainfall return periods was compared in the LISEM model and the results were presented as follows.
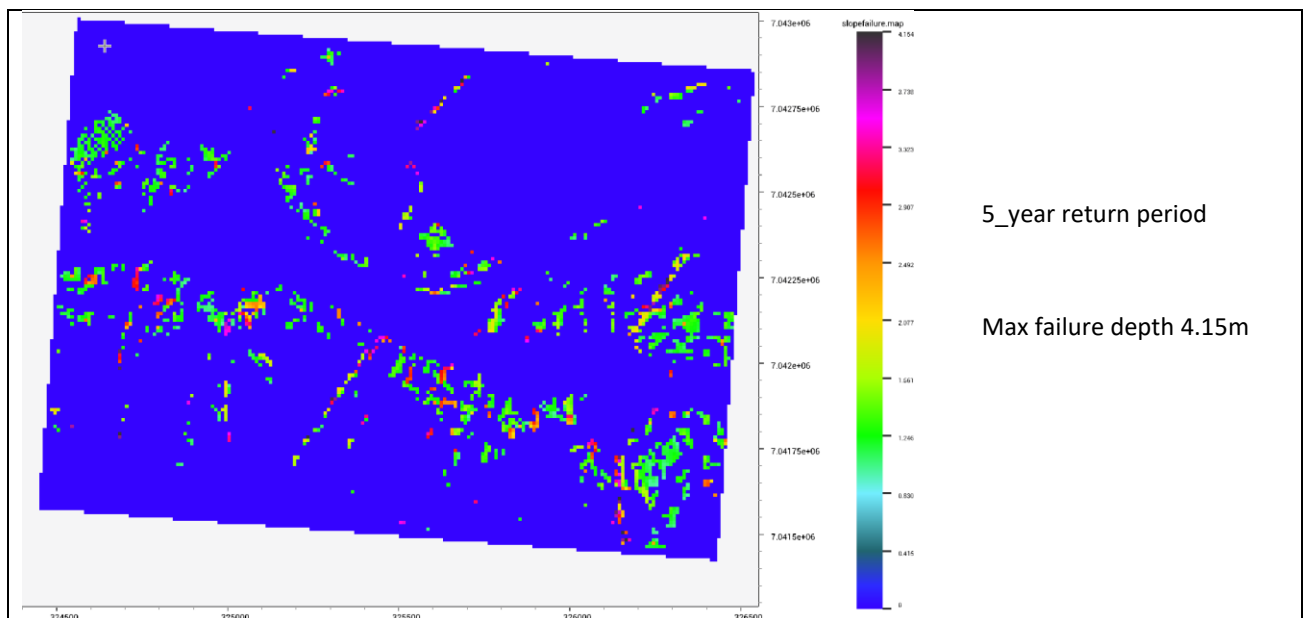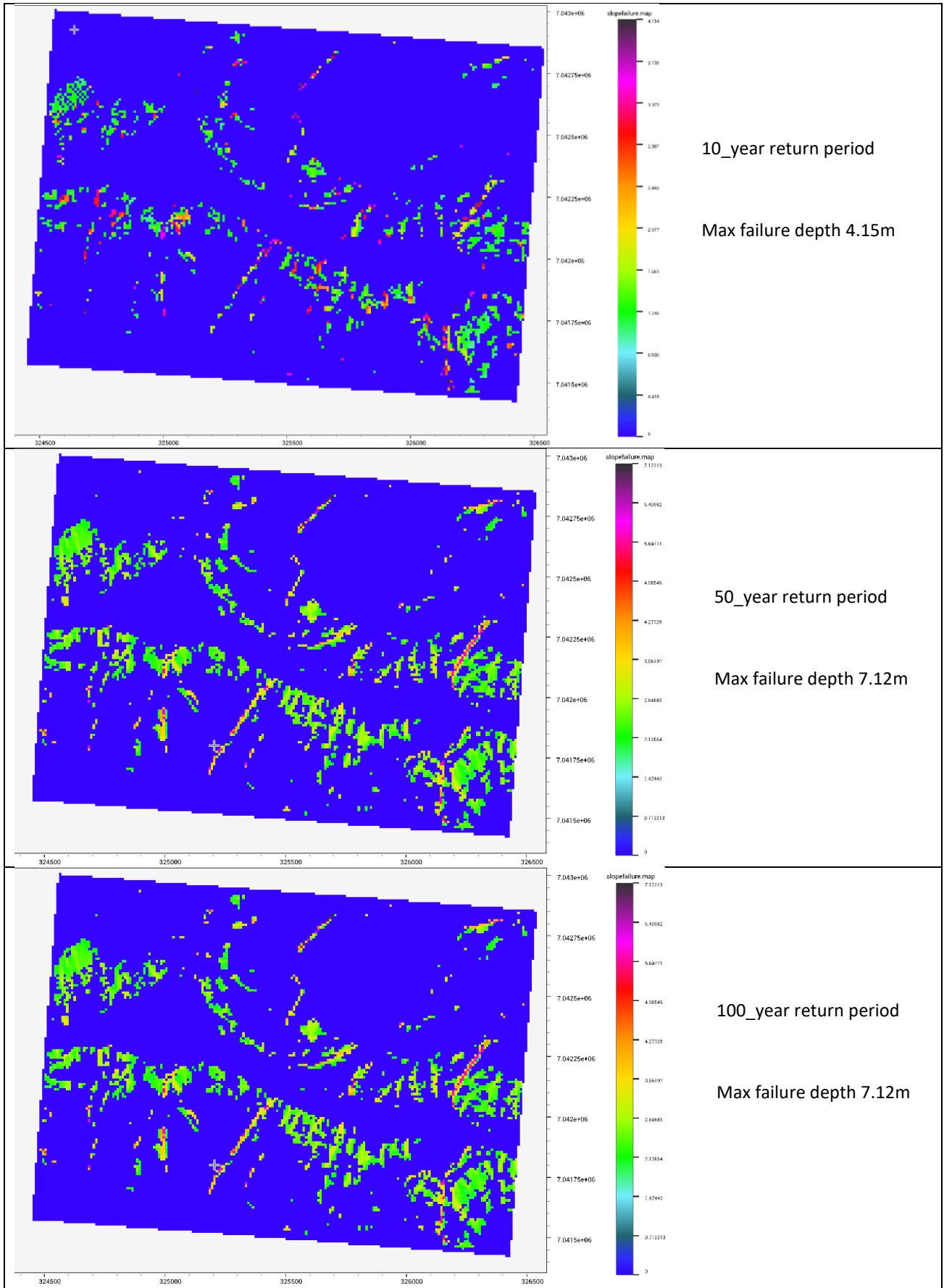
Figure 53. Sensitivity analysis of slope failure for the different rainfall return period.

The initial soil moisture is directly affected by the rainwater. Soil water content at the onset of a rain event is an essential factor that influences the water storage capacity of the catchment as well as the hydrological response of rainfall events. Low intensity tends to result in low moisture on the deep surface because most of the rainwater will be retained in the shallow layer. For that reason, there will be high soil moisture on the surface soil. High rainfall amounts tend to result in high moisture content in the deep soil and increased deep soil moisture content. As shown in figure (53), variation in rainfall amount doesn't significantly affect the slope stability. However, (initial soil saturation) variation directly affects slope stability results. The VWC of the study area is in the range of (0.15-0.3) (Depina & Oguz, 2021). These data were used in the assessment of slope stability therefore, for the high amount of rainfall the maximum value of VWC was used. Consequently, a higher failure result is obtained for a 50 and 100-year return period rainfall.

5.6. Runout result

Landslide inventory is usually used as a reference for modelling the landslide runout distance. Photographs, reports, and inventory maps were used for verification of the landslide modelling. The landslide runout simulation model is important to detect the extent of the debris flow and the maximum solid height along with its probable initiation. On physically based model inputs and outputs, there are expected errors and uncertainties therefore, interpretation and calibration of the input and output results are crucial factors for the appropriate modelling results. Input parameters used for the runout model in the LISEM software are the DEM map, Manning map, and soil parameters which are considered boundary conditions for the model (Initial fluid hight, initial solid height, initial density, initial IFA, initial rock size, initial cohesion) failure depth result from the slope stability model used as an input for the initial solid height map. The provides simulation in time. One hour of simulation time is used for this case study and a shorter time step in seconds for the flow simulation is used. Rainfall data (duration (min) Vs. Intensity(mm/hr)) is used for the analysis. The figure below shows the screenshot of the model during the simulation.
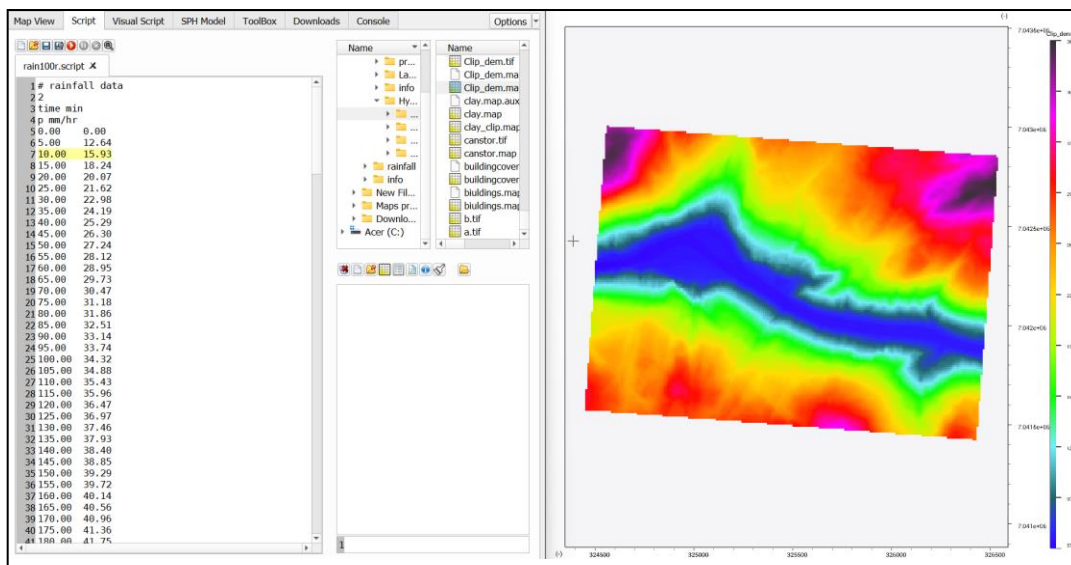
Figure 54. Rainfall data was used for the runout model analysis (duration (min) Vs. Intensity(mm/hr).
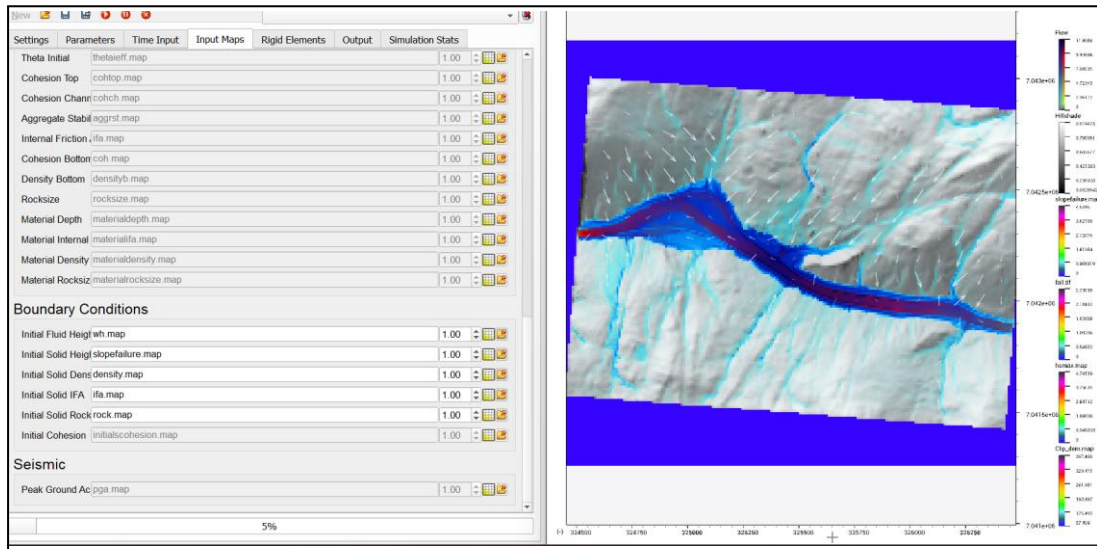
Figure 55. Fluid and solid flow during runout simulation In LISEM.
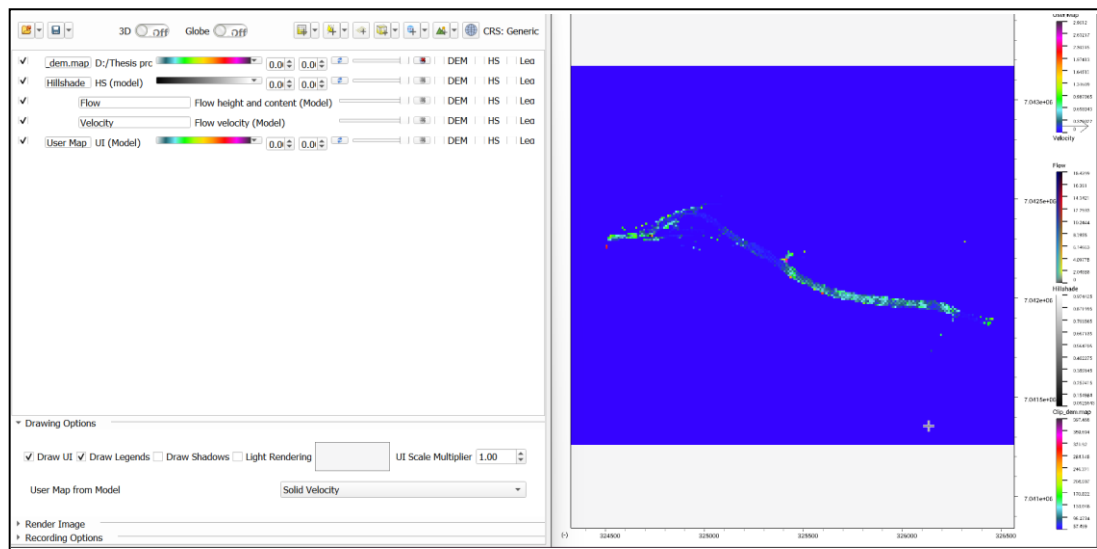
Figure 56. Solid velocity map result during model simulation

The simulation of the model is presented in the figure below. The blue colour represents the water flow whereas the red colour represents the solid flow in figure (55). It is also possible to obtain several maps from the map user during the simulation. Screenshot Image from the model presented, the left side of the image indicates the processing of data while the right side is runout simulation.

The runout map is presented using the reference slope failure result. The maximum runout height is 2.44m. This value is obtained using the reference value of the failure depth result. As shown in the figure below, the maximum solid height with red colours was observed on the failure location.

Max_Soildepth (m)	Cohesion (Pa)	IFA (rad)	GWH	Max_FD (m)
5.22	1500	0.57	flow transient	2.44
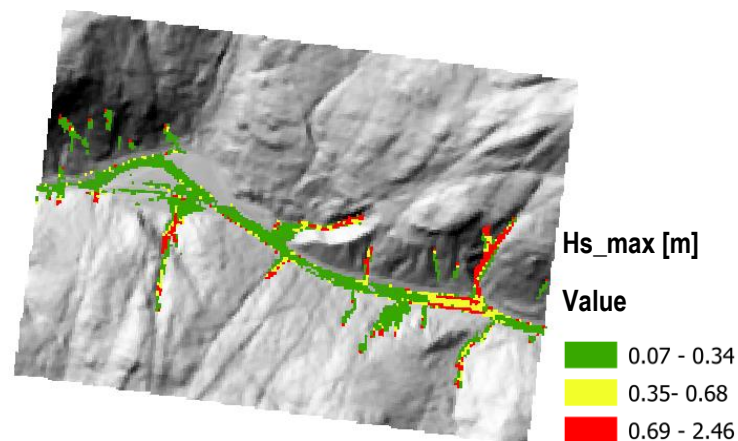
Figure 57. Runout model result using the reference value of slope failure.

The different cases adopted in slope stability assessment can be used in the runout simulation.to observe the maximum solid height due to the changed parameters. The parameters were selected from the sensitivity analysis part in chapter 5.

Case 1. High soil saturation

Max_Soildepth (m)	Cohesion (Pa)	IFA (rad)	GWH	Max_FD (m)
5.22	1500	0.57	80% of Sd	2.44
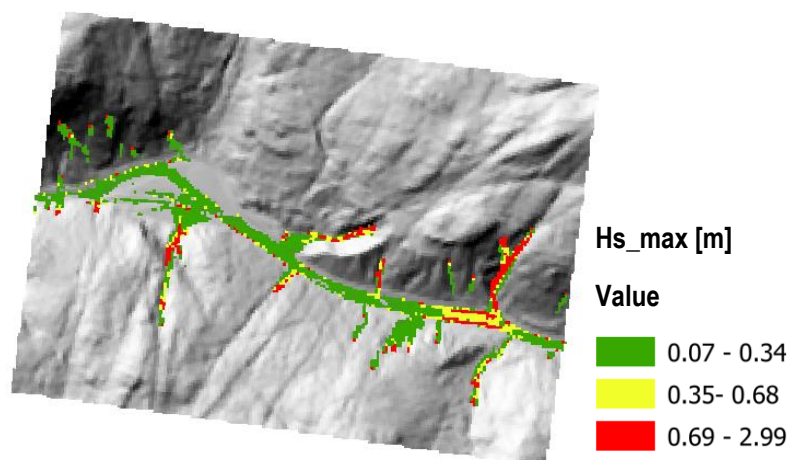
Figure 58. Runout models result due to high soil saturation.

Case 2. 50% increase in soil depth from the reference value.

Max_Soildepth (m)	Cohesion (Pa)	IFA (rad)	GWH	Max_FD (m)
10.44	1500	0.57	Flow transient	4.88
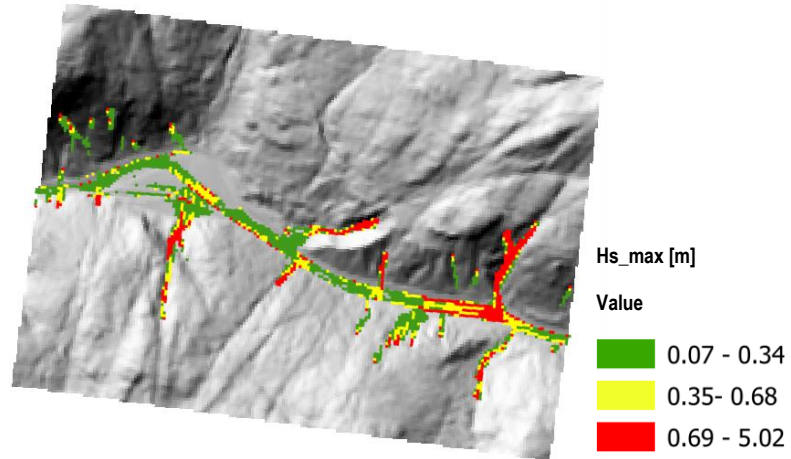
Figure 59. The runout model results in a 50% increase in soil depth from the reference value.

Case 3. Low cohesion value and 20% increased soil depth

Max_Soildepth (m)	Cohesion (Pa)	IFA (rad)	GWH	Max_FD (m)
6.65	1200	0.57	Flow transient	3.05
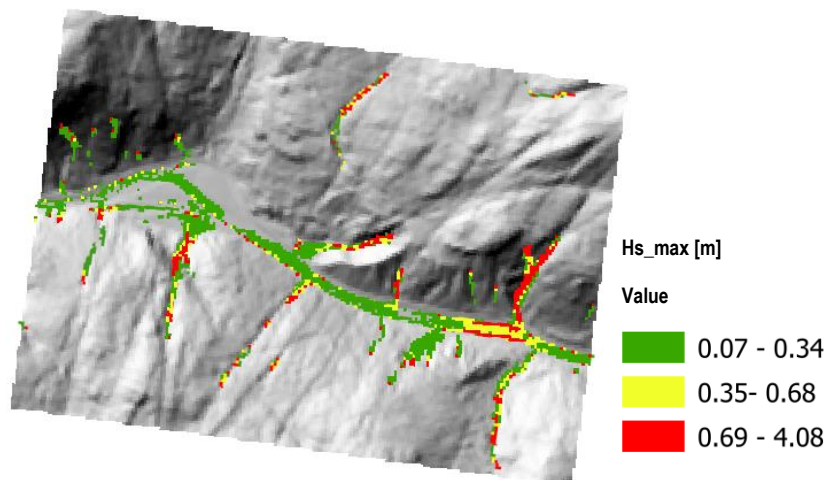
Figure 60. Runout model result for low cohesion value and increased soil depth

Case 4. High water saturation and 50% increased soil depth

Max_Soildepth (m)	Cohesion (Pa)	IFA (rad)	GWH	Max_FD (m)
10.44	1500	0.57	80% of sd	4.88
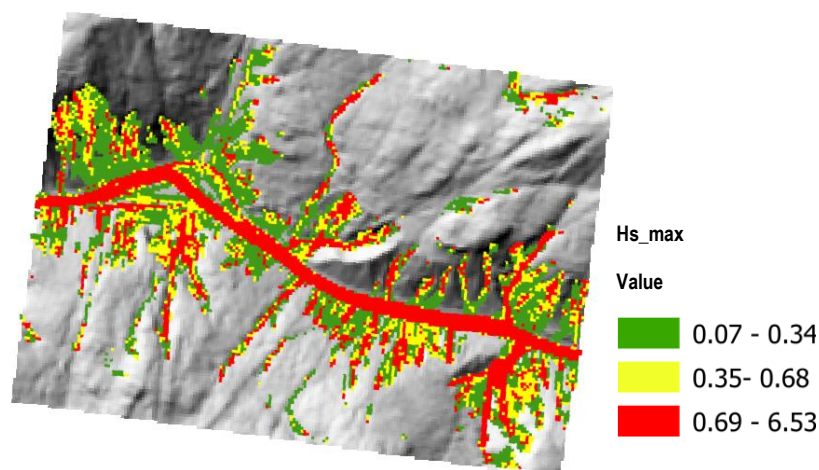
Figure 61. Runout model result for High water saturation and 50% increased soil depth

The runout model result must be validated based on the landslide inventory maps. Figure (57) depicts the landslide runout in the specified failure area. Hs_max represents the maximum solid (debris height). The maximum solid height is 2.46m, and the failure depth and the maximum solid height are almost the same. The inventory map showed the location where the landslide is accumulated. The runout result from figure (57) also identified this location. However, there are some slope failures detected which are not recorded on the inventory data. on the contrary, landslide failures that are recorded on the inventory maps are not completely predicted in the figure (57).

Case 1 and case 2 predicted the landslide where the landslide occurred. In case 2 the landslide is nearly predicted in the location where the inventory is found. Case 3 and case 4 give a huge amount of solid height which is not expected in the actual condition. The reason for this is a huge amount of soil depth is assumed consequently the failure depth is huge. The landslide due to rainfall is depicted in the loose material. The maximum solid height (Hs_max) in this case is very big due to the assumed high value of soil depth and low value of cohesion. The predicted landslide in case 4 is massive and covers the road with a huge amount of solid materials this is in the worst-case scenario with high soil saturation and high-level of soil depth. Using the ArcGIS tool. The area of the predicted landslide from LISEM was computed. Case 4 revealed a huge amount of landslide prediction almost 50% of the total area is covered by the predicted landslide which is not realistic as shown in figure (61). Therefore, the runout result from figure (57) gives a better result. The other cases overestimate the failure depth as well as the soil height. Using LISEM volume of the landslide can be predicted by a simple volume calculation approach which is Area x failure depth. However, it is impossible to say all the slopes failed at once and all the soil eroded.

6. Element at risk assessment

After analysing the landslide hazard and its triggering factors with different sensitivity analyses, it is nothing but worthless not to mention the element at risk. Roads, railways, and buildings are the most vulnerable elements in the study area. The population number and population density were gathered from Statistics Norway. The total population of Meråker and Stjørdal municipality is 26,685. The total population for different age groups is also classified. The total population number of Meråker and Stjørdal municipalities is presented in Annex. The most vulnerable buildings were depicted from the runout model result and slope failure result. However, a detailed risk assessment is required to investigate the damage cost of a landslide. This thesis project doesn't show a detailed risk assessment however, the element at risk and the possible EWS investigated to recommend further study of risk assessment.
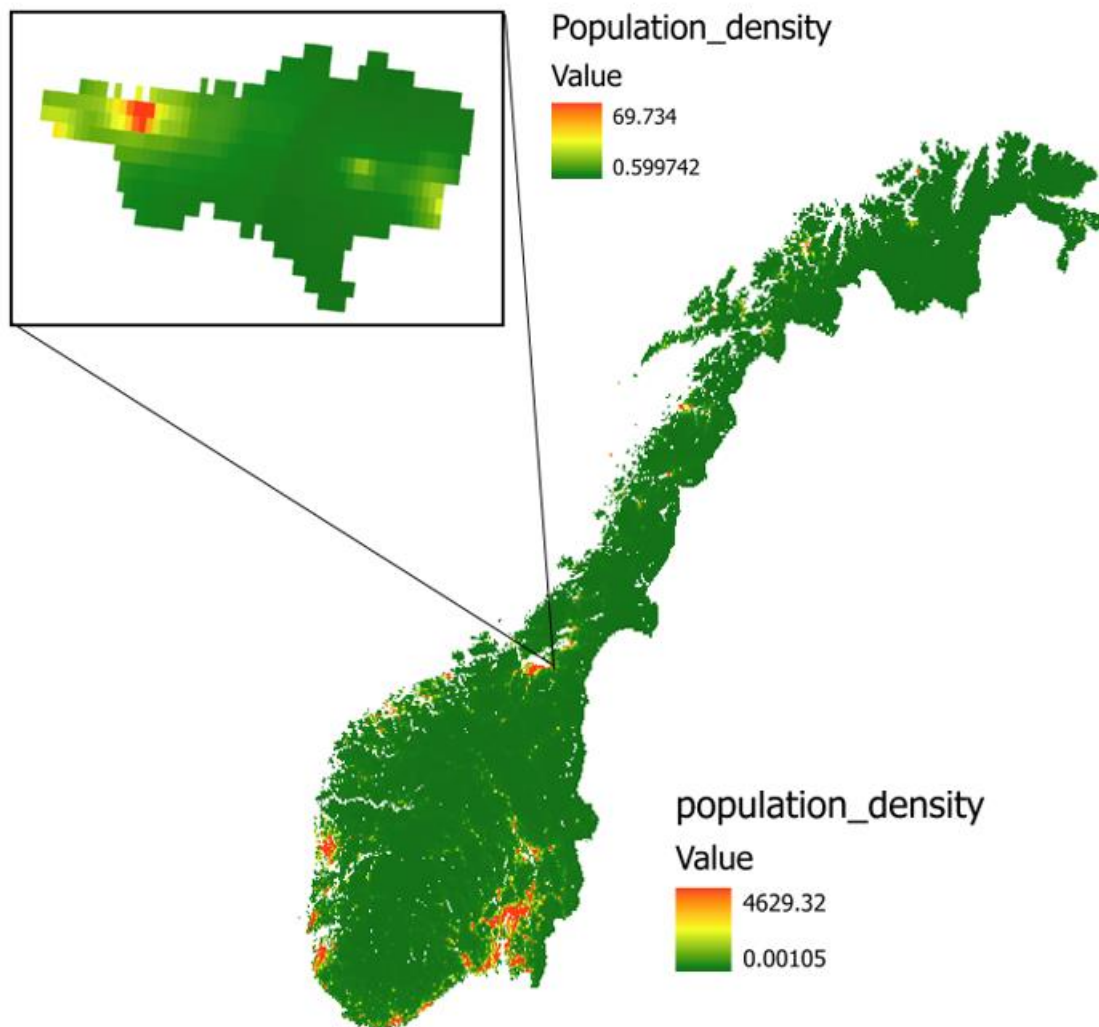
Figure 62. Population density data.

Buildings with the red box are considered to be the most vulnerable areas considering the case 3 runout model result. However, considering the worst-case scenario, which is case 4, all the buildings are vulnerable. Consequently, road E124 (Mellomriksvegen) is also vulnerable to landslides. Case 3 landslide

runout model is considered for risk assessment due to its comparable result with the previous landslide runout propagation.
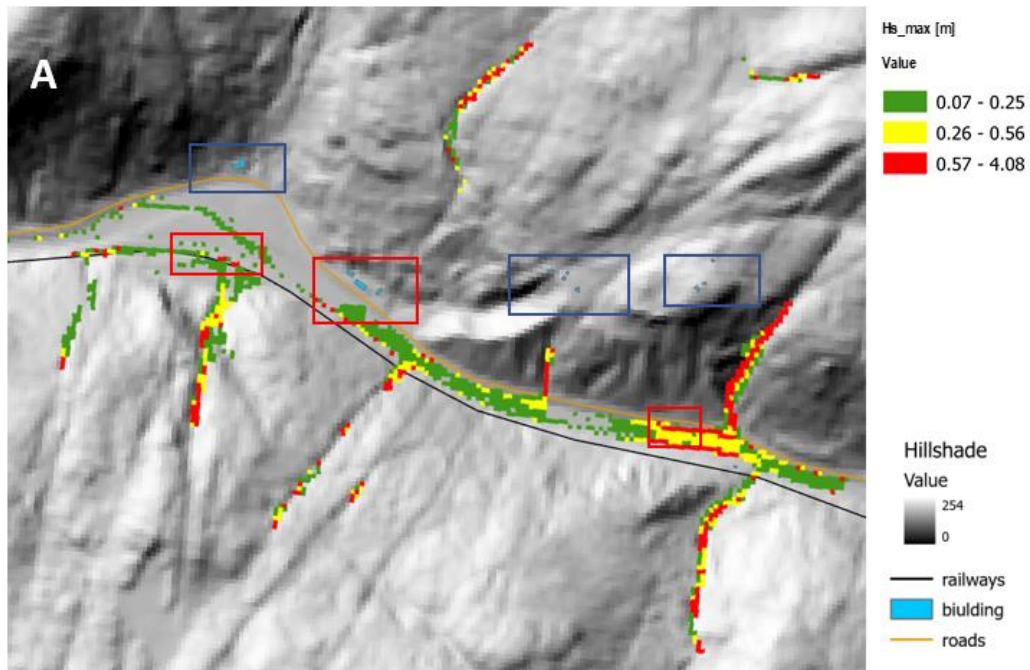
In addition to this, vulnerable buildings due to slope failure were investigated. As shown in the figure below. Most of the buildings are located on unstable slope areas. Human activities can also be considered the possible triggering factor for this instability. The previous landslide in this area is very few. However, the road and the railway are vulnerable to slope failure impact.
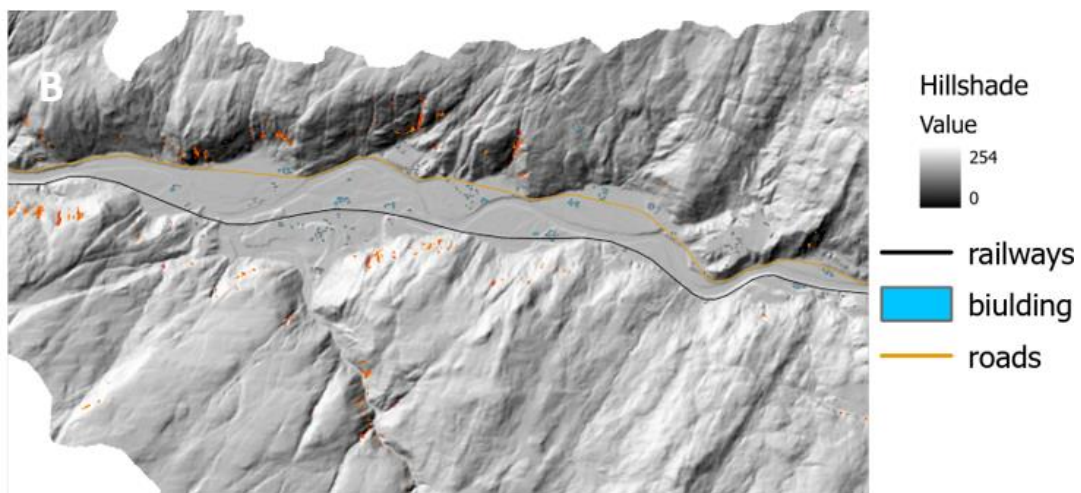
Figure 63. A Proposed runout model and vulnerable buildings, B elements at risk dueto slope failure

According to the Norwegian LEWS methodologies classified as setting parameters to be monitored and threshold values, developing monitoring devices and systems, coordinating satellite radar data with local monitoring stations, planning monitoring programs for high-risk areas, and developing computer-aided decision-making tools with e.g. mobile mapping and retrieval, and information management using

geographical information technology, remote sensing, and 3d modelling (NGI, n.d.). The flowchart below indicates the methodologies adopted for geohazard EWS in Norway.
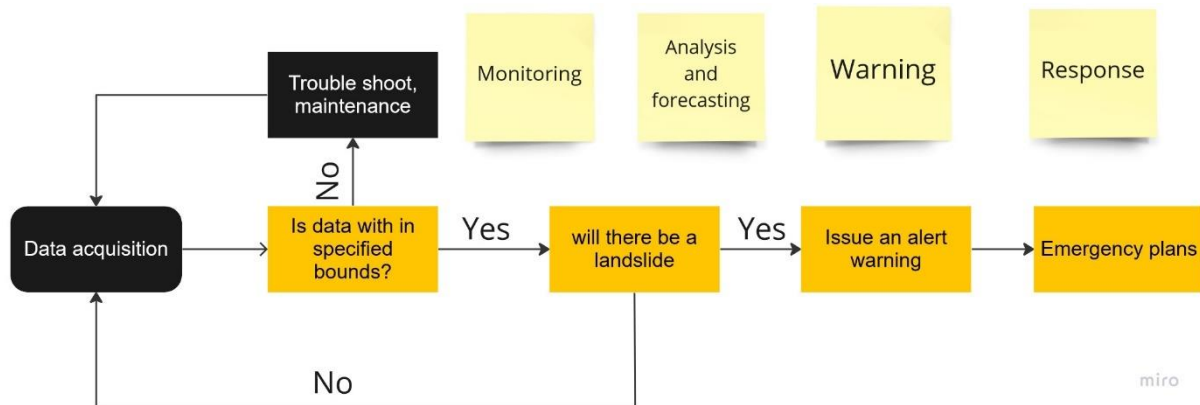
Figure 64. diagram of EWS used in Norway (NGI, n.d.)

Several approaches to LEWS were implemented in the previous studies. Sensor and empirical-based approaches were implemented in the study area (Depina & Oguz, 2021). Sensor-based warnings are issued directly based on observations from single or multiple sensors. In this study, it was possible to predict the slope failure location and runout direction. Landslide sensor-based triggering systems strongly correlated with landslide stability in the considered area. The threshold level is determined by collecting long-term data serious from the sensor, landslide observations, and physical-based models. The runout model presented may indicate that landslide could potentially be triggered in the Fluvial/Alluvial deposits. As it is known Precise prediction of landslides is not always possible because it depends on the visibility of the model and the accuracy of input data. However, the location of the landslide can be estimated by observing the slope failure and runout results from different input parameters. For instance, if the location of slope failure is the same for the different rainfall conditions and soil parameters. An assumption can be made that in that location there is a potential landslide. Nevertheless, for a model like LISEM since the model is not significantly sensitive to the different rainfall conditions it is quite difficult to determine the accurate location and time of slope failure. Particularly for rainfall-triggered landslides a model that precisely investigates the effect of rainfall on an unstable slope is very important for a reliable landslide early warning system (LEWS). LISEM investigates the effects of different soil parameters on slope failure. The observed slope failure location and magnitudes are somehow comparable with the inventory results. As shown in the sensitivity analysis results, most of the slope failure location is on the **Fluvial/Alluvial deposits** and in the **thin moraine deposits**. Likewise, these areas are considered to be unstable from the previous slope stability analysis and field observation. According to the (Depina & Oguz, 2021) report, sensor based IoT devices were installed. The sensors measure the VWC of the soil due to rainfall and snow-melting. Consequently, it is recommended to install sensor-based devices on

fluvial deposits where the factor of safety is less than 1. Because instability of slope is already depicted in this area using LISEM for different soil conditions. Subsequently, the possible triggering factor such as rainfall or snowmelt will increase the magnitude of slope failure on the fluvial deposits. Considering the four runout case studies for different conditions, it was possible to observe that the failure propagates on the same location with different amounts of failure depth.

7. Discussion and Conclusion

The rainfall-induced landslide susceptibility assessment in central Norway required several data and sufficient knowledge about the triggering factor of rainfall and the parameters that causes the slope to become unstable. Susceptibility assessment using a physical-based landslide model for slope stability assessment and runout model gives detailed information about the triggering parameters and their impact on the study area. LISEM was found to be the most applicable software for the assessment of slope stability and runout model. The slope stability assessment and its failure mechanism are intensively studied in the case study. January 13, 2022, back analysis of recent rainfall-triggered shallow landslide events considered for the calibration of the model.

During the assessment, it was possible to understand the possible slope instability triggering factors in dry conditions (before the rainfall). As it is well-known rainfall by itself doesn't cause the slope to fall. The instability condition of the slope due to the topography condition and the possible weak soil materials in combination with the heavy rainfall triggers landslides. Because landslide starts as the consequence of terrain instability, it is important in geotechnical practice to ascertain instability conditions of the soil. The dry condition instability assessment was found to be reasonable. From the assessment result, the areas which are susceptible to failure during rainfall were observed after the sensitivity analysis of slope stability assessment on dry conditions. The stability of the slope depends on several factors and weak soil conditions occurred due to many reasons. However, LISEM considers three basic sensitive parameters for slope failure, cohesion, IFA, and soil depth. This is reasonable because the slope stability (IS) approach also considers these parameters in the FOS calculation. The limit of stability is a value of 1. From the geotechnical information, the resistance of soil or rock is formed by the combined effect of friction and cohesion. The lower value of these parameters affects the stability condition. Water destabilizes slopes mainly due to the increase in pore water pressure. The LISEM model was calibrated to provide FOS>1 for slope stability assessment in dry conditions and FOS<1 after the rainfall in unstable areas. However, the areas which are susceptible to slope failure can easily be detected. The assessment after rainfall also approved this result. FOS becomes lower than 1 in the detected areas.

The calibration to validate the result with the inventory also used parameters which are cohesion and IFA. Availability and accuracy of inventory data were challenging parts of this project. The methodology adopted for calibration is due to the shortage of data. For that reason, a qualitative method is adopted. Even though this method also gives good quality result assessment quantitative method would give a better estimation of errors. The quantitative calibration method used inventory data recorded from NVE (NVE, Velkommen til skredregistrering, 1921) shapefiles. This data is not sufficient for a detailed result validation. That means it gives the location where the landslide was detected and not the location of

landslide initiation. This is a common type of data recording. However, for the susceptibility assessment using the physical based model, the landslide data that indicate the initiation and its propagation along the slope is very important for accurate calibration of the model. This project used additional data from satellite images for the estimation of landslide initiation and its propagation from image analysis. This is the other savvy way of result validation in the case of data shortage. Simply images were gathered from the satellite data and using engineering assessment the polygons on a scarp of the landslide were recorded. The result from LISEM result applied on the base map match on the selected scarp. Consequently, validation was easily adopted for those polygons that coincide with the inventory image. However, some landslide polygons observed from the inventory are not predicted from the LISEM and vice versa.

From the satellite image and inventory map, it was possible to observe that most of the unstable areas are on the fluvial deposit as was detected from the model assessment. Less vegetated areas are prone to landslides. However, there is also a very well-vegetated unstable area. In these areas, it was clear to understand that there was a previous shallow landslide. Vegetations also do not always positively influence slope stability. The stability could be influenced by mechanical cohesion and the removal of water via evapotranspiration. If the vegetation is also in the slopy area the root can either positively or negatively influence the stability. Overall, slope stability assessment and runout model using LISEM indicated the susceptible area where the most previous landslide was recorded. However, this model required several iterations of input parameters. This is not applicable in real conditions. A landslide could occur anywhere in a stable area where it shows on the model. Because there are several triggering factors along the slope, this was possible to investigate from the site visit. It is not always possible to be dependent on these input parameters. In addition, this model didn't give slope failure result on the expected location from the parameters obtained in the laboratory. Even though these values were not recently recorded value, an iteration of this parameter was conducted to obtain the most optimal result that coincides with the inventory.

The other motivation for this research was sensitivity analysis. This analysis was found to be very important to investigate the sensitive parameters for this model and study the extent of failure magnitude due to variation of these parameters. (Cohesion, IFA, and soil depth) value was analysed using the reference value. As it was expected these parameters significantly change the failure depth and failure extent in the area. The combination of these parameters in the worst-case scenario was also assessed and the result showed a huge failure on the map. The higher the soil depth the higher the failure depth since the failure depth is predefined as the bottom of the soil layer. The lower cohesion and IFA also the higher the failure amount. LISEM is user-friendly for sensitivity analysis. one can easily change the

parameters and assess the stability of the area. Rainfall data used for the assessment is from the previous landslide event on January 13, 2022, the rainfall amount was heavy this year. Sensitivity analysis for 5, 10, 50, and 100 rainfall return periods was applied in this model. The result didn't change significantly for each period. This is because rainfall is considered due to the rise of GWH in the model. The wetting front height will create contact with the existing GHW to raise the level of the water from the bottom. This process slightly changes the slope stability result because of the different amounts of rainfall. Also, this condition is not very much applicable in real conditions.

The runout model investigated the element at risk in the study area. The simulation takes 1 hour. However, this can be adjusted for the different resolutions of DEM. The same rainfall data were used for the runout model. The motive was to investigate the soil deposition height and the propagation of debris flow along the slope. The model gives several results solid height and fluid height can be extracted among the other results. The failure depth from the slope stability assessment was used as an initial solid height value during the simulation. A solid height above 2.5m is unrealistic in the study area due to the thin soil cover on the slopes. The runout case due to the combination of parameters that are considered as the triggering factor also resulted a huge solid height. Soil depth above 2.5m is not found in the study area specially along the slope. However, the result can be used for investigating the element at risk. Buildings, E14road, and railways are the exposed elements in the study area. The susceptibility assessment investigated the fluvial/Alluvial deposit is highly susceptible to a landslide. The soil material type (lithology type) description is presented in the geological map. Consequently, there are quite a few residential buildings in this area. The implemented landslide model LISEM reasonably assessed the landslide-prone areas in the case study. The sensitivity analysis and calibration result showed the same location of slope failure, and these areas were observed from the inventory and image analysis. Thus, qualitative analysis is particularly important in susceptibility assessment. The method greatly depends on the expert's experience and discussion. Therefore, the assessment is reinforced by the professionals from the field study. The zoning map and susceptibility assessment using the qualitative method are generally more consistent with reality in the study area.

7.1. Limitations of the study

Rainfall-induced landslide susceptibility assessment was conducted using a physically based model LISEM on a case study in central Norway. This approach requires data for model simulation and result validation. The input data required by LISEM are detailed geotechnical and hydrological parameters of the study area. The topography data are also very important for accurate model simulation and susceptibility assessment. Data in this case study are not accurately recorded. The laboratory results used for model simulation are not recent data, in addition, the most triggering factor of landslide in Norway is rainfall and snowmelt or the combination of both triggers shallow to deep landslide. Rainfall data only consider the recent landslide event recorded on January 13, 2022. However, the snow melt data are not simultaneously considered in the same year.

The calibration of the model is very important for any simulation result. Finding accurate landslide inventory data was the most challenging part of this project. The runout model requires landslide inventory for a detailed investigation of the runout propagation and its deposition. However, this model results used data from satellites image and inventory shapefiles obtained from the available data resource. It is very difficult to precisely draw a polygon that indicates the landslide propagation from a satellite image. The accuracy of image analysis for the calibration of the model could be tricky. Consequently, the calibration depends on the sensitivity analysis of input soil parameters which required several assumptions.

LISEM assumes slope failure is caused by the change in the surrounding or the conditions in the slope. However, this assumption is not correct if we consider the real condition of slope failure. In addition, LISEM assumes that the groundwater level is changed only when the wetting front height reaches the groundwater level. However, soil can be partially saturated everywhere, Therefore, the model doesn't precisely account for the effect of different rainfall amounts on slope failure. This may lead to an underestimation of the FOS value. Most rainfall-induced landslides are not caused by slow infiltration of the wetting front, but by rainfall infiltrating into cracks. Therefore, soil layer discontinuities are not accounted on the model. A runout simulation was performed for a smaller area. For larger areas, the model required a longer time to run which leads to further limitations regarding the performance and accuracy of the output model.

7.2. Recommendation

For accurate calibration of the model the historical topography, soil data, and triggering factors data with a high level of detail are required. However, when dealing with an area where landslide hazard is frequent the quality of such data is problematic. The pre-event data was mostly gathered from a topography map, expert visual observation, and digitalizing existing inventory maps, which can result in errors. Landslide types and dates are probably unknown if a good event-based landslide inventory is not available. Faulty landslide information may lead to incorrect landslide sensitivity models, which may have a negative impact on the susceptibility assessment. Therefore, when preparing data, we should thoroughly investigate the area, and catalogue detailed landslide information in the area. For appropriate runout prediction runout inventory, underground information on soil depth, soil characteristics, and groundwater system is required. Many physical base models required adequate data for calibration, however, insufficient data will result in significant uncertainties in landslide prediction and susceptibility assessment.

This study recommends to extend the conducted work with a landslide risk assessment of the study area. The landslide susceptibility assessment presented with calibration and runout model discussion. However, risk assessment is not included in this thesis project. Therefore, adequate information on exposure elements such as buildings, roads, railways, population data, exposed utility lines, and so on is required for a complete investigation of risk assessment.

8. References

(CLC), C. L. (2018). Retrieved from https://land.copernicus.eu/pan-european/corine-land-cover

(IPCC), I. P. (2013). *AR5 Synthesis Report: Climate Change 2014.* AR5 Synthesis Report: Climate Change 2014.

(Kartverket), N. M. (2021). Retrieved from https://www.kartverket.no/en/about-kartverket/media

Bobrowsky, J. H. (2009). Mapping inventory, susceptibility, Hazard, and risk. In J. H. Bobrowsky, *Mapping inventory, susceptibility, Hazard, and risk.* Landslides - Disaster Risk Reduction.

Bout, B. (2018). Integration of two-phase solid-fluid equations in a catchment model for flash floods, debris flows, and shallow slope failures.

Cepda, N. (2012). Using Spacing to Enhance Diverse Forms of Learning: Review of Recent Research and Implications for Instruction.

Chin-Tung Cheng. (2013). Landslide Susceptibility Map.

Chiyang, M. (2018). Comparing and evaluating two physical-based models: OpenLISEM and SCOOPS3D, FOR landslide volume prediction.

De Roo et al. (1996). *OpenLISEM.* Retrieved from https://lisemmodel.com/docs/about/

Depina, I., & Emir, A. (2022). A Case Study on IoT-based Hydrological Monitoring of Water-Induced Landslides in Central Norway.

Depina, I., & Oguz, E. (2021). Dissemination of sensor data and landslide predictions through an early-warning system.

Depina, I., & Oguz, E. (2021). KlimaDigital Case Study.

Dibaba, M. (2019). THE INFLUENCE OF SOIL DEPTH MODELS ON SIMULATING SLOPE INSTABILITY.

Dyf, H., & Delwyn, F. (1982). A multistage triaxial test for unsaturated soil.

Fernanda, D. (2022). Landslide Early warning runout modeling case study in Norway.

Godoy Leiva, C. (2019). Susceptibility assessment of rainfall (Hegra-Meråker).

Godoy Leiva, C. (2019). Susceptibility assessment of rainfall-induced landslides case study: Hegra-Meraker.

Goodman, & Bray. (1976). Toppling-of-Rock-Slopes.

Graziella Devoli (NVE). (2019). Susceptibility map at catchment level, to be used in landslide forecasting, Norway.

Greco, R., & Gargano, R. (2016). Is there Predictive Power in Hydrological Catchment Information for Regional Landslide Hazard Assessment.

Green&Ampt. (1911). The Flow of Air and Water through Soils. *Open Journal of Soil Science*.

Guzzetti, F. (2005). Probabilistic landslide hazard assessment at the basin scale.

Hisdal et al. (2017). Heavy weather events, water quality and gastroenteritis in Norway. *one Health*.

Kirschbaum, D., & Hong, R. (2006). *Evaluation of a Satellite-Based landslide Algorithm Using Global and Regional Landslide Inventories.* The University of Oklahoma, school of civil and environmental engineering.

Krøgli et al. (2018). The Norwegian forecasting and warning service for rainfall- and snowmelt-induced landslides.

Longoni, L., Scaioni, M., & Melillo, V. (2014). Remote Sensing for Landslide Investigations: An Overview of Recent Achievements and Perspectives.

Lotte Ciska, d. (2018). Mapping and modelling of landslide and flood hazards on St. Eustatius with openLISEM.

Melchiorre , & Frattini. (2010). Modelling probability of rainfall-induced shallow landslides in a changing climate, Otta, Central Norway.

Mikoš, M., & Sassa, K. (2015). Advancing Culture of living with landslides.

Nadim, B. K. (2016). Landslide risk management in Norway. *Landslide risk management*, 215.

NAGAD. (2016). *Geoteknisk Datarapport E14 TS-tiltak Nr. Vd1399A (Statens vegvesen,*. Retrieved from Geoteknisk Datarapport E14 TS-tiltak Nr. Vd1399A (Statens vegvesen,: https://geo.ngu.no/kart/nadag-avansert/

NGI. (2013). *InfraRisk NGI*. Retrieved from https://www.ngi.no/eng/Projects/InfraRisk

NGI. (n.d.). *Early warning systems*. Retrieved from Systems need to be developed to monitor both short-term and long-term geohazards and their effects, and to forewarn of impending danger, in areas

where geohazards could affect life and property.: https://www.ngi.no/eng/Projects/ICG-International-Centre-for-Geohazards/Prevention-and-mitigation/Early-warning-systems

Norwegian Center for climate , S. (2022). Retrieved from https://seklima.met.no/observations/

NPS. (2018). *Geohazards*. Retrieved from Geohazards: https://www.nps.gov/subjects/geohazards/landslide-hazards.htm

NVE. (n.d.). *Norwegian Water Resources and Energy Directorate*. Retrieved from Norwegian Water Resources and Energy Directorate.

NVE. (n.d.). *Velkommen til skredregistrering*. Retrieved from Velkommen til skredregistrering: https://www.skredregistrering.no/#Forsiden

NVE. (2022). Retrieved from Climate and Average Weather Year Round in Meråker: https://weatherspark.com/y/71653/Average-Weather-in-Mer%C3%A5ker-Norway-Year-Round

Oguzhan Akbas, S., & Sterlacchini, S. (2016). Critical assessment of existing physical vulnerability estimation approaches.

oldrich, H., Luciano, p., & serge, L. (2014). The Varnes classification of landslide types, an update.

Peter T, B. (2016). Mapping: Inventories, Susceptibility, Hazard, and Risk.

Safeland. (2011). *Living with landslide risk in Europe: Assessment,.*

Salciarini, D. (2007). Modelling the rainfall-induced development of shallow landslides in eastern Umbria, central Italy, using the TRIGRS (Transient Rainfall Infiltration and Grid-based Slope-stability).

Saxton, & J. Rawls. (2006). Field and pond Hydrologic Analysis with the spaw model.

Science, S. (2011). Friction, Cohesion, and Slope Stability.

T.K., T., & David G., T. (2009). Modeling Soil Depth from Topographic and Land Cover Attributes.

THE INFLUENCE OF SOIL DEPTH MODELS ON SIMULATING SLOPE INSTABILITY. (n.d.).

Trøan. (2017). *Trøan.*

Van Beek , R. (2002). Assessment of the influence of changes in climate and land use on landslide activity in a Mediterranean environment.

van den Bout, B. (2017). *LISEM (Lisem Integrated Spatial Earth Modeller).* Retrieved from LISEM:
https://lisemmodel.com/

Von Ruette, & Lehmann. (2013). Rainfall-triggered shallow landslides at catchment scale:
Thresholdmechanics-based modeling for abruptness and localization.

9. Appendix

9.1. LISEM script

Soil depth MAP	```void main()```
	```{```
	```soildepth.map = SteadyStateSoil(dem.map,dem.map```
	```* 0.0 + 0.1,dem.map * 0.0 + 0.1,100);```
	```}```

Groundwater (flow transient) MAP	```void main()```
	```{```
	``` Map dem = dem.map;```
	``` Map sd= soil depth. map;```
	``` Map thetas = dem*0.0 + 0.3;```
	``` Map gwh = sd * 0.2;```
	``` UILayer l = AddViewLayer(gwh,"gwh");```
	``` for(int i = 0; i < 1000; i++)```
	``` {```
	``` Map gwhn = FlowTransient(dem,sd,sd *0.0 +```
	```0.0001,thetas,gwh,60 * 30,true);```
	
	``` ReplaceViewLayer(l,gwh);```
	``` gwh = gwhn;```
	``` Print(i);```
	``` }```
	
	```}```

hydrological parameters using the Saxton relationships	```wfhn.map = GreenAndAmpt(wfh.map,wh.map,soil``` ```depth.map,ksat.map,thetas2.tif,thetai2.tif,psi.tif,1.0);```

	```void main()```
	```{```
	
	``` Map sand = sg_sand.tif/1000.00;```
	``` Map clay = sg_clay.tif/1000.0;```
	``` Map silt = sg_silt.tif/1000.0;```
	``` Map om = sg_om.tif/100.0;```
	
	``` thetas.tif =```
	```SaxtonPorosity(sand,clay,om,om*0.0,1.0);```
	``` theta.tif = thetas.tif * 0.9; //assume 90 percent```
	```saturation```
	``` a.tif = SaxtonA(sand,clay,om,om*0.1,1.0);```
	``` b.tif = SaxtonB(sand,clay,om,om*0.1,1.0);```
	``` ksat.tif = SaxtonKSat(sand,clay,om,om*0.0,1.0);```
	``` psi.tif = a.tif * ((theta.tif) **(-b.tif));```
	
	```}```

SlopeStability (IS) MAP	```void main()``` ```{```

	array <Map> results = **SlopeStabilityIS(**clip_dem.map,soildepth.map, ,soildepth.map * 0.0 + 1500, soildepth.map * 0.0 + 0.57,soildepth.map * 0.0 + 1900,fgwh.map,1.0); fail.tif = results[1]; FoS.tif = results[0];
	
	}

9.2. Rainfall data

	Return period					
Time (minute)	2YEAR	5YEAR	10YEAR	25YEAR	50YEAR	100YEAR
5.00	77.81	116.73	142.49	175.05	199.20	223.17
10.00	45.02	74.09	93.34	117.66	135.70	153.60
15.00	34.44	60.34	77.49	99.16	115.23	131.19
20.00	28.03	51.56	67.14	86.83	101.43	115.93
25.00	23.86	45.71	60.17	78.45	92.01	105.47
30.00	20.91	41.46	55.08	72.27	85.03	97.70
35.00	18.68	38.21	51.14	67.48	79.60	91.63
40.00	16.94	35.62	47.99	63.61	75.20	86.71
45.00	15.53	33.49	45.38	60.41	71.55	82.62
50.00	14.37	31.71	43.19	57.69	68.45	79.14
55.00	13.38	30.18	41.30	55.36	65.78	76.13
60.00	12.54	28.86	39.66	53.32	63.44	73.49
65.00	11.81	27.70	38.22	51.51	61.37	71.16
70.00	11.17	26.67	36.94	49.90	59.52	69.07
75.00	10.61	25.76	35.78	48.46	57.86	67.19
80.00	10.10	24.93	34.74	47.15	56.35	65.48
85.00	9.65	24.18	33.80	45.95	54.97	63.92
90.00	9.24	23.49	32.93	44.85	53.70	62.48
95.00	8.86	22.86	32.13	43.85	52.53	61.16
100.00	8.52	22.29	31.40	42.91	51.45	59.93
105.00	8.21	21.75	30.72	42.04	50.45	58.79
110.00	7.92	21.25	30.08	41.23	49.51	57.72
115.00	7.65	20.79	29.49	40.48	48.63	56.72
120.00	7.41	20.36	28.93	39.77	47.80	55.78
125.00	7.17	19.95	28.41	39.10	47.03	54.90
130.00	6.96	19.57	27.92	38.47	46.29	54.06
135.00	6.76	19.21	27.45	37.87	45.60	53.27
140.00	6.57	18.87	27.02	37.31	44.94	52.52
145.00	6.39	18.55	26.60	36.77	44.32	51.81
150.00	6.22	18.24	26.20	36.26	43.72	51.13
155.00	6.06	17.96	25.83	35.78	43.16	50.48
160.00	5.91	17.68	25.47	35.31	42.62	49.87
165.00	5.77	17.42	25.13	34.87	42.10	49.27

170.00	5.64	17.17	24.80	34.45	41.61	48.71
175.00	5.51	16.93	24.49	34.04	41.13	48.17
180.00	5.39	16.70	24.19	33.65	40.68	47.65
185.00	5.27	16.48	23.90	33.28	40.24	47.15
190.00	5.16	16.27	23.63	32.92	39.82	46.66
195.00	5.05	16.07	23.36	32.58	39.41	46.20
200.00	4.95	15.87	23.11	32.24	39.02	45.75
205.00	4.85	15.69	22.86	31.92	38.65	45.32
210.00	4.76	15.51	22.62	31.61	38.28	44.90
215.00	4.67	15.33	22.39	31.31	37.93	44.50
220.00	4.58	15.17	22.17	31.02	37.59	44.11
225.00	4.50	15.00	21.96	30.74	37.26	43.73
230.00	4.42	14.85	21.75	30.47	36.94	43.37
235.00	4.34	14.70	21.55	30.21	36.63	43.01
240.00	4.27	14.55	21.36	29.96	36.33	42.67
245.00	4.20	14.41	21.17	29.71	36.04	42.33
250.00	4.13	14.27	20.99	29.47	35.76	42.01
255.00	4.06	14.14	20.81	29.23	35.49	41.69
260.00	4.00	14.01	20.64	29.01	35.22	41.39
265.00	3.94	13.88	20.47	28.79	34.96	41.09
270.00	3.88	13.76	20.31	28.57	34.71	40.80
275.00	3.82	13.64	20.15	28.36	34.46	40.51
280.00	3.76	13.53	19.99	28.16	34.22	40.24
285.00	3.71	13.42	19.84	27.96	33.99	39.97
290.00	3.66	13.31	19.70	27.77	33.76	39.70
295.00	3.60	13.20	19.55	27.58	33.54	39.45
300.00	3.55	13.10	19.41	27.40	33.32	39.20
305.00	3.50	12.99	19.28	27.22	33.11	38.95
310.00	3.46	12.90	19.15	27.04	32.90	38.71
315.00	3.41	12.80	19.02	26.87	32.70	38.48
320.00	3.37	12.71	18.89	26.70	32.50	38.25
325.00	3.32	12.61	18.77	26.54	32.30	38.03
330.00	3.28	12.53	18.65	26.38	32.12	37.81
335.00	3.24	12.44	18.53	26.22	31.93	37.60
340.00	3.20	12.35	18.41	26.07	31.75	37.39
345.00	3.16	12.27	18.30	25.92	31.57	37.18
350.00	3.12	12.19	18.19	25.77	31.40	36.98
355.00	3.08	12.11	18.08	25.63	31.23	36.78
360.00	3.05	12.03	17.97	25.49	31.06	36.59
365.00	3.01	11.95	17.87	25.35	30.89	36.40
370.00	2.98	11.88	17.77	25.21	30.73	36.22
375.00	2.94	11.80	17.66	25.07	30.56	36.02
380.00	2.91	11.73	17.57	24.95	30.42	35.85

385.00	2.88	11.66	17.47	24.82	30.27	35.68
390.00	2.85	11.59	17.38	24.69	30.12	35.51
395.00	2.82	11.52	17.29	24.57	29.97	35.34
400.00	2.79	11.46	17.20	24.45	29.83	35.17
405.00	2.76	11.39	17.11	24.33	29.69	35.01
410.00	2.73	11.33	17.02	24.21	29.55	34.85
415.00	2.70	11.26	16.93	24.10	29.41	34.69
420.00	2.67	11.20	16.85	23.98	29.28	34.53
425.00	2.64	11.14	16.77	23.87	29.15	34.38
430.00	2.62	11.08	16.68	23.76	29.02	34.23
435.00	2.59	11.02	16.60	23.66	28.89	34.08
440.00	2.57	10.96	16.53	23.55	28.76	33.94
445.00	2.54	10.91	16.45	23.45	28.64	33.79
450.00	2.52	10.85	16.37	23.34	28.52	33.65
455.00	2.49	10.80	16.30	23.24	28.40	33.51
460.00	2.47	10.74	16.22	23.14	28.28	33.38
465.00	2.44	10.69	16.15	23.05	28.16	33.24
470.00	2.42	10.64	16.08	22.95	28.05	33.11
475.00	2.40	10.59	16.01	22.86	27.94	32.98
480.00	2.38	10.54	15.94	22.76	27.83	32.85
485.00	2.36	10.49	15.87	22.67	27.72	32.73
490.00	2.33	10.44	15.80	22.58	27.61	32.60
495.00	2.31	10.39	15.74	22.49	27.50	32.48
500.00	2.29	10.34	15.67	22.40	27.40	32.36
505.00	2.27	10.30	15.61	22.32	27.30	32.24
510.00	2.25	10.25	15.54	22.23	27.19	32.12
515.00	2.23	10.20	15.48	22.15	27.09	32.00
520.00	2.22	10.16	15.42	22.06	26.99	31.89
525.00	2.20	10.12	15.36	21.98	26.90	31.77
530.00	2.18	10.07	15.30	21.90	26.80	31.66
535.00	2.16	10.03	15.24	21.82	26.70	31.55
540.00	2.14	9.99	15.18	21.74	26.61	31.44
545.00	2.12	9.94	15.12	21.67	26.52	31.34
550.00	2.11	9.90	15.07	21.59	26.43	31.23
555.00	2.09	9.86	15.01	21.51	26.34	31.13
560.00	2.07	9.82	14.95	21.44	26.25	31.02
565.00	2.06	9.78	14.90	21.36	26.16	30.92
570.00	2.04	9.75	14.85	21.29	26.07	30.82
575.00	2.02	9.71	14.79	21.22	25.99	30.72
580.00	2.01	9.67	14.74	21.15	25.90	30.62
585.00	1.99	9.63	14.69	21.08	25.82	30.52
590.00	1.98	9.59	14.64	21.01	25.74	30.43
595.00	1.96	9.56	14.59	20.94	25.65	30.33

600.00	1.95	9.52	14.54	20.87	25.57	30.24
605.00	1.93	9.49	14.49	20.81	25.49	30.15
610.00	1.92	9.45	14.44	20.74	25.41	30.05
615.00	1.90	9.42	14.39	20.67	25.34	29.96
620.00	1.89	9.38	14.34	20.61	25.26	29.87
625.00	1.88	9.35	14.29	20.54	25.17	29.78
630.00	1.86	9.32	14.25	20.48	25.11	29.70
635.00	1.85	9.28	14.20	20.42	25.03	29.61
640.00	1.84	9.25	14.16	20.36	24.96	29.52
645.00	1.82	9.22	14.11	20.30	24.89	29.44
650.00	1.81	9.19	14.07	20.24	24.81	29.36
655.00	1.80	9.15	14.02	20.18	24.74	29.27
660.00	1.79	9.12	13.98	20.12	24.67	29.19
665.00	1.77	9.09	13.94	20.06	24.60	29.11
670.00	1.77	9.09	13.94	20.06	24.60	29.11
675.00	1.76	9.06	13.89	20.00	24.53	29.03
680.00	1.75	9.03	13.85	19.94	24.46	28.95
685.00	1.74	9.00	13.81	19.89	24.40	28.87
690.00	1.73	8.97	13.77	19.83	24.33	28.79
695.00	1.71	8.94	13.73	19.78	24.26	28.72
700.00	1.70	8.91	13.69	19.72	24.20	28.64
705.00	1.69	8.89	13.65	19.67	24.13	28.56
710.00	1.68	8.86	13.61	19.61	24.07	28.49
715.00	1.67	8.83	13.57	19.56	24.00	28.42
720.00	1.66	8.80	13.53	19.51	23.94	28.34
725.00	1.65	8.77	13.49	19.46	23.88	28.27
730.00	1.64	8.75	13.46	19.40	23.82	28.20
735.00	1.63	8.72	13.42	19.35	23.76	28.13
740.00	1.62	8.69	13.38	19.30	23.69	28.06
745.00	1.61	8.67	13.34	19.25	23.63	27.99
750.00	1.60	8.64	13.31	19.20	23.58	27.92
755.00	1.59	8.62	13.27	19.15	23.52	27.85
760.00	1.58	8.59	13.24	19.10	23.46	27.78
765.00	1.57	8.57	13.20	19.06	23.40	27.71
770.00	1.56	8.54	13.16	19.01	23.34	27.65
775.00	1.55	8.52	13.13	18.96	23.29	27.58
780.00	1.54	8.49	13.10	18.91	23.23	27.51
785.00	1.53	8.47	13.06	18.87	23.17	27.45
790.00	1.52	8.44	13.03	18.82	23.12	27.38
795.00	1.51	8.42	12.99	18.78	23.06	27.32
800.00	1.50	8.40	12.96	18.73	23.01	27.26
805.00	1.49	8.37	12.93	18.69	22.96	27.19
810.00	1.48	8.35	12.90	18.64	22.90	27.13

815.00	1.47	8.33	12.86	18.60	22.85	27.07
820.00	1.46	8.30	12.83	18.55	22.80	27.01
825.00	1.46	8.28	12.80	18.51	22.74	26.95
830.00	1.45	8.26	12.77	18.47	22.69	26.89
835.00	1.44	8.24	12.74	18.42	22.64	26.83
840.00	1.43	8.22	12.71	18.38	22.59	26.77
845.00	1.42	8.19	12.68	18.34	22.54	26.71
850.00	1.42	8.17	12.65	18.30	22.49	26.65
855.00	1.41	8.15	12.62	18.26	22.44	26.60
860.00	1.40	8.13	12.59	18.22	22.39	26.54
865.00	1.39	8.11	12.56	18.18	22.34	26.48
870.00	1.38	8.09	12.53	18.14	22.30	26.43
875.00	1.38	8.09	12.53	18.14	22.30	26.43
880.00	1.38	8.07	12.50	18.10	22.25	26.37
885.00	1.37	8.05	12.47	18.06	22.20	26.32
890.00	1.36	8.03	12.44	18.02	22.15	26.26
895.00	1.35	8.01	12.41	17.98	22.11	26.21
900.00	1.35	7.99	12.38	17.94	22.06	26.15
905.00	1.34	7.97	12.36	17.90	22.01	26.10
910.00	1.33	7.95	12.33	17.86	21.97	26.05
915.00	1.32	7.93	12.30	17.83	21.92	25.99
920.00	1.32	7.91	12.27	17.79	21.88	25.94
925.00	1.31	7.89	12.25	17.75	21.83	25.89
930.00	1.30	7.87	12.22	17.71	21.79	25.84
935.00	1.30	7.85	12.19	17.68	21.75	25.79
940.00	1.29	7.83	12.17	17.64	21.70	25.73
945.00	1.28	7.82	12.14	17.61	21.66	25.68
950.00	1.28	7.80	12.11	17.57	21.62	25.63
955.00	1.27	7.78	12.09	17.53	21.57	25.58
960.00	1.26	7.76	12.06	17.50	21.53	25.53
965.00	1.26	7.74	12.04	17.46	21.49	25.49
970.00	1.25	7.73	12.01	17.43	21.45	25.44
975.00	1.24	7.71	11.99	17.40	21.41	25.39
980.00	1.24	7.69	11.96	17.36	21.37	25.34
985.00	1.23	7.67	11.94	17.33	21.33	25.29
990.00	1.22	7.66	11.91	17.29	21.28	25.25
995.00	1.22	7.64	11.89	17.26	21.24	25.20
1000.00	1.21	7.62	11.87	17.23	21.20	25.15

9.3. Population data

Population Age	K-5034 Meråker		K-5035 Stjørdal	
	Males	Females	Males	Females
0 years	12.00	3.00	106.00	124.00
1 year	20.00	6.00	113.00	133.00
2 years	10.00	16.00	117.00	109.00
3 years	10.00	7.00	132.00	109.00
4 years	18.00	7.00	141.00	145.00
5 years	14.00	10.00	153.00	121.00
6 years	12.00	11.00	149.00	141.00
7 years	13.00	7.00	165.00	127.00
8 years	18.00	15.00	156.00	146.00
9 years	15.00	10.00	154.00	147.00
10 years	19.00	12.00	173.00	162.00
11 years	15.00	15.00	155.00	160.00
12 years	10.00	11.00	184.00	170.00
13 years	10.00	16.00	167.00	157.00
14 years	14.00	14.00	172.00	179.00
15 years	11.00	13.00	170.00	158.00
16 years	11.00	10.00	150.00	167.00
17 years	17.00	13.00	155.00	159.00
18 years	15.00	10.00	157.00	170.00
19 years	12.00	7.00	159.00	129.00
20 years	18.00	15.00	174.00	136.00
21 years	8.00	8.00	154.00	117.00
22 years	10.00	14.00	152.00	134.00
23 years	15.00	9.00	154.00	141.00
24 years	9.00	8.00	169.00	137.00
25 years	13.00	12.00	154.00	138.00
26 years	14.00	12.00	131.00	116.00
27 years	9.00	11.00	160.00	128.00
28 years	13.00	11.00	140.00	143.00
29 years	11.00	16.00	144.00	129.00
30 years	10.00	10.00	130.00	134.00
31 years	11.00	11.00	142.00	152.00
32 years	15.00	13.00	123.00	131.00
33 years	16.00	16.00	166.00	175.00
34 years	13.00	7.00	133.00	144.00
35 years	10.00	12.00	155.00	137.00
36 years	13.00	16.00	141.00	154.00
37 years	12.00	13.00	152.00	133.00
38 years	10.00	14.00	136.00	137.00

39 years	14.00	12.00	154.00	168.00
40 years	15.00	11.00	119.00	160.00
41 years	8.00	16.00	138.00	134.00
42 years	15.00	12.00	158.00	140.00
43 years	22.00	13.00	150.00	134.00
44 years	4.00	10.00	158.00	153.00
45 years	13.00	16.00	143.00	135.00
46 years	15.00	16.00	155.00	175.00
47 years	21.00	16.00	150.00	164.00
48 years	19.00	10.00	191.00	172.00
49 years	16.00	16.00	204.00	166.00
50 years	20.00	18.00	203.00	176.00
51 years	26.00	15.00	171.00	199.00
52 years	10.00	18.00	191.00	159.00
53 years	17.00	22.00	175.00	177.00
54 years	21.00	20.00	178.00	170.00
55 years	25.00	15.00	175.00	152.00
56 years	14.00	13.00	184.00	180.00
57 years	16.00	18.00	157.00	168.00
58 years	18.00	20.00	167.00	150.00
59 years	12.00	13.00	159.00	146.00
60 years	20.00	18.00	130.00	137.00
61 years	20.00	24.00	130.00	134.00
62 years	12.00	14.00	144.00	129.00
63 years	13.00	19.00	123.00	139.00
64 years	21.00	17.00	146.00	140.00
65 years	17.00	10.00	127.00	141.00
66 years	22.00	18.00	120.00	145.00
67 years	18.00	15.00	137.00	116.00
68 years	18.00	26.00	137.00	129.00
69 years	12.00	14.00	127.00	121.00
70 years	17.00	17.00	134.00	128.00
71 years	27.00	17.00	111.00	131.00
72 years	22.00	11.00	138.00	126.00
73 years	16.00	13.00	141.00	123.00
74 years	20.00	20.00	103.00	122.00
75 years	16.00	13.00	121.00	122.00
76 years	13.00	5.00	110.00	134.00
77 years	14.00	9.00	101.00	109.00
78 years	11.00	9.00	86.00	94.00
79 years	6.00	12.00	87.00	80.00
80 years	8.00	13.00	71.00	80.00
81 years	11.00	7.00	67.00	69.00

82 years	8.00	8.00	58.00	62.00
83 years	6.00	7.00	37.00	57.00
84 years	5.00	5.00	54.00	58.00
85 years	3.00	9.00	28.00	49.00
86 years	2.00	2.00	27.00	42.00
87 years	2.00	6.00	29.00	24.00
88 years	3.00	4.00	25.00	44.00
89 years	3.00	7.00	13.00	42.00
90 years	0.00	5.00	9.00	23.00
91 years	2.00	2.00	8.00	25.00
92 years	4.00	6.00	9.00	11.00
93 years	3.00	2.00	7.00	15.00
94 years	3.00	0.00	9.00	18.00
95 years	0.00	2.00	4.00	10.00
96 years	0.00	3.00	0.00	8.00
97 years	0.00	0.00	1.00	6.00
98 years	1.00	1.00	1.00	4.00
99 years	0.00	1.00	0.00	2.00
100 years	0.00	1.00	0.00	0.00
101 years	0.00	0.00	1.00	1.00